



UNIVERSIDADE FEDERAL DE SANTA CATARINA  
CENTRO TECNOLÓGICO  
PROGRAMA DE PÓS-GRADUAÇÃO EM ENGENHARIA QUÍMICA

Arthur Poester Cordeiro

**mRNA Encapsulation in Lipid Nanoparticles Formulations for Macrophage-based  
Immunotherapy and Pulmonary Lung Delivery**

Florianópolis  
2023

Arthur Poester Cordeiro

**mRNA Encapsulation in Lipid Nanoparticles Formulations for Macrophage-based  
Immunotherapy and Pulmonary Lung Delivery**

Tese submetida ao Programa de Pós-Graduação em Engenharia Química da Universidade Federal de Santa Catarina como requisito parcial para a obtenção do título de Doutor em Desenvolvimento de Processos Químicos e Biotecnológicos

Orientadora: Prof.<sup>a</sup> Dr.<sup>a</sup> Cláudia Sayer  
Coorientador: Prof. Dr. Pedro Henrique  
Hermes De Araújo e Dr.<sup>a</sup> Tamara Agner

Florianópolis

2023

Poester Cordeiro, Arthur

mRNA Encapsulation in Lipid Nanoparticles Formulations for Macrophage-based Immunotherapy and Pulmonary Lung Delivery / Arthur Poester Cordeiro ; orientador, Claudia Sayer, coorientador, Pedro Henrique Hermes De Araújo, coorientador, Tamara Agner, 2023.

107 p.

Tese (doutorado) - Universidade Federal de Santa Catarina, Centro Tecnológico, Programa de Pós-Graduação em Engenharia Química, Florianópolis, 2023.

Inclui referências.

1. Engenharia Química. 2. Nanopartículas Lipídicas. 3. mRNA. 4. Drug Delivery. 5. Lung and Macrophages. I. Sayer, Claudia. II. Hermes De Araújo, Pedro Henrique. III. Agner, Tamara IV. Universidade Federal de Santa Catarina. Programa de Pós-Graduação em Engenharia Química. V. Título.

Arthur Poester Cordeiro

**mRNA Encapsulation in Lipid Nanoparticles Formulations for Macrophage-based  
Immunotherapy and Pulmonary Lung Delivery**

O presente trabalho em nível de Doutorado foi avaliado e aprovado, em 14 de dezembro de 2023, pela banca examinadora composta pelos seguintes membros:

Prof.a Ana Paula Serafini Immich Boemo, Dr.a  
Universidade Federal de Santa Catarina

Prof. Odinei Hess Gonçalves, Dr.  
Universidade Federal de Santa Catarina

Prof.a Maria Eliane Merlin Rocha, Dr.a  
Universidade Federal Do Paraná

Certificamos que esta é a versão original e final do trabalho de conclusão que foi julgado adequado para obtenção do título de Doutor em Engenharia Química.

---

Coordenação do Programa de Pós-Graduação

---

Prof.(a) Claudia Sayer, Dr.(a)  
Orientador(a)

Florianópolis, 2023.

## AGRADECIMENTOS

Agradeço primeiramente aos meus pais e minha irmã pelo apoio incondicional na jornada que culminou nesse momento. Sem dúvida sem a força de vocês nos bons, e principalmente, nos maus momentos essa conquista não seria possível. Muito obrigado por tudo, por serem os pilares dos meus sonhos. Eu agradeço todos os dias pela família incrível que eu tenho. Amo vocês!

Agradeço a minha orientadora Dr<sup>a</sup>. Claudia Sayer e pela confiança depositada, pelos ensinamentos e pela disponibilidade, principalmente durante o período do doutorado sanduíche, onde ter uma orientadora experiente foi fundamental para a conclusão deste trabalho. Gostaria de agradecer meu coorientador Pedro Henrique Hermes De Araújo. E a minha coorientadora Dr.<sup>a</sup> Tamara Agner, que muitas vezes foi uma amiga fundamental no dia a dia caótico e uma grande incentivadora para a realização do meu doutorado sanduíche.

Agradeço imensamente ao meu supervisor de doutorado sanduíche Prof. Dr. Sandro da Rocha pelo carinho, generosidade, e orientação durante o último do meu doutorado. Foi, talvez, o período mais difícil dessa jornada, mas o modo como fui recebido e integrado ao *The da Rocha and Sweet Labs* na *Virginia Commonwealth University* tornou essa experiência menos dolorosa e ainda mais incrível e enriquecedora. Levarei ensinamentos deste período, deste grupo e das pessoas que conheci para minha vida. Gostaria de agradecer em especial ao grupo do mRNA, Prof. Dr. Douglas Sweet, Raneem Al-Daqqá e Asma AlTerawi por tantas horas que passamos discutindo cálculos, formulações, ensaios e resultados e principalmente ao trabalho em equipe, que nos permitiram dar início a esse trabalho que com certeza ainda irá gerar respostas incríveis.

Agradeço ao meu amigo Thiago Machado Neubauer, que me ajudou em tudo que foi possível nesses 4 anos e meio, mostrando que pesquisadores podem ser colegas e contribuir mesmo sem precisar ser coautor dos artigos uns dos outros. Agradeço por ouvir minhas loucuras, ideias revoltas, frustrações e de vez em quando vitórias. Obrigado por toda a força, pessoal e profissional.

Agradeço ao meu colega e amigo Luiz Paulo Soares Pereira, por todas as horas que passamos dentro do LCP, fossem elas para trabalhar, dar risada, fazer fofoca, ou resolver problemas que não eram nossos. Obrigado por ser meu contraponto muitas vezes e por trazer um ponto de vista único para nossas discussões.

Ao programa de pós-graduação em engenharia química e à Coordenação de Aperfeiçoamento de Pessoal de Nível Superior (CAPES) pelo suporte financeiro.

## RESUMO

Nas últimas décadas, o uso de agentes terapêuticos baseados em ácidos nucleicos tem sido amplamente investigado para o desenvolvimento de terapias genéticas, tornando-se uma estratégia interessante para o tratamento de diversos tipos de doenças pulmonares, desde condições hereditárias até câncer. A imunoterapia pode ser feita pela modulação de células do sistema imune inato, como os macrófagos. A administração de mRNA requer um transportador apropriado capaz de evitar sua degradação, e garantir sua expressão sem gerar efeitos colaterais indesejados. Nesse contexto, as nanopartículas lipídicas (NPLs) são atualmente a melhor plataforma aprovada pela FDA para a administração *in vivo* de mRNA. No entanto, para maximizar ainda mais os benefícios das terapias baseadas em mRNA, é preferível direcioná-las diretamente ao local-alvo específico. Assim, o objetivo deste trabalho foi propor uma formulação de NPLs para a encapsulação de mRNA e investigar o uso dessas NPLs para a entrega pulmonar de medicamentos como ferramenta de imunoterapia baseada em macrófagos. Duas formulações à base de lecitina foram investigadas para a encapsulação do mRNA-Revilla em emulsão dupla água/óleo/água (A/O/A) usando duas abordagens diferentes de emulsificação ultrassônica. Ambas as formulações e abordagens de emulsificação permitiram a produção de NPLs submicrométricas estáveis e capazes de encapsular a molécula de mRNA. A presença de cera de abelha na formulação promoveu a inibição completa de células HEK 293T nas concentrações testadas. A formulação composta apenas por lecitina de soja e Crodamol mostrou-se o sistema de entrega de mRNA mais promissor, com uma eficiência de encapsulação de 31% e com baixos níveis de citotoxicidade em células Vero. No entanto, a expressão de mRNA em células HEK 293T não foi detectada usando o sistema de entrega a base de lecitina de soja e Crodamol. A aplicação de ultrassom com uma sonda invertida para promover a emulsificação não comprometeu a integridade do mRNA. Dessa forma, lecitina de soja e Crodamol têm o potencial de serem usados como formulação alternativa para a encapsulação e entrega de mRNA. Em seguida, oito formulações diferentes de NPLs contendo mRNA-FLuc foram preparadas pela técnica de autoagregação por adição gota-a-gota, e avaliadas para a entrega direcionada de mRNA a macrófagos. Todas as formulações apresentaram tamanho submicrométrico, estabilidade coloidal e níveis de encapsulamento acima de 80%. A mistura lipídica provou ser um aspecto crucial na entrega e expressão do mRNA, impactando o nível de bioluminescência *in vitro* das células RAW 264.7 e K7M2. A combinação de SM-102, DOPE e  $\beta$ -sitosterol teve o melhor nível geral de transfecção em células de macrófagos. Finalmente, formulações de NPLs de autoagregação contendo mRNA-FLuc foram preparadas pelo método de microfluídica, o que impactou significativamente o tamanho das NPLs, atingindo um nível de encapsulamento de 90%. A entrega pulmonar *in vivo* da formulação composta por DLin-MC3-DMA/DSPC/colesterol/DMG-PEG carregada com mRNA-FLuc foi investigada em camundongos Balb/c, com a expressão de mRNA-FLuc apresentando um pico de bioluminescência após 6 h. O rastreamento das NPLs usando o corante DiD revelou sua presença *in vivo* e *ex vivo* nos pulmões, assim como no fluido de lavagem broncoalveolar (BALF). No entanto, mesmo sendo observada *in vivo* e *ex vivo* nos pulmões, a expressão de mRNA-FLuc não foi detectada no BALF. Assim, as NPLs são uma estratégia promissora para promover a entrega direta de mRNA aos pulmões, e o ajuste da formulação lipídica pode ser usado para direcionar as NPLs aos macrófagos, para o desenvolvimento de uma ferramenta de imunoterapia.

**Palavras-chave:** lecitina de soja, nanopartículas lipídicas, mRNA, lipídios ionizáveis, macrófagos, pulmão

## RESUMO EXPANDIDO

### Introdução

Nas últimas décadas, medicamentos utilizando ácidos nucleicos (e.g. mRNA - *messenger ribonucleic acid*) como agentes terapêuticos têm sido amplamente investigados para o desenvolvimento de terapias gênicas e imunoterapias, como alternativa aos tratamentos convencionais que frequentemente enfrentam obstáculos biológicos como resistência e mutação patológica. O uso desta abordagem é interessante para o tratamento de diversos tipos de doenças pulmonares, desde condições hereditárias até câncer. O uso de imunoterapias contra o câncer pode se dar pela ativação e modulação das atividades de células do sistema imune como os macrófagos. O uso da administração local é um aspecto chave na utilização de terapias gênicas, e a administração pela via pulmonar se torna crucial quando o pulmão é o alvo da terapia uma vez que a utilização das rotas tradicionais limita o alcance dos medicamentos nesta região. A administração de mRNA extracelular como formulação terapêutica, por sua vez, exige um transportador apropriado capaz de evitar a degradação da molécula e garantir sua transfecção e expressão, sem gerar efeitos colaterais indesejados. Nesse contexto, as nanopartículas lipídicas (NPLs) são atualmente a plataforma mais avançada e aprovada pelo órgão de regulamentação de Administração de Alimentos e Medicamentos dos Estados Unidos (FDA - *Food and Drug Administration*) para a administração *in vivo* de mRNA. Diferentes métodos podem ser empregados na produção de NPLs carregadas com mRNA, e a transição de métodos de preparo em batelada para métodos de manufatura contínua vêm sendo amplamente explorada no desenvolvimento de novas formulações.

### Objetivos

O objetivo do presente trabalho é propor uma nova formulação lipídica para produção de carreadores nanoestruturados para entrega de mRNA, bem como investigar a administração pulmonar de nanopartículas lipídicas carregadas com mRNA e sua entrega em macrófagos visando o desenvolvimento de uma ferramenta imuno terapêutica.

### Metodologia

Inicialmente duas formulações a base de lecitina de soja foram propostas para realizar a encapsulação de Renilla-Luc-mRNA em NPLs utilizando a combinação do método dupla emulsão água/óleo/água (A/O/A) e de uma abordagem para protonação da lecitina de soja em meio ácido. As formulações foram compostas por: I – cera de abelha, lecitina, Crodamol (mistura de triglicerídeos de cadeia média do ácido cáprico e caprílico) e Tween 80; e II – lecitina, Crodamol e Tween 80. As NPLs contendo Renilla-Luc-mRNA foram caracterizadas em relação a sua morfologia, eficiência de encapsulação, citotoxicidade e expressão de Renilla-Luc-mRNA *in vitro* em células Vero e HEK 293T, respectivamente. Posteriormente, investigou-se o efeito da composição lipídica das NPLs na entrega direcionada e expressão de proteínas em macrófagos. Seis lipídios, sendo dois lipídios ionizáveis, dois fosfolipídios auxiliares e dois lipídios esteróis foram utilizados para preparação de oito formulações de NPLs carregadas com FLuc-mRNA pelo método de autoagregação por adição gota-a-gota. As formulações foram caracterizadas em relação a sua morfologia, eficiência de encapsulação e testadas *in vitro* para expressão de proteínas mediante a entrega de FLuc-mRNA utilizando NPLs em células RAW 264.7 e K7M2. Finalmente investigou-se a capacidade de uma formulação a base de lipídio ionizável de promover a entrega de FLuc-mRNA no pulmão de camundongos balb/c após administração intratraqueal das NPLs. As formulações foram preparadas utilizando uma combinação de DLin-MC3-DMA (heptatriaconta-6,9,28,31-tetraen-19-yl-4-(dimethylamino)butanoate), DSPC (1,2-distearoyl-sn-glycero-3-phosphocholine),

Colesterol e DMG-PEG (1,2-dimyristoyl-rac-glycero-3-methoxypolyethylene glycol-2000) na proporção molar de 50:10:38,5:1,5 em um sistema de microfluídica para encapsulação de FLuc-mRNA com e sem a adição do corante lipofílico DiD'. As NPLs foram caracterizadas em relação a sua morfologia, eficiência de encapsulação e testadas *in vivo* para quantificação do perfil de bioluminescência. Ainda, realizou-se a avaliação *in vivo*, *ex vivo* e no líquido de lavagem bronco alveolar (BALF) da biodistribuição das NPLs e da expressão de FLuc-mRNA.

## Resultados e Discussão

Inicialmente, Renilla-Luc-mRNA foi encapsulado em NPLs preparadas usando a abordagem de emulsão dupla A/O/A associada à dispersão por fusão. As NPLs feitas de cera de abelha, lecitina de soja e Crodamol apresentaram um diâmetro médio de 255 e 283 nm, dependendo do pH da fase aquosa interna, índice de polidispersão (PDI) relativamente estreito e estabilidade coloidal proporcionada pelo potencial zeta abaixo de -30 mV. Esta abordagem foi capaz de encapsular o Renilla-Luc-mRNA na NPLs, porém a análise de eletroforese em gel indicou sinais de degradação, possivelmente causada pelo cisalhamento ultrassônico, uma vez que o procedimento foi realizado usando uma sonda de imersão onde há o contato direto entre sonda e emulsão. Finalmente, a exposição das células HEK 293T a esta formulação mostrou ser citotóxica, promovendo a inibição total das células em todas as concentrações testadas (3,15, 6,3 e 9,45  $\mu\text{g}/\mu\text{L}$ ). Em seguida, o Renilla-Luc-mRNA foi encapsulado em NPLs preparadas usando a abordagem de emulsão dupla A/O/A, porém utilizando uma matriz lipídica composta apenas por lecitina de soja e Crodamol, e empregando uma aparato de sonda ultrassônica invertida para promover a emulsificação e evitar o contato direto entre a sonda e a emulsão. Essas NPLs apresentaram um diâmetro médio menor em comparação com a formulação anterior, de 166 nm, PDI relativamente estreito (0,228) e estabilidade coloidal proporcionada pelo potencial zeta abaixo de -30 mV. Ainda, esta formulação atingiu uma eficiência de encapsulação de 31,6%, e a cadeia de mRNA não foi significativamente afetada pelo após ser exposta as condições de emulsificação por ultrassom, provavelmente em função da utilização da sonda ultrassônica invertida que permite realizar a emulsificação em condições mais brandas de temperatura e sem contato direto entre sonda e emulsão, se tornando menos agressivo para o mRNA. A análise de microscopia eletrônica de transmissão confirmou o tamanho submicrométrico das NPLs e permitiu a visualização de estruturas no interior das NPLs que podem ser associadas ao Renilla-Luc-mRNA encapsulado. A remoção da cera de abelha da formulação teve impacto sobre a tolerabilidade *in vitro* da formulação em células Vero, apresentando níveis de inibição de 17%, 30,1% e 36,4% nas concentrações de 0,49, 2,48 e 4,97  $\mu\text{g}/\mu\text{L}$ , respectivamente. Porém nenhuma expressão de proteína foi detectada em células HEK 293T, o que poderia estar relacionado à baixa concentração de mRNA encapsulado e à capacidade da lecitina de soja e do Crodamol de promover adequadamente o escape endossomal do mRNA. Mudando o foco da encapsulação de mRNA utilizando formulação e método alternativos, seis lipídios, sendo dois lipídios ionizáveis, dois fosfolipídios auxiliares e dois lipídios esteróis, foram testados *in vitro* para a entrega direcionada de NPLs para macrófagos. Estas NPLs contendo FLuc-mRNA foram preparadas usando o método de autoagregação por adição gota-a-gota e apresentaram um tamanho médio submicrométrico em torno de 130 nm, distribuição de tamanho estreita e eficiência de encapsulamento acima de 80%. Após 24 h, seis das oito formulações apresentaram um nível de transfecção mais alto em células RAW 264.7 comparado as células K7M2, e duas não tiveram nenhum sinal de transfecção em nenhuma das células. As formulações de NPLs contendo SM-102 como lipídio ionizável apresentaram um nível mais alto de expressão de proteína, e o uso de  $\beta$ -sitosterol aprimorou seu desempenho em comparação com o colesterol. A combinação de SM-102, DOPE  $\beta$ -sitosterol teve o melhor nível geral de expressão de proteína em células RAW 264.7. O maior nível de ramificação do lipídio SM-102, a geometria molecular cônica do DOPE e a incorporação de  $\beta$ -sitosterol à casca das



NPLs mostraram ter um efeito positivo sobre a capacidade das NPLs de promover a expressão de FLuc-mRNA. No entanto, o efeito da adição de DOPE em função da mistura de lipídios à formulação de NPLs precisa ser investigado mais a fundo. Finalmente, a administração pulmonar *in vivo* das NPLs foi investigada utilizando a formulação de autoagregação DLin-MC3-DMA/DSPC/Colesterol/DMG-PEG contendo FLuc-mRNA e preparada usando o sistema microfluídico. A utilização deste método impactou positivamente as características das NPLs, reduzindo significativamente o tamanho médio para 71 nm, mantendo a distribuição de tamanho estreita e elevando o nível de encapsulação para 90%. As NPLs entregaram com sucesso o mRNA nos pulmões dos camundongos, e o perfil de expressão de proteína revelou um pico de bioluminescência após 6 h de administração. Por último, o corante DiD' foi adicionado ao sistema, e a biodistribuição das NPLs e a expressão de FLuc-mRNA após administração intratraqueal foram monitoradas. O rastreamento *in vivo* e *ex vivo* do sinal de DiD' revelou a presença das NPLs nos pulmões e no BALF dos animais. O FLuc-mRNA promoveu um aumento no sinal basal de bioluminescência *in vivo* e *ex vivo*, mas não foi detectada expressão de FLuc-mRNA no BALF.

### **Considerações Finais**

A estratégia sugerida para a encapsulação de mRNA empregando uma combinação do método de dupla emulsão A/O/A com a protonação da lecitina de soja, se mostrou capaz de promover a encapsulação do mRNA em NPLs submicrométricas estáveis. Todavia, o uso de cera de abelha, lecitina de soja e Crodamol como matriz para encapsulação de mRNA usando uma sonda ultrassônica de imersão para promover a emulsificação não é apropriado para a aplicação pretendida, por não ser capaz de evitar a degradação do ácido nucleico. No entanto, o uso de Crodamol e lecitina de soja como matriz para encapsulação de mRNA usando a técnica de emulsão dupla A/O/A com um aparato de sonda ultrassônica invertida e condições brandas de temperatura, afetou positivamente as NPLs carregadas com Renilla-Luc-mRNA, se apresentando como uma estratégia viável encapsulação e entrega de ácidos nucleicos. Entretanto, trabalhos futuros são necessários para aumentar o teor de mRNA encapsulado e promover a expressão de mRNA *in vitro*. Em relação à entrega direcionada para macrófagos, a mistura de lipídios utilizada para a produção de NPLs se mostrou um fator determinante para a geração de bioluminescência mediante a entrega de FLuc-mRNA em NPLs, impactando o nível de expressão de proteína em função da célula alvo. A utilização de um lipídio ionizável com alto grau de ramificação na cadeia, associado a um fosfolipídio com estrutura molecular cônica, e um esteroide mais lipofílico se mostrou a combinação mais promissora para promover entrega direcionada de NPLs em macrófagos. Por fim, as NPLs representam uma estratégia com potencial interessante para a entrega direta de mRNA aos pulmões, com grande potencial para serem utilizados como medicamentos anticancerígenos, no entanto estudos adicionais se fazem necessários para investigar e identificar precisamente o local de entrega das NPLs e da expressão de FLuc-mRNA após administração intratraqueal. Por fim, o ajuste da formulação lipídica pode ser usado para direcionar a entrega das NPLs para células e tecidos alvo, podendo explorar a vasta população de macrófagos no microambiente tumoral como ferramenta de imunoterapia.

**Palavras-chave:** lecitina de soja, nanopartículas lipídicas, mRNA, lipídios ionizáveis, macrófagos, pulmão

## ABSTRACT

Over the past few decades, nucleic acid-based therapeutic agents have been vastly investigated for gene therapy, becoming an interesting strategy for the treatment of several types of lung diseases, from hereditary conditions to cancer. Immunotherapies can be used to modulate innate immune cells, such as macrophages. The administration of extracellular mRNA demands an appropriate carrier capable of avoiding its degradation and securing the mRNA transfection and expression, without generating undesirable side effects. In this context lipid nanoparticles (LNPs) are currently the best FDA-approved platform for *in vivo* mRNA administration. Nevertheless, to further maximize the benefits of mRNA-based genomic medicines, they must be preferably delivered to the specific target site. Thus, the aim of the present work was to propose a bio-based LNPs formulation for mRNA encapsulation and investigate the use of these LNPs for pulmonary drug delivery as macrophage-based immunotherapy tool. Two lecithin-based formulations were investigated for water/oil/water (W/O/W) double emulsion encapsulation of Revilla-mRNA using two different approaches of ultrasonic emulsification. Both formulations and emulsification approaches allowed the production of submicrometric, and stable LNP structures, which successfully encapsulated the mRNA molecule. The presence of beeswax in the formulation promoted the complete inhibition of HEK 293T cells at the tested concentrations making unfeasible its use for the intended application. The formulation composed only of soy lecithin and Crodamol proved to be the most promising mRNA delivery system, with an encapsulation efficiency of 31% and low levels of cytotoxicity in Vero cells. However, mRNA expression in HEK 293T cells was not detected using the soy lecithin and Crodamol delivery system. The application of ultrasound using an invert probe to promote the emulsification did not compromise the mRNA integrity. In this way, soy lecithin and Crodamol have the potential to be used as alternative formulation for mRNA encapsulation and delivery. Next, eight different self-assembly LNP formulations containing FLuc-mRNA were prepared by the dropwise addition technique and screened for macrophages mRNA targeting delivery. All the formulations presented submicrometric size, stability, and encapsulation level above 80%. The lipid mixture proved to be a key aspect of the mRNA delivery and expression, impacting the *in vitro* bioluminescence level of RAW 264.7 and K7M2 cells, with the combination of SM-102, DOPE  $\beta$ -sitosterol having the best overall transfection level in macrophages cells. Finally, self-assembly LNP formulations containing FLuc-mRNA were prepared by the microfluidics method, which significantly impacted the LNPs size and reached an encapsulation level of 90%, and also proved to be the most reproducible one. The *in vivo* lung delivery of the self-assembly formulation DLin-MC3-DMA/DSPC/Cholesterol/DMG-PEG LNPs loaded with FLuc-mRNA was investigated on balb/c mice, with the FLuc-mRNA expression presenting a bioluminescence pic at 6 h. The LNPs tracking using DiD' dye revealed its *in vivo* and *ex vivo* presence in the lungs, as well as in the bronchoalveolar lavage fluid (BALF). However, even being *in vivo* and *ex vivo* identified in lungs, the FLuc-mRNA expression was not detected in the BALF. Thus, LNPs are a promising strategy to promote the direct delivery of mRNA to the lungs, and the adjustment of the lipid formulation can be used as an advantage to target LNPs to macrophages to be used as an immunotherapy tool.

**Keywords:** soy lecithin, lipid nanoparticles, mRNA, ionizable lipids, macrophages, lung

## FIGURES LIST

Figure 1 – Structural types of lipid-based nanoparticles: (I) Solid lipid nanoparticles and (II) Nanostructured lipid carrier. The types of NLC are: a) imperfect crystal, b) amorphous and c) multiple type. ....	23
Figure 2 – Generic structure of current used nanoparticles for RNA encapsulation using ionizable lipids...	32
Figure 3 – Soy lecithin (L- $\alpha$ -Phosphatidylcholine) structure.....	34
Figure 4 – Schematical representation of the inverted ultrasound probe apparatus used to prepare the C-mRNA-LNPs .....	44
Figure 5 – Schematical representation of a 96 well plate configuration used for encapsulation efficiency quantification by RiboGreen assay .....	52
Figure 6 – Schematical representation of the characterization performed with B-mRNA-LNPs and C-mRNA-LNPs .....	56
Figure 7 – TEM analyzes of C-mRNA-LNPs.....	58
Figure 8 – Agarose gel electrophoresis from Renilla-Luc-mRNA extracted from LNPs (A), extracted from the supernatant (B), and control (C).....	59
Figure 9 – Cellular viability of HEK 293T after 24h treatment with different concentrations of C-mRNA-LNPs .....	61
Figure 10 – Renilla-Luc activity on HEK 293T cells after 24h treatment with five C-mRNA-LNPs concentrations (■) and Lipofectamine 2000 (■)#.....	62
Figure 11 – Bioluminescence signal on RAW 264.7 (■) and K7M2 (■) cells (n=3) after 24h treatment with 100 $\mu$ g of Fluc-mRNA loaded in different LNPs formulations .....	65
Figure 12 – Chemical structures of cholesterol (A) and $\beta$ -sitosterol (B).....	67
Figure 13 – Chemical structures and geometrical arrangement of DSPC and DOPE.....	68
Figure 14 – Proposed mechanism for mRNA-LNP endosomal escape .....	69
Figure 15 – <i>In vivo</i> bioluminescence signal profile obtained from FLuc mRNA (2 $\mu$ g) expression on balb/c (n=4) after F05 pulmonary administration.....	72
Figure 16 – <i>In vivo</i> bioluminescence signal after pulmonary administration of 1 $\mu$ g FLuc-mRNA on balb/c (n=3) mice. F05 (■) and DiD'-F05 (●).....	73
Figure 17 – <i>In vivo</i> fluorescent signal after pulmonary administration of DiD'-F05 on balb/c mice.....	74
Figure 18 – <i>Ex vivo</i> bioluminescence signal after pulmonary administration of 1 $\mu$ g FLuc-mRNA on balb/c (n=3) mice. F05 (■) and DiD'-F05 (●).....	75
Figure 19 – <i>Ex vivo</i> fluorescent signal after pulmonary administration of DiD'-F05 on balb/c mice (n=3)..	75
Figure 20 – BALF bioluminescence signal after pulmonary administration of 1 $\mu$ g FLuc-mRNA on balb/c (n=3) mice. F05 (■) and DiD'-F05 (●).....	76
Figure 21 – BALF fluorescent signal after pulmonary administration of DiD'-F05 on balb/c mice (n=3) ...	77
Figure A1 – Schematical representation of how to use the Amicon® ultra centrifugal filter for LNP recovery .....	92
Figure A2 – K7M2 + NIH-3T3 Spheroids after three (A) and six days (B).....	96
Figure A3 – K7M2+RAW 264.7+NIH-3T3 spheroids using 168:32:20 (A - B), 100:100:20 (C - D) and 32:168:20 (E - F) initial cells ratio; After 3 (A,C and E) and 6 days (B, D and F).....	97
Figure A4 – K7M2+RAW 264.7+NIH-3T3 spheroids using 168:32:50 (A - B), 100:100:50 (C - D) and 32:168:50 (E - F) initial cells ratio; After 3 (A,C and E) and 6 days (B, D and F).....	99
Figure A5 – K7M2+RAW 264.7+NIH-3T3 spheroids using 110:55:55 (A - B), 92:45:83 (C - D) and 74:36:110 (E - F) initial cells ratio; After 3 (A,C and E) and 6 days (B, D and F).....	100

## TABLE LIST

Table 1 – Nano drug delivery systems: potential advantages and drawbacks .....	21
Table 2 – Major applications areas for lipid nanoparticles .....	24
Table 3 – Ionizable lipids used for nanoparticles production .....	32
Table 4 – Lipid composition of LNPs prepared by dropwise addition .....	48
Table 5 – Details of formulation and operational conditions for LNPs preparation by microfluidics.....	50
Table 6 – RNA standard curve preparation for encapsulation efficiency quantification by RiboGreen assay .....	52
Table 7 – Intensity mean diameter of nanoparticles (Dp), polydispersity index (PDI), and Zeta potential ( $\xi$ ) of B-mRNA-LNP and C-mRNA-LNP.....	57
Table 8 – HEK cellular viability after 24h treatment with B-mRNA-LNPs.....	60
Table 9 – C-mRNA-LNPs and Renilla-Luc-mRNA concentrations used in the <i>in vitro</i> luciferase expression assay.....	62
Table 10 – LNPs Intensity mean diameter of nanoparticles (Dp), polydispersity index (PDI), Zeta potential ( $\xi$ ), and Encapsulation Efficiency (EE%) achieved with different lipid formulation (n=2) .....	64
Table 11 – Intensity mean diameter of nanoparticles (Dp), polydispersity index (PDI), Zeta potential ( $\xi$ ), and Encapsulation Efficiency (EE%) of F05 achieved with different manufacture methods (n=4).....	71
Table 12 – Intensity mean diameter of nanoparticles (Dp), polydispersity index (PDI), Zeta potential ( $\xi$ ), and Encapsulation Efficiency (EE%) of F05 and DiD'-F05 .....	73
Table A1– Lipids stock solutions used in the Dropwise Addition method.....	92
Table A2 – Intensity mean diameter of nanoparticles (Dp), polydispersity index (PDI), Zeta potential ( $\xi$ ), and Encapsulation Efficiency (EE%) of DLin-MC3-DMA/DSPC/Cholesterol/DMG-PEG LNPs prepared by microfluidics .....	93
Table A3 – Spheroids composition and percentage of NIH-3T3 cells over the total amount of K7M2 or K7M2+RAW 264.7 .....	95
Table A4 – K7M2+RAW 264.7 spheroids average Feret's diameter for each cell ratio using 10% of NIH-3T3 after 3 and 6 days.....	97
Table A5 – K7M2+RAW 264.7 spheroids average Feret's diameter for each cell ratio using 25% of NIH-3T3 after 3 and 6 days.....	98
Table A6 – K7M2+RAW 264.7 spheroids average Feret's diameter using 2:1 cell ratio and 33.3%, 60.6% and 100% of NIH-3T3 after 3 and 6 days.....	99

## ABBREVIATIONS AND ACRONYMS LIST

A/O/A	Dupla Emulsão Água/Óleo/Água
BALF	Bronchoalveolar Lavage Fluid
B-mRNA-LNPs	Beeswax, Soy lecithin, and Crodamol Lipid Nanoparticles Loaded with mRNA
C-mRNA-LNPs	Crodamol and Soy lecithin Lipid Nanoparticles Loaded with mRNA
CSF1R	Colony-Stimulating Factor 1 Receptor
DiD	1,1'-dioctadecyl-3,3,3',3'-tetramethylindodicarbocyanine, 4-chlorobenzenesulfonate salt
DLin-MC3-DMA	Heptatriaconta-6,9,28,31-tetraen-19-yl-4-(dimethylamino)butanoate
DMG-PEG	1,2-dimyristoyl-rac-glycero-3-methoxypolyethylene glycol-2000
DOPE	1,2-dioleoyl-sn-glycero-3-phosphoethanolamine
Dp	Diameter of Nanoparticles
DSPC	1,2-distearoyl-sn-glycero-3-phosphocholine
EE%	Encapsulation Efficiency
FDA	U.S. Food and Drug Administration
FFR	Flow Phase Ratio
HEK 293T	Human Embryonic Kidney Cells
IRF5	Interferon Regulatory Factor 5
K7M2	Murine Osteosarcoma Lung Metastasis Cells
LNPs	Lipid Nanoparticles
M0	Resting State Macrophages
M1	Pro-Inflammatory Macrophages
M2	Anti-inflammatory Macrophages
mRNA	Messenger Ribonucleic Acid
N/P	Lipid Amine Nitrogen/Nucleic Acid Phosphate
NIH-3T3	Mouse Embryonic Fibroblast Cells
NLCs	Nanostructured Lipid Carriers
NPLs	Nanopartículas Lipídicas
P.A.	Pulmonary Administration
PBAE	Poly( $\beta$ -amino ester)
PDI	Polydispersity Index
PEI	Polyethylenimine
pGFP	Green Fluorescent Protein-Encoding Plasmid
PLGA	Poly(lactic acid-co-glycolic acid)

PLGA-PEG	Poly(lactic acid-co-glycolic acid)-poly(ethylene glycol)
PLX3397	Pexidartinib
RAW 264.7	Murine Macrophage Cells
SLNs	Solid Lipid Nanoparticles
SM-102	Heptadecan-9-yl 8-((2-hydroxyethyl) (6-oxo-6-(undecyloxy) hexyl) amino
Vero	Monkey Kidney Epithelial Cells
W/O/W	Water/Oil/Water Double Emulsion

## SUMMARY

<b>CHAPTER I</b> .....	18
<b>1 INTRODUCTION</b> .....	18
1.1 AIMS.....	21
<b>1.1.1 General Aim</b> .....	221
<b>1.1.2 Specific Aims</b> .....	221
<b>CHAPTER II</b> .....	23
<b>2 LITERATURE REVIEW</b> .....	23
2.1 NANOTECHNOLOGY FOR DRUG DELIVERY.....	23
2.2 LIPID NANOPARTICLES.....	26
2.3 NANOCARRIERS FOR mRNA DELIVERY.....	29
<b>2.3.1 Lipid-based carriers for mRNA delivery</b> .....	31
2.3.1.1 <i>Ionizable Lipids Based Nanoparticles (ILN) for mRNA delivery</i> .....	32
<b>2.3.2 Currently used lipid carriers for mRNA delivery</b> .....	35
<b>2.3.3 Beeswax, Crodamol and Lecithin as potential mRNA delivery systems</b> .....	37
2.4 LNPs PRODUCTION METHODS FOR NUCLEIC ACID ENCAPSULATION.....	39
<b>2.4.1 Double emulsion</b> .....	39
<b>2.4.2 Batch (Dropwise Addition) and Continuous (Microfluidization) Self-Assembly</b> .....	40
2.5 MACROPHAGE-BASED IMMUNOTHERAPY.....	41
2.6 OSTEOSARCOMA LUNG METASTASIS.....	43
2.7 LNPs PULMONARY LUNG DELIVERY.....	44
<b>CHAPTER III</b> .....	46
<b>3 MATERIAL AND METHODS</b> .....	46
3.1 mRNA LOADED IN LECITHIN BASED LIPID NANOPARTICLES.....	46
<b>3.1.1 Material</b> .....	46
<b>3.1.2 Methods</b> .....	46
3.1.2.1 <i>mRNA Encapsulation in Beeswax, Crodamol and Lecithin LNPs (B-mRNA-LNPs)</i> .....	46
3.1.2.2 <i>mRNA Encapsulation in Crodamol and Lecithin LNPs (C-mRNA-LNPs)</i> .....	47
3.1.2.3 <i>Encapsulation Efficiency (EE%)</i> .....	48
3.1.2.4 <i>Morphology and Surface Characterization</i> .....	48
3.1.2.5 <i>Agarose Gel Electrophoresis</i> .....	49
3.1.2.6 <i>Cell Culture</i> .....	49
3.1.2.7 <i>In vitro Cell Viability</i> .....	50
3.1.2.8 <i>In Vitro Luciferase Expression Promoted by mRNA-LNP Delivery</i> .....	50
3.2 MRNA LOADED IN IONIZABLE LIPID NANOPARTICLES.....	51

<b>3.2.1</b>	<b>Material</b> .....	51
<b>3.2.2</b>	<b>Methods</b> .....	52
3.2.2.1	<i>mRNA Encapsulation in LNP by Dropwise addition</i> .....	52
3.2.2.2	<i>Purification and Concentration of mRNA Loaded LNP Prepared by Dropwise Addition</i> .....	53
3.2.2.3	<i>mRNA Encapsulation in LNP by Microfluidics</i> .....	53
3.2.2.4	<i>Purification and Concentration of mRNA Loaded LNP Prepared by Microfluidics</i> .....	55
3.2.2.5	<i>Morphology and Surface Characterization</i> .....	55
3.2.2.6	<i>Encapsulation Efficiency (EE%)</i> .....	55
3.2.2.7	<i>Cell Culture</i> .....	57
3.2.2.8	<i>In Vitro Luciferase Expression promoted by mRNA-LNP Delivery</i> .....	57
3.2.2.9	<i>Co-Culture of Spheroids Using K7M2, RAW 264.7 and NIH-3T3 Cells</i> .....	58
3.2.2.10	<i>In Vivo Luciferase Expression Profile promoted by mRNA-LNP Delivery</i> .....	58
3.2.2.11	<i>Luciferase Expression In Vivo, Ex Vivo, and in BALF's Macrophages promoted by mRNA-LNP Delivery</i> .....	58
3.2.2.12	<i>Luciferase Expression and DiD'-LNPs Tracking In Vivo, Ex Vivo, and in BALF's Macrophages promoted by mRNA-LNP Delivery</i> .....	59
3.2.2.13	<i>Statistical Analyses</i> .....	59
	<b>CHAPTER IV</b> .....	60
<b>4</b>	<b>RESULTS AND DISCUSSION</b> .....	60
4.1	LECITHIN BASED LIPID NANOPARTICLES PREPARED BY W/O/W DOUBLE EMUSION.....	60
4.1.1	<b>Nanoparticle characterization</b> .....	60
4.1.2	<b>Agarose Gel Electrophoresis</b> .....	62
4.1.3	<b>Cell Viability</b> .....	64
4.1.4	<b><i>In Vitro</i> Luciferase Expression</b> .....	65
4.2	IONIZBLE LNPs PREPARED BY DROPWISE ADDITION.....	67
4.2.1	<b>Nanoparticle characterization</b> .....	67
4.2.2	<b><i>In Vitro</i> Formulation Screening on RAW 264.7 and K7M2 cells</b> .....	69
4.3	IONIZBLE LNPs PREPARED BY MICROFLUIDIC.....	74
4.3.1	<b>Nanoparticle characterization</b> .....	74
4.3.2	<b>In Vivo Lung Fluc Expression Profile</b> .....	75
4.3.3	<b>Lung Fluc Expression and mRNA-LNP's Uptake Quantification <i>In Vivo, Ex Vivo, and in BALF</i></b> .....	76
	<b>CHAPTER V</b> .....	82
<b>5</b>	<b>CONCLUSION</b> .....	82
<b>6</b>	<b>FURTHER SUGGESTIONS</b> .....	83
<b>7</b>	<b>REFERENCES</b> .....	84



**APPENDIX.....96**

## CHAPTER I

### 1 INTRODUCTION

Currently, most therapeutic drugs available in the market are either classified as small molecules or protein-based platforms. Although they have been proven effective in many scenarios, they still have limitations (YAMADA, 2021). For instance, small molecules have poor bioavailability due to their inability to efficiently penetrate cellular membranes, while protein-based therapeutics are susceptible to degradation and can trigger an immune response (LANGER; TIRRELL, 2004). Moreover, traditional drugs may become ineffective when drug-resistant pathogens and disease mutations emerge (ROMANELLI et al., 2015).

Over the past few decades, nucleic acid-based therapeutic agents have been vastly investigated for gene therapy as a potential strategy to overcome the limits of traditional small molecule and protein-based drugs and address diseases at the gene level (KACZMAREK; KOWALSKI; ANDERSON, 2017). Messenger Ribonucleic Acid (mRNA) is a single-stranded molecule that carries genetic code from DNA to ribosomes, which plays a key role in protein synthesis, such as antibodies (WANG et al., 2021).

The use of mRNA as a therapeutic approach has gained significant attention in recent years, particularly in the development of vaccines against infectious diseases (e.g. COVID-19 and Influenza) (PILKINGTON et al., 2021) and cancer immunotherapy (PARDI et al., 2018). Currently, mRNA vaccines already have demonstrated their effectiveness against infectious diseases and two formulations have been successfully approved by the FDA for COVID-19 immunization (SADARANGANI; MARCHANT; KOLLMANN, 2021). However, there are no mRNA cancer immunotherapies approved by the FDA yet. Despite this, there have been significant advancements in the field, with one immunotherapy formulation receiving the *breakthrough therapy* designation from the regulatory institution for the use of mRNA as an adjuvant in melanoma treatment. This status intends to accelerate the development and review of drugs for serious or life-threatening conditions, and phase 3 clinical trials are scheduled to start in 2023 (INC, 2023). The use of mRNA as an anti-cancer immunotherapy strategy offers several advantages over conventional gene therapy such as flexibility, versatility, lower oncogenic potential, well-tolerated (VISHWESHWARAIAH; DOKHOLYAN, 2022), transient protein expression, and a lack of genomic integration (ORLANDINI VON NIESSEN et al., 2019).

The main concept of cancer immunotherapies is to activate the host anti-tumor immunity modulating cellular immune responses, especially the T-cell-mediated tumor-specific antigen and tumor-associated antigens-directed cytotoxicity, which can cause tumor depletion (LAHIRI et al., 2023; Miao; ZHANG; HUANG, 2021). The immune-modulatory formulations also can act against cancer cells by raising the level of tumor-specific antibodies, natural killer cells (e.g. dendritic cells and macrophage), and cytokines in the blood plasma (LAHIRI et al., 2023). Macrophages that are located in cancer sites are designated as tumor-associated macrophages, which can have proinflammatory or anti-inflammatory activity and are one of the main elements of the tumor microenvironment forming approximately 50% of the tumor mass (CENDROWICZ et al., 2021; MERZ et al., 2021; VINOGRADOV; WARREN; WEI, 2014). The tumor microenvironment provides the essential conditions for cancer start and progression, with considerable diversity in the inflammatory elements of the tumor microenvironment from different cancer tissues. Nevertheless, the infiltration of myelomonocytic cells, particularly monocytes, macrophages, and dendritic cells, is a regular aspect of cancers, regardless of their origin and localization (MANTOVANI et al., 2022). Thus, considering its abundance and versatility in the tumor microenvironment, the idea of exploring macrophages as a cancer immunotherapy instrument could be an advantageous approach.

Although the use of mRNA is a promising approach for multiple types of therapies, such as vaccines and cancer immunotherapy (VISHWESHWARAI AH; DOKHOLYAN, 2022), the stability and translation of mRNA are crucial aspects of the success of nucleic acid-based therapies. In this context, delivery carriers are frequently used to prevent the eventual digestion of mRNA by ribonucleases and promote an efficient target cell uptake (ZHANG et al., 2019a).

Different types of nanostructured drug-delivery systems have been explored as potential platforms for mRNA delivery, including lipids, lipid-like compounds, polymers, and protein derivatives (HOU et al., 2021). Regarding these nanostructured drug-delivery systems, the knowledge and understanding of lipid nanoparticles (LNPs) are relatively mature when it comes to the development of nucleic acid delivery systems (ISLAM et al., 2015). The most used lipid-based nanoparticles include liposomes, solid lipid nanoparticles (SLNs), nanostructured lipid carriers (NLCs), and micro/nanoemulsions. Liposomes are vesicular structures consisting of phospholipid bilayers that can encapsulate both hydrophilic and lipophilic drugs, being a versatile drug delivery option. SLNs have a solid lipid core that provides improved drug stability and controlled release characteristics to the system. NLCs are composed of a mixture of solid and liquid lipids, offering enhanced drug-loading capacity and

improved stability compared to conventional lipid nanoparticles. Micro- and nanoemulsions are, respectively, thermodynamically stable and colloiddally stable systems composed of oil, water, surfactants, and co-surfactants for microemulsions or co-stabilizer for nanoemulsions, which enable the encapsulation of both hydrophobic and hydrophilic drugs (MAHMOUD et al., 2022). Until this date, there are only two formulations approved by the U.S. Food and Drug Administration (FDA) for mRNA use: the Pfizer-BioNTech COVID-19 and the Moderna COVID-19 vaccines (SADARANGANI; MARCHANT; KOLLMANN, 2021). Both use lipid nanoparticles as carriers. However, there is ongoing research to develop new lipid-based formulations that can further improve the delivery and efficacy of mRNA therapeutics in various diseases (DUAN et al., 2022; XU et al., 2022).

Looking for the encapsulation of nucleic acids, the application of cationic lipids or cationic polymeric matrices is preferable due to the presence of tertiary or quaternary amines in the lipid molecule that exerts an electrostatic interaction with negatively charged mRNA, which favors the internalization of the nucleic acid (BLAKNEY et al., 2019; WADHWA et al., 2020). However, the clinical application of cationic lipid-based drug delivery systems has faced complications due to pro-inflammatory reactions, undesirable side effects, and loss of *in vivo* performance (ISLAM et al., 2015; WADHWA et al., 2020).

The development of a bio-based lipids NLC formulation using beeswax, a mixture of triglycerides from caprylic and caproic acids (commercially available as Miglyol 812 and Crodamol) and soy-lecithin is a promising alternative to produce mRNA delivery systems using FDA approved materials. Beeswax has desirable biocompatibility, biodegradability, and stability at various pH levels (KYOBULA et al., 2017; MILANOVIC et al., 2017). In addition, triglycerides, such as Crodamol, have already been shown to enhance the permeation of drugs through biological barriers, including the nasal mucosa (CLEMENTINO et al., 2021). The beeswax and Crodamol matrix for NLC formulation can be powered by soy lecithin, a natural surfactant that possesses a quaternary amine in its structure. At the right conditions, this quaternary amine can be protonated to interact with the phosphate group of RNA molecules, similar to what ionizable lipids do (PÉREZ et al., 2012).

To further maximize the benefits of mRNA-based genomic medicines, they must be preferably delivered to specific cells, tissues, or organs (XU; XIA, 2023). While surface tissues such as muscles and eyes can be easily reached through local administration, deep organs (e.g., lungs) within the body require systemic administration for optimal delivery. However, traditional lipid nanoparticles that are commonly used for systemic administration tend to accumulate in the liver after intravenous injection, and the pulmonary biodistribution of

systemic administration drugs is poor with only 2-4% of the administered dose reaching the lungs, which in turns demand a total dose over than the therapeutic dose resulting in off-target side effects (SULAIMAN, 2021). In this way, the targeted mRNA delivery beyond the liver is difficult and requires new engineered drug delivery systems to properly deliver the nucleic acid cargo to the lungs (WEI; TAO; CHENG, 2022).

The increasing knowledge about mRNA versatility, safety, efficacy, and industrial production has paved the way for exploring mRNA as a tool against several malignant and infectious diseases (HEINE; JURANEK; BROSSART, 2021; WANG et al., 2021). With the appropriate combination of mRNA and pharmaceutical formulation design, the alternatives to the application of mRNA can be considered endless (VAN HOECKE et al., 2021).

## 1.1 AIMS

### 1.1.1 General Aim

Based on the challenges related to the development of mRNA delivery systems and its pulmonary administration, the main objective of the present work is to propose a bio-based lipids formulation of lipid carriers for mRNA delivery and investigate the pulmonary administration of mRNA lipid nanoparticles and its delivery on macrophages for immunotherapy.

### 1.1.2 Specific Aims

To address the current challenges associated with mRNA delivery systems the aim of the work is to propose a novel lipid formulation made of beeswax, Crodamol, which is a mixture of triglycerides from caprylic and caproic acids and soy-lecithin for the encapsulation of mRNA, using the water/oil/water double emulsion approach. In addition, to enhance the *in vitro* transfection capacity of mRNA-loaded nanoparticles in macrophages, as well as their *in vivo* performance for pulmonary administration the goal is to investigate the FDA-approved ionizable lipid-based formulation and assess the potential enhancements.

- Promote the encapsulation of mRNA by the water/oil/water double emulsion process;
- Develop a formulation for mRNA encapsulation and delivery;

- Produce stable LNPs made of bio-based lipids with narrow PDI by water/oil/water double emulsion technique without employing organic solvents;
- Investigate the feasibility of using lecithin as a substitute for ionizable lipids;
- Evaluate the effect of different lipid compositions as LNPs matrix for mRNA encapsulation and delivery;
- Investigate the influence of the encapsulation process conditions on RNA stability and structural integrity;
- Investigate the *in vitro* cytotoxicity dose-dependence effect caused by LNPs made of bio-based lipids;
- Evaluate the RNA-loaded LNPs dose dependence effect over the response produced by the mRNA;
- Test the *in vitro* selectivity of the developed lipid nanoparticle formulations over different types of cells that compose the osteosarcoma lung metastasis tumor microenvironment (e.g., cancer cells, macrophages);
- Adjust the LNP formulation to enhance the mRNA transfection in macrophages as well as the *in vitro* protein expression
- Verify the *in vivo* mRNA-mediated protein expression on balb/c mice lungs after LNP delivery.

## CHAPTER II

### 2 LITERATURE REVIEW

#### 2.1 NANOTECHNOLOGY FOR DRUG DELIVERY

Research involving bio-systems at the nanoscale considers nanotechnology as the key to overcoming medical and biological barriers (POPE-HARMAN et al., 2007). Nanotechnology is science, engineering, and technology conducted at the atomic and molecular level, where unique phenomena enable novel applications in various fields, from chemistry, physics, and biology, to medicine, engineering, and electronics (NATIONAL NANOTECHNOLOGY INITIATIVE, 2020). Nanomaterials have powered the incorporation of nanotechnology into various fields of biomedicine science, such as drug delivery, gene therapy, biomarkers, tissue engineering, diagnoses, and images (YETISGIN et al., 2020).

Traditional medicine and pharmaceutical sciences have been facing several challenges with the constant upsurge of new diseases and the remarkable capability of quick mutation of usual infections (ROMANELLI et al., 2015). The most common problems associated with established drugs include limitations linked to insufficient drug concentration, fast opsonization, heterogeneous biodistribution, poor drug solubility, and unpredictable bioavailability. Also, sick cells can become resistant to a single drug or a class of drugs with an analogous action mechanism by changing the drug's cellular target or by increasing the repair rate of drug-induced damage (GOTTESMAN; FOJO; BATES, 2002; LAGE, 2008). However, the application of new drug delivery systems capable of delivering drugs to specific body locations could be an alternative to solve these critical concerns.

Nanomaterials possess interesting properties for an efficient delivery vehicle (THILAKARATHNA; VASANTHA RUPASINGHE, 2013). Nanoparticles are one of the nanomaterials that have raised major interest related to physiological applications due to their capacity to remain in the bloodstream for a long period associated with the ability to release lower and sustained drug doses, causing fewer adverse effects. Particles and molecules with a size ranging from 1 to 10  $\mu\text{m}$  have their uptake and biodistribution compromised. Nanosized drugs and delivery systems can penetrate the tissue and cellular systems, helping the appropriate uptake by cells and optimizing the drug delivery once that the drug can directly interact with the infected body region (MIRZA; SIDDIQUI, 2014; PATRA et al., 2018).

The term nanoparticle is a general classification used for both nanospheres and nanocapsules. Nanospheres are solid particles in which drugs are dissolved, entrapped, encapsulated, chemically bound, or adsorbed at their surface. Nanocapsules are core-shell systems in which the drug is confined in a cavity surrounded by a membrane or coating that can also contain the drug (SCHAFFAZICK et al. 2003; REIS et al. 2006; LETCHFORD and BURT 2007; ROMIO et al. 2009).

The targeting mechanism is a crucial aspect of nanomaterials and nanoformulations used as a drug delivery system, and it can be classified as passive or active. In the former, the drug carrier travels through the bloodstream, being preferably directed to the target site by the influence of characteristics like pH, temperature, molecular size, and shape. In an opposite way, the latter approach uses an identifying molecule (e.g., antibodies and peptides) anchored to the carrier structure, which guides the drug delivery system to the specific location where the receptor is expressed or overexpressed (KUMARI; KUMAR; YADAV, 2012; PATRA et al., 2018).

Nanotechnology proposes several benefits for the treatment of human chronic and emergent diseases by site-specific and targeted-oriented delivery of therapeutic agents. However, the inadequate knowledge of the risks and drawbacks of the pretend nanomaterials is one of the biggest concerns of the researchers to guarantee the safer implementation of these classes of medicines with the promised therapeutic efficiency (OBEID et al., 2017). Currently, the development of materials and structures in the field of drug delivery systems has been receiving a significant investment in terms of money, time, effort, and technology. The growth projection for the pharmaceutical drug delivery market is to reach USD 2,015.3 billion by 2025 from USD 1,430.5 billion with a compound annual growth rate of 7.1% (SUR et al., 2019).

Table 1 presents an overview of the advantages and drawbacks of the principal nano-drug delivery systems.



Table 1 – Nano drug delivery systems: potential advantages and drawbacks

Nano Drug Delivery System	Advantages	Drawbacks	References
Nanoemulsion	Different types of use (e.g., cream, liquid, and spray), ability to carry either hydrophilic or hydrophobic drugs	High concentration of surfactant required, presence of potentially cytotoxic surfactants	(AZMI et al., 2019; SALEEM et al., 2019)
Liposomes	Stability, ability to carry either hydrophilic or hydrophobic drugs, biocompatibility, biodegradability, possibility of surface functionalization, low toxicity, low immunogenicity, structural flexibility, and easiness of handling	High production cost, the likelihood of undesirable drug release in the bloodstream during the transportation step	(BARBA et al., 2019; TRUCILLO; CAMPARDELLI ; SALEEM et al., 2019; REVERCHON, 2020)
Nanocochleates	More stable than traditional liposomes, ability to carry either hydrophilic or hydrophobic drugs, non-immunogenic, non-inflammatory, and non-toxic	High production cost, storage condition, and the possibility of aggregation during long storage times	(NAYEK; VENKATACHALA; CHOUDHURY, 2019)
Lipid Nanoparticles	Drug protection against aggressive environmental conditions, easily scale-up, biodegradability, biocompatibility, capacity to simultaneously carry lipophilic and hydrophilic molecules, no organic solvent required	Low drug-loading, there is a chance of drug expulsion during the storage, and initial burst release can occur	(GHASEMIYE; MOHAMMADI-SAMANI, 2018; MAZUR et al., 2018)
Polymeric Nanoparticles	Stability, biocompatibility, low toxicity, cost-effectiveness, possible surface functionalization, ability to carry either hydrophilic or hydrophobic drugs	Difficult to scale up, possible toxicity	(SALEEM et al., 2019; SINGH et al., 2017; SUR et al., 2019)
Peptide Nanoparticles	High drug loading efficiency, biodegradability, biocompatibility, high potential for functionalization, increased cellular uptake	High cost, possible immunogenicity, difficulty in achieving an adequate release pattern, fast degradation	(HONG et al., 2020; JAIN, 2020; KIANFAR, 2021)
Metallic Nanoparticles	Stability, uniform structure, therapeutic effect, drug targeting	Potentially cytotoxic	(DOS SANTOS et al., 2020; SALEEM et al., 2019)
Dendrimers	Solubility enhancers of highly lipophilic drugs, presence of functionable groups for targeted delivery, biocompatibility, capacity to carry lipophilic and hydrophilic molecules,	Potentially cytotoxicity for cationic dendrimers, high cost, rapid clearance, poor drug release profile	(KAHRAMAN; GÜNGÖR; ÖZSOY, 2017; RATEMI et al., 2016; VEGA-VÁSQUEZ; MOSIER; IRUDAYARAJ, 2020)

Source: The Author (2023)

## 2.2 LIPID NANOPARTICLES

Lipid-based drug delivery systems are an accepted and commercially viable approach to produce dose-controlling pharmaceutical therapies (SUGAWARA; NIKAIDO, 2014). In the early 1990s, investigations about SLNs emerged as an alternative for the traditional polymeric nanoparticles. The attention of the research groups was attracted by the biocompatibility of the nanoparticle matrix-like vesicular lipid carriers (e.g., liposomes and emulsions) combined with the presence of a solid core like polymeric nanoparticles (PALIWAL et al., 2020). This combination opened the possibility for the development of complex systems with stability and capable of performing controlled release to and be modified for specific and active delivery (DOKTOROVOVA; SOUTO; SILVA, 2014; GORDILLO-GALEANO; MORA-HUERTAS, 2018).

SLNs are particles made from solid lipids with a submicrometric mean diameter (EKAMBARAM; SATHALI; PRIYANKA, 2012). By definition, SLNs are submicron colloidal carriers composed of highly purified triacylglycerols, complex triacylglycerol mixtures or waxes, stabilized by a surfactant(s) or polymer(s), and their mixtures are capable of being dispersed in pure water or in an aqueous surfactant solution (MÜLLER et al., 2000; SARMENTO et al., 2007).

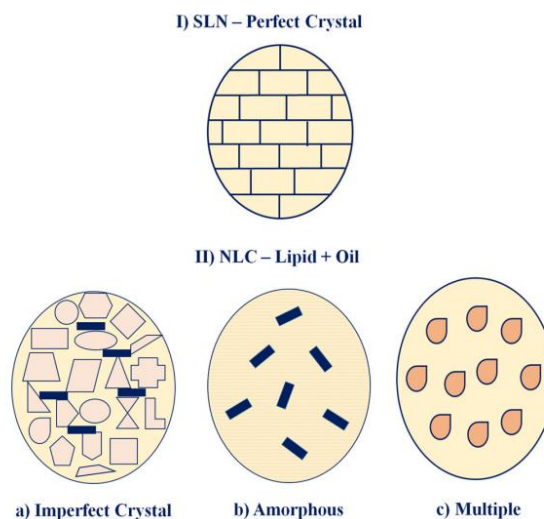
After more than two decades of investigations, SLNs proved to have the advantages of other carrier systems as polymeric macro/nanoparticles (e.g., physical stability, protection of incorporated drugs from degradation, controlled release) while at the same time overcoming eventual associated problems due to the biodegradable and physiological nature of the matrix material (GANESAN; NARAYANASAMY, 2017; MÜLLER et al., 2000; WISSING; KAYSER; MÜLLER, 2004). However, one of the characteristics of interest of SLNs, the solid core, showed itself as an undesirable and significant problem. The solidification and subsequent crystallization of the lipid matrix promotes the expulsion of the encapsulated drug from the structure. This phenomenon occurs due to the progressive crystallization of the dispersed lipid molecules in more stable forms, which leads to an increase in the particle size and in the drug load capacity (GORDILLO-GALEANO; MORA-HUERTAS, 2018).

In order to solve the drug expulsion problem, a new alternative was the design based on the binary mixture of short-chain solid lipids with long-chain liquid lipids (oil) or a mixture of liquid lipids, called NLC in which the solid-state of the system is preserved at room and body temperature (GORDILLO-GALEANO; MORA-HUERTAS, 2018). NLCs are classified as second-generation of lipid drug delivery systems having an average size of 10 - 500 nm and a

hybrid structure usually composed of a solid-lipid:liquid-lipid ratio ranging from 70:30 to 99.9:0.1 and stabilized by a surfactant solution of 0.5 - 5%. Nevertheless, in the case of multiple emulsion systems, a higher proportion of oil can be used (GORDILLO-GALEANO; MORA-HUERTAS, 2018; KHOSA; REDDI; SAHA, 2018). The presence of the long-chain lipids increases the drug loading capacity of NLC compared to SLNs due to the creation of imperfections in the nanoparticle structure. Also, NCLs are more stable than SLNs once that NLC disables the recrystallization of the solid lipid keeping the particle size consistent during storage (GORDILLO-GALEANO; MORA-HUERTAS, 2018; HAIDER et al., 2020).

The different possibilities of proportion in the mixture between oil and solid lipid associated with several methods of production divide the NLCs into three categories: imperfect, amorphous, and multiple oil-in-solid fat-in-water (O/F/W). In the first one, the mixing of lipids with different molecular sizes creates imperfections in the crystal order, forming an imperfect crystalline structure in the nanoparticle. In the second type, the correct type of lipids associated with the adequate preparation procedure can completely prevent the crystallization process while keeping the matrix solid, creating an amorphous nanoparticle capable of preventing drug expulsion. In the last category, the multiple O/F/W is formed by various nanosized oil cavities distributed in the solid matrix, which increases drug loading by the higher solubility of the drug in the oil cavities and extends the release time once there exists a solid barrier covering the oil droplets (KHOSA; REDDI; SAHA, 2018; SUGAWARA; NIKAIDO, 2014). Figure 1 presents the structure of the different types of lipid-based nanoparticles.

Figure 1 – Structural types of lipid-based nanoparticles: (I) Solid lipid nanoparticles and (II) Nanostructured lipid carriers. The types of NLC are: a) imperfect crystal, b) amorphous, and c) multiple type.



Source:(SUGAWARA; NIKAIDO, 2014)

NLCs have a series of characteristics that make them attractive to be applied as a drug delivery system. These include low toxicity, high drug entrapment efficiency, the feasibility of carrying lipophilic and hydrophilic drugs, the capacity to project stealth carriers capable of avoiding the reticuloendothelial system, modulate the drug release profile, and increase the bioavailability and permeability of the therapeutic agent through the cell membrane (DATE et al., 2018; GORDILLO-GALEANO; MORA-HUERTAS, 2018). Recent reports in different areas have demonstrated the versatility of different types of lipid nanoparticles (LNPs). Table 2 summarizes some of the recent reviews published about the applications of LNPs.

Table 2 – Major application areas for lipid nanoparticles

Application Area	Article Title	Reference
Gene therapy	Nanostructured lipid carriers for MicroRNA delivery in tumor gene therapy	(WANG et al., 2018)
Brain targeted delivery	Critical review of lipid-based nanoparticles as carriers of neuroprotective drugs and extracts	(FERNANDES et al., 2021)
Cancer immunotherapy	mRNA vaccine for cancer immunotherapy	(MIAO; ZHANG; HUANG, 2021)
Improvement of the efficiency of anticancer drugs	Nanostructured lipid carriers for delivery of chemotherapeutics: A review	(HAIDER et al., 2020)
Topical, dermal, and transdermal delivery	SLN and NLC for topical, dermal, and transdermal drug delivery	(SOUTO et al., 2020)
Cutaneous delivery	Formulations based on solid lipid nanoparticles (SLN) and nanostructured lipid carriers (NLC) for cutaneous use: a review	(GARCÊS et al., 2018)
Nasal drug delivery	Targeting pulmonary tuberculosis using nanocarrier-based dry powder inhalation: status and futuristic need	(PATIL et al., 2019)
Oral drug delivery	Solid lipid nanoparticles and nanostructured lipid carriers in oral cancer drug delivery	(NASIRIZADEH; MALAEKEH-NIKOUEI, 2020)
Ocular drug delivery	Application of lipid nanoparticles to ocular drug delivery	(BATTAGLIA et al., 2016)

Source: The Author (2023)

Different types of lipid matrices are reported in the literature (GORDILLO-GALEANO; MORA-Hadas, 2018). Beeswax is a non-paraffin organic composite mostly composed of a combination of fatty acid esters, long-chain alcohols, paraffinic hydrocarbons, and free fatty acids (AMIN et al., 2017). Beeswax has large applications in food and pharmaceutical areas, being a potential material for nanoparticle formulation due to its stability at various pH and moisture levels, hydrophobicity (MILANOVIC et al., 2017), and to the antibacterial proprieties against *Staphylococcus aureus*, *Salmonella enterica*, *Candida albicans*, and *Aspergillus Niger* (FRATINI et al., 2016).

The production of lipid-based nanoparticles has already been studied in our research group. Becker Peres (2016) investigated the application of the melt dispersion and double emulsion technique to simultaneously encapsulate both hydrophilic and lipophilic compounds in stearic acid nanoparticles. Meneses (2016) explored the SLNs to encapsulate clove oil by O/W emulsion, also applying stearic acid as a lipid matrix. Cordeiro (2021) produced beeswax-based lipid nanoparticles to perform the simultaneous encapsulation of hydrophilic and lipophilic compounds.

### 2.3 NANOCARRIERS FOR mRNA DELIVERY

Messenger RNA (mRNA) is a crucial intermediary molecule in the life cycle responsible for carrying the genetic information transcribed from DNA, which in turn is translated into proteins. mRNA possesses singular characteristics that allow it to have a wide and flexible therapeutic application: mRNA is neither a permanent genetic blueprint nor a final functional product (HAJJ; WHITEHEAD, 2017).

The best strategy to control disease and infections involves the manipulation of protein expression, so in theory, a therapeutic system based on mRNA has the capacity to treat or prevent multiple diseases and infections (HAJJ; WHITEHEAD, 2017). However, mRNA possesses a size of  $10^5$  -  $10^6$  Da, which is about three to four times larger than molecules capable of easily diffusing into cells. In addition, mRNA has a strong negative charge that leads to a natural repulsive electrostatic answer with the anionic cell membrane. Nevertheless, naked mRNA is highly vulnerable to degradation by 5' exonucleases, 3' exonucleases, and endonuclease (WADHWA et al., 2020). The instability of naked mRNA (not encapsulated) at physiologic conditions leads to a poor cellular uptake rate, less than 1 in 10,000, and an intracellular half-life of only 7 hours (HAJJ; WHITEHEAD, 2017).

The development of mRNA-based therapies has had a slow growth over the years because of its remarkable instability *in vivo*. However, the interest in incorporating mRNA into a delivery system has increased due to its potential for higher transfection efficiencies in non-dividing cells (no nuclear entry required), rapid expression, predictable kinetics, as well as higher safety profile compared to plasmid DNA (ERASMUS et al., 2018; PHUA; NAIR; LEONG, 2014). Currently, the incorporation of mRNA into protein/peptide carriers, lipid-based nanoparticles, and polymeric nanoparticles has been investigated as a promising approach to transport the molecule across the lipid bilayer of the cell membrane (COFFEY; GAIHA; TRAVERSO, 2021; ZENG et al., 2020).

Peptide-based nanoparticles are a class of devices that make part of the so-called cell-penetrating peptides. This type of delivery device uses short-chain peptides (less than 30 amino acids) to perform the encapsulation by the formation of non-covalent complexes between the peptides and the RNA. The peptides used for this approach are capable of promoting the movement of the encapsulated biomolecule across the cell membrane into the cytoplasm and, thereby, simplifying the interaction with the target (CROMBEZ et al., 2008; KONATE et al., 2019). However, some of the drawbacks faced by peptide-based nanoparticles include short circulation half-lives, poor chemical and physical stability in serum, and low DNA binding ability (KANG; MENG; LIU, 2019).

Polymers are the most used materials for the production of biomedical nanoparticles due to their biocompatibility, ease of functionalization, and modulable drug release profile (COFFEY; GAIHA; TRAVERSO, 2021). For the preparation of vectors for RNA delivery, cationic polymers are preferable due to their electrostatic interactions with negatively charged nucleic acids and cell membranes (ISLAM et al., 2015). Polyethylenimine (PEI) and its derivatives are one of the most used cationic polymers because of the high density of positive charges associated with the amino groups. Even with an already recognized capacity for *in vivo* delivery of mRNA, vectors based on cationic polymers still have problems associated with acute cytotoxicity (COFFEY; GAIHA; TRAVERSO, 2021; LEHNER et al., 2017). Thus, to overcome this complication, biodegradable polymers such as poly(lactide) (PLA) and poly(lactic-co-glycolic acid) (PLGA) have been considered to promote gene delivery systems. However, the anionic profile of these polymers harms the interaction with the mRNA molecule, and the encapsulation efficiency decreases to low levels (COFFEY; GAIHA; TRAVERSO, 2021; WADHWA et al., 2020). Pollard et al. (2013) conducted an assay comparing the immune activity of naked mRNA, mRNA associated with cationic lipid carriers, and cationic polymeric carriers. The authors reported that the only system capable of promoting antigen-encoding mRNA was the one composed of mRNA complex to cationic lipids.

Even with a considerable number of approaches to facilitate the entrance of nucleic acid into cells, the field has recently converged to ionizable lipid-based systems as the preferred choice for RNA delivery systems (GEBRE et al., 2021).

### 2.3.1 Lipid-based carriers for mRNA delivery

The first clinical trial with a lipid-based mRNA delivery system as potential vaccines for H10 and H7 influenza hemagglutinin were performed in 2015 and 2016, respectively. The phase I clinical data showed promising therapeutic effects with a similar side event profile to other approved vaccines. Until 2020, and the COVID-19 pandemic, 8 other mRNA vaccines have passed the clinical test phase, and of these, 5 have applied lipid-based delivery carriers. The pandemic state caused by COVID-19 had an impact on vaccines development, and since then, 8 new programs have emerged to implement mRNA vaccines (GEBRE et al., 2021).

The knowledge about the development of lipid nanoparticles for nucleic acid delivery is relatively mature regarding other types of nanocarriers. Among these systems, liposomes are the most traditional system. Liposomes are simple vesicular systems composed of a phospholipid arranged in a double lipid layer encapsulating an aqueous phase with multiple favorable characteristics, including excellent biocompatibility, biodegradability, low toxicity, low immunogenicity, capacity to deliver a large piece of nucleic acids, structural flexibility, and easiness of handling (BARBA et al., 2019; TRUCILLO; CAMPARDELLI; REVERCHON, 2020). Neutral liposomes are well known for their low toxicity and good stability under physiological conditions. However, compared to cationic liposomes, they exhibit a reduced ability to interact with nucleic acids (ANGELINI et al., 2013). Thus, cationic liposomes are preferable for RNA delivery because the positively charged lipids interact with the negatively charged phosphate groups of nucleic acid, forming a compacted structure, which can also electrostatically interact with the negatively charged cell membrane, helping their cellular uptake (BARBA et al., 2019).

When the focus is the construction of the nanocarrier, the application of cationic lipid matrixes is strongly preferable due to the presence of tertiary or quaternary amines in the lipid molecule that exert an electrostatic interaction with negatively charged mRNA, which favors the internalization of the nucleic acid (ISLAM et al., 2015; WADHWA et al., 2020). However, the clinical application of cationic lipid-based drug delivery systems has faced complications due to their pro-inflammatory reactions and undesirable side effects (WADHWA et al., 2020). In addition, another crucial aspect of positively charged lipids is that the desirable effects observed *in vitro* showed itself less promising *in vivo* because of the capacity of the mononuclear phagocyte system to quickly remove cationic lipid carriers (ISLAM et al., 2015).

Qi, Zhao, and Zhuang (2011) compared the *in vitro* and *in vivo* performance of neutral and cationic liposomes loaded with Doxorubicin. The authors reported that the *in vitro* uptake

of cationic nanoparticles by rat aortic endothelial cells was faster than that of the neutral ones. Although, when the *in vivo* antitumor effect over hepatocellular carcinoma-bearing mice was tested, the authors observed that the positively charged nanoparticles had their pharmacokinetics, biodistribution, and anticancer effect compromised in comparison to the neutral ones. According to the authors, the liposomes with the highest positive charge presented a reduction in the circulation times and poor distribution in tumors, resulting in the worst *in vivo* anticancer efficiency among the tested formulations.

More recently, the substitution of cationic lipids by ionizable lipids has emerged as a new alternative for the development of lipid-based gene delivery systems. The use of this type of lipids in the composition of lipid nanoparticle formulations has been proposed to overcome the limitations pointed out for cationic lipids while keeping their desirable transfection properties (WADHWA et al., 2020).

#### *2.3.1.1 Ionizable Lipids Based Nanoparticles (ILN) for mRNA delivery*

The design of the modern nucleic acid delivery platforms is derived from the traditional liposomal systems, such as Doxil®, which is a liposomal formulation of Doxorubicin and is composed of 1,2-distearoyl-sn-glycero-3-phosphocholine (DSPC), cholesterol, and PEG-lipid at a 56:38:5 molar ratio. This formulation layout was optimized over the years looking for desirable properties such as high encapsulation efficiencies, low unfavorable interactions with serum proteins, longer circulation lifetime, enhanced drug accumulation at the target location, and fewer dose-limiting toxicities. However, to apply this type of system to nucleic acid delivery, an additional charge-related functionality was revealed to be necessary to complex the lipids with the highly negative charge density of nucleic acids and promote the active loading of this large molecule (HALD ALBERTSEN et al., 2022).

The use of permanently charged lipids, mainly as liposomal formulations in clinical trials has been unsuccessful due to obstacles related to its toxicity, short circulation half-life, and non-specific association with negatively charged cellular and extracellular components. Aiming to overcome the charge related limitations, new lipids were designed replacing the quaternary ammonium head of cationic lipids by a titratable moiety, creating the concept of ionizable lipids. From this modification, the resulting lipid is able to acquire an electrostatic charge according to its own pKa and the pH of the surrounding environment (SCHLICH et al., 2021).



The utilization of ionizable lipids in nanostructured delivery systems for nucleic acids holds significant interest related to the manipulation of the electrostatic state of this type of molecule. Initially, during nanoparticle production, these lipids become positively charged under acidic conditions, making them well-suited for complexation with mRNA, enhancing the encapsulation efficiency and mRNA delivery. However, after purification and post-production steps the lipids exhibit a neutral charge at physiological pH, thereby minimizing the eventual charge related cytotoxic issues associated with the delivery system. In addition, after administered and engaged in the intracellular endocytosis pathway, these lipids can be protonated again due to the endosome acidic pH, favoring mRNA endosomal escape and delivery in the cytosol (HAN et al., 2021; SUN; LU, 2023). One critical aspect related to the ionizable lipid addition to the formulation is the N/P ratio, which is the molar ratio of ionizable lipid nitrogen/nucleic acid phosphate and represents the charge balance between the tertiary amine headgroup of the ionizable lipid and the anionic phosphate group in the nucleic acid chain backbone. This property is the basis for the complexation of ionizable lipids with nucleic acids in the LNP formulations, which commonly have an N:P ratio around 6 (YANG et al., 2022).

As mentioned, the strategy of using ionizable lipids to form a complex lipid-based gene delivery system is derived from the traditional liposomal systems which also includes the use of three other components: a helper phospholipid, a sterol (e.g. cholesterol) and a PEGylated-lipid (DE GROOT et al., 2018; GASPAR; COELHO; SILVA, 2020; HALD ALBERTSEN et al., 2022).

The presence of the helper phospholipids in ILN formulations is crucial for their architecture and functionality. The most widespread are DSPC and 1,2-dioleoyl-sn-glycero-3-phosphoethanolamine (DOPE) (HALD ALBERTSEN et al., 2022). The choice of the helper phospholipid can have a significant impact on the characteristics of the ILN formulation and mRNA delivery properties based on the geometry of its chemical structure. Phospholipids with a small head group and unsaturated lipid chains, such as DOPE, present their kinked structure and are referred to as "cone shape" phospholipids (HALD ALBERTSEN et al., 2022; SUN; LU, 2023). Due to the cone shape, these lipids are known to favor membrane fusion and bilayer disruption processes, facilitating mRNA endosomal escape (IBBA et al., 2021). This property is particularly advantageous for promoting efficient intracellular delivery of mRNA. On the other hand, saturated lipids, like DSPC, possess a structure referred to as a "cylindrical shape" (HALD ALBERTSEN et al., 2022). The cylindrical shape of these lipids is associated with higher bilayer stability, which is crucial for *in vivo* administration of ILNs (SUN; LU, 2023).

The stability provided by cylindrical-shaped lipids like DSPC helps to prevent premature disintegration of the nanoparticles during systemic circulation, allowing them to reach the target cells and achieve their desired therapeutic effects.

Cholesterol plays a pivotal role in ILN formulations for mRNA delivery, offering various benefits and contributing to the system's overall success. Its rigid and hydrophobic nature allows it to insert into the inter-lipid space filling the gaps between phospholipids, which prevents net efflux or influx, contributing to vesicle stability and membrane integrity (IBBA et al., 2021; SUN; LU, 2023). Moreover, the increase in the membrane rigidity promoted by cholesterol reduces the drug leakage from the ILN core enhancing the encapsulation of nucleic acids. In addition to its stabilizing and encapsulating effects, cholesterol can improve intracellular ILN delivery and transfection efficiency both *in vitro* and *in vivo* (KIAIE et al., 2022). Cholesterol limits the interaction between ILN and blood proteins improving circulation half-lives, and possibly favors cellular transfection by promoting membrane fusion and translocation across the endosomal membrane aiding the mRNA release from ILN (BUSCHMANN et al., 2021; SUN; LU, 2023). Nevertheless, recent studies in the literature demonstrate that the type of sterol incorporated into the ILN formulation could positively impact the mRNA endosomal escape and protein expression (KIM et al., 2022; MEDJMEDJ et al., 2022).

Finally, the PEGylated lipid, is the lipid component with the smallest mole percentage in ILNs and affects multiple characteristics and properties of the carrier (IBBA et al., 2021). During ILN formation, PEG chains form a hydrophilic steric barrier on the ILN surface promoting the lipid's self-assembly around the mRNA cargo and as the PEG chain extends away from the surface of the emerging particle, the particle stability is increased by preventing its aggregation (HALD ALBERTSEN et al., 2022; IBBA et al., 2021). The size can be influenced by the PEG presence and is reported that increasing the molar ratio of the PEG-lipid tends to lead to the formation of smaller ILN, independent of other lipid components (KULKARNI et al., 2019). According to the literature, this could be explained by the PEG-lipid being located only at the ILN surface, hence raising the mol% of the PEGylated lipid leads to a higher surface area:volume ratio causing the decrease of particle size (HALD ALBERTSEN et al., 2022). The PEGylation is a widely used stealth strategy to prevent rapid clearance and increase the circulation time of carriers. The lipid tail structure in PEG-lipids also influences LNPs biological activity and enhances the nonspecific cellular uptake (KIAIE et al., 2022). Since the PEG-lipid is incorporated into the ILN membrane through the hydrophobic tail (the alkyl/acyl chains), PEG-lipids with longer tails are less likely to dissociate from the ILN (SUN; LU, 2023).

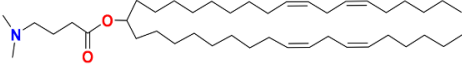
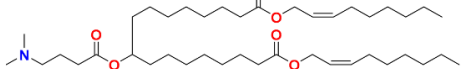
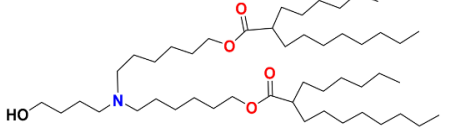
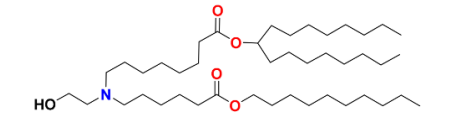
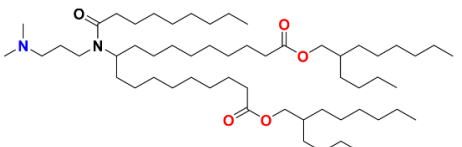
Generally, longer alkyl chains improve LNP stability in biological fluids, however, it is reported that there exists a correlation between desorption rate and lipid tail length both *in vitro* and *in vivo* (HALD ALBERTSEN et al., 2022). As showed by Wheeler et al. (1999), who encapsulated luciferase encoding plasmids in PEG-coated lipid nanoparticles and observed that the use of shorter acyl chain PEGs resulted in higher *in vitro* luciferase expression.

### 2.3.2 Currently used lipid carriers for mRNA delivery

In 2018, the FDA approved the RNA-based drug, and the prescription medicine Onpattro™ was approved for clinical application against hereditary transthyretin-mediated amyloidosis. This medicine formulation established an ionizable lipid-base delivery system capable of increasing 200 times the potency of the transported siRNA and reducing the effective dose in the same order while achieving durable suppression of the target gene in more than 80% (AKINC et al., 2019; BUSCHMANN et al., 2021). The Onpattro™ formulation presented the combination of DLin-MC3-DMA/DSPC/Cholesterol/PEG–lipid in the molar proportion of 50/10/38.5/1.5 (BARBA et al., 2019; BUSCHMANN et al., 2021; GEBRE et al., 2021).

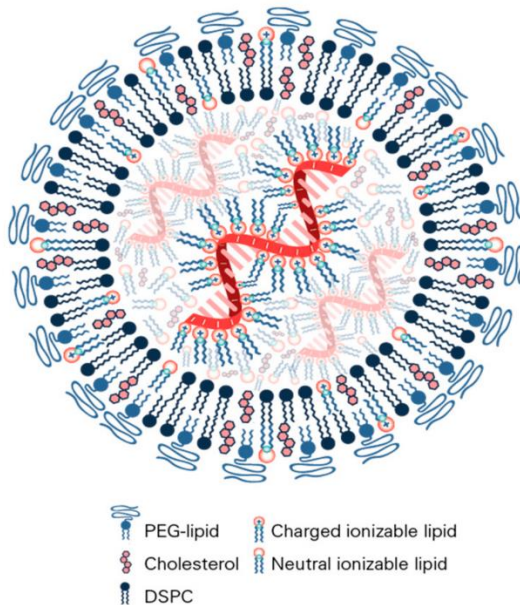
The Onpattro™ formulation was used as the basis for the subsequent development of several lipid-based carriers for nucleic acid delivery, including the programs that were established as emergency use for SARS-CoV-2 mRNA vaccines. However, MC3-based lipid structures present a worryingly slow degradability that is associated with multiple dosing could be the reason for a potential toxic effect. Thus, one of the biggest efforts during the COVID-19 global immunization program was to adapt the pharmaceutical formulations with a less aggressive ionizable lipid (BUSCHMANN et al., 2021). Table 3 presents the structures of MC3 and of other promising ionizable lipids, including the ones engineered by Moderna and Pfizer-BioNTech which already have been approved by FDA for general use. Figure 2 shows a generic structure of the current used ionizable lipids nanoparticles for mRNA encapsulation.

Table 3 – Ionizable lipids used for nanoparticles production

Company	Ionizable Lipid	
	Name	Structure
-	MC3	
BioNTech/Pfizer	Lipid 319	
BioNTech/Pfizer and CureVac	Acuitas ALC-0315	
Moderna	Lipid H, SM-102	
Imperial College	Acuitas A9	

Source: Adapted from (BUSCHMANN et al., 2021)

Figure 2 – Generic structure of current used nanoparticles for RNA encapsulation using ionizable lipids



Source: (BUSCHMANN et al., 2021)

Currently, the ionizable lipid is considered the crucial point for the system to perform as best as possible. Recently, researchers have centered efforts to identify or create biodegradable ionizable lipids once that these materials present some level of challenges regarding their biodegradability (BARBA et al., 2019; BUSCHMANN et al., 2021; GEBRE et al., 2021). The addition of

biodegradable lipids in lipid-based carriers for injectable vaccines leads to a reduction in the inflammatory answer in the application site, improving the tolerability of the formulation. The enhancement in the acceptability of the vaccine is associated with the quick metabolic breakdown and removal of the lipid from the injection site, which reduces the exposure of other tissues to the material (GEBRE et al., 2021). Preclinical and clinical studies for COVID-19 from BioNTech report the use of Lipid 319, that is a modified version of MC3, that replaces one of the two double bonds in each alkyl chain with a primary ester that can be easily degraded by esterases *in vivo* (BUSCHMANN et al., 2021). The final formulation of BioNTech/Pfizer uses Acuitas ALC-0315 ionizable lipid that has the ester groups for enhancing the degradability but also has structural modifications related to the branching level.

The number of branches also is a strategy in the development of alternative ionizable lipids. It is believed that the increase in the number of branches creates more cone-shaped lipid structures, which, after paired with the anionic phospholipids in the endosome, will have a greater membrane-disrupting capacity. In this way, the ionizable lipid based on MC3 developed by Moderna (Lipid H, SM-102) was added two ester groups to the structure to decrease the degradability problems but is focused on increasing the potency of the molecule, connecting a second saturated tail that branches after seven carbons into two saturated C8 tails (BUSCHMANN et al., 2021).

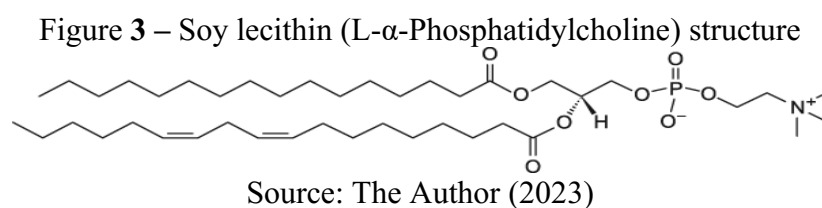
### **2.3.3 Beeswax, Crodamol and Lecithin as potential mRNA delivery systems**

Beeswax is obtained from the honeycombs of bees and is composed of esters of saturated fatty acids and long-chain alcohols (mainly hydrocarbons monoesters, diesters, triesters, free myristic acid, and a variable number of hydroxy acids and diols groups). The material is solid at room and body temperature and is water-insoluble. Beeswax is commonly used in the food industry, but the biodegradability and biocompatibility of beeswax associated with high availability and relatively low industrial cost have been attracting the interest of beeswax for new forms of use, such as the production of drug delivery systems (S, 2018; SOLEIMANIAN et al., 2018; SOUZA; DE FREITAS; MAIA CAMPOS, 2017; ZAMBRANO-ZARAGOZA et al., 2020). The use of natural fatty acids such as triglycerides from caprylic and caproic acids (commercially available as Miglyol 812 and Crodamol) in LNP formulations for drug delivery has several advantages. The application of a natural oil as a co-stabilizer maintains the biocompatible character of LNPs and increases the system stability, which is crucial for ensuring the efficacy of the drug-loaded in the nanoparticles during the shelf-life storage and during the *in vivo* transportation to the target site. Also, using this type of oil in drug delivery formulations has demonstrated to be effective to overcome bio barriers, and natural obstacles

related to oral drug absorption, such as acid and enzymatic degradation, pH variations, and mucosal irritation (LE BARS et al., 2015; MEHTA et al., 2023; ORTIZ et al., 2021).

In our research group, the combination of beeswax and Crodamol already proved to be a very promising lipid matrix to produce drug delivery systems, having a high level of stability, encapsulation efficiency, and cellular uptake associated with a non-cytotoxic profile. Cordeiro et al. (2021) used beeswax-based solid lipid nanoparticles for the generation of synergistic therapeutic effects between hydrophilic and lipophilic drugs against Melanoma. Mazur et al. (2018) incorporated Diethyldithiocarbamate in beeswax-based solid lipid nanoparticles for the development of an alternative treatment for Leishmaniasis.

Soy lecithin (L- $\alpha$ -Phosphatidylcholine) is a complex mixture containing ca. 65 – 75% phospholipids used as natural surfactant for several types of products in both food and non-food industries (SCHOLFIELD, 1981). One of the applications of lecithin is as an emulsifier, which allows lecithin to be used to produce drug delivery systems, such as liposomes. Structurally, lecithin possesses a head quaternary amine (Figure 3) (LIST, 2015).



For the development of RNA delivery systems, the quaternary's lecithin amine can be protonated under the right conditions to interact with the phosphate group of RNA molecules. Pérez et al. (2012) promoted the encapsulation of siRNA in lecithin-based nanoparticles and demonstrated that formulations prepared at pH 5.0 favored the encapsulation of siRNA when compared to the same process performed at pH 7.0. Also, the lecithin-based nanoparticles showed an efficient delivery of siRNA in MCF-7 human breast cancer cells.

The association of beeswax and soy lecithin in an RNA delivery system has the potential to apply the electrochemical principle used in ionizable lipid-based delivery systems, as well as overcoming the drawbacks associated with the low biodegradability and cytotoxic risks of the traditional ionizable lipids (Table 3).

## 2.4 LNPs PRODUCTION METHODS FOR NUCLEIC ACID ENCAPSULATION

Different types of approaches have been reported for nucleic acid encapsulation in LNP formulations, such as thin-film hydration, reverse-phase evaporation, passive encapsulation, dropwise addition, spontaneous vesicle formation, and microfluidization (HOU et al., 2021; LOPES et al., 2022; MACLACHLAN, 2007).

### 2.4.1 Double emulsion

The double emulsion technique allows the encapsulation of hydrophilic compounds. Also, the possibility of using different types of oils, lipids, waxes, and emulsifiers turned this approach highly versatile, increasing the possibilities for the elaboration of biocompatible, biodegradable, and surface modifiable particles. In addition, when combined with hot melt dispersion, the procedure can be performed without organic solvents and is considered simple with the use of convenient and low complexity instruments (CAMPANI; GIARRA; DE ROSA, 2018; CORDEIRO et al., 2021).

The production of LNPs by the double emulsion process can be conducted by single or two-step emulsification. In the first one, an emulsion with a nonionic emulsifier or a mixture of different emulsifiers is heated to cause phase inversion, which leads to the formation of a double emulsion. The second one can be structured in two ways: water/oil/water (W/O/W) and oil/water/oil emulsification. For the former method, initially, a water/oil emulsion is prepared in the presence of a low HLB surfactant and subsequently added to an aqueous phase containing a high HLB surfactant, which enables the formation of a second water/oil/water emulsion. Alternately, in the latter approach, an oil/water emulsion is primarily stabilized by a low HLB surfactant, which is then emulsified in an oil phase containing a high HLB surfactant, creating the oil/water/oil emulsion. This type of system has already shown great potential in areas such as medicine, pharmaceuticals, cosmetics, and the food industry, mainly for encapsulation and sustained release of substances, production of low-fat foods and surface coatings to maintain aroma and flavor integrity (CORDEIRO et al., 2021; LAMBA; SATHISH; SABIKHI, 2015).

The combination of the double emulsion method with the solvent evaporation approach already proved to be useful to incorporate RNA into polymeric and lipid-based nanoparticles (CUN et al., 2010; HU et al., 2014; LI et al., 2020).

Li et al., (2020) applied the double-emulsion solvent evaporation method to encapsulate a green fluorescent protein-encoding plasmid (pGFP) in poly(lactic acid-co-glycolic acid)-poly(ethylene glycol)(PLGA-PEG)/poly( $\beta$ -amino ester)(PBAE) nanoparticles. Previously, the

authors observed that using only PLGA-PEG, the internalization of RNA was strongly affected by their large size, polar profile, and electrostatic repulsion. In this recent work, the authors reported that the incorporation of cationic polymer (PBAE) in a weight ratio of 1:1.3 with PLGA-PEG led to an encapsulation efficiency of 97% and was capable of keeping the gene stability and sustained release for 8 days with a minimal toxicity effect over HEK 293 cells. The authors observed a decrease in the encapsulation efficiency with the decrease of the cationic polymer content in the formulation, reaching 18% at a weight ratio of 1:4. Also, the use of only PBAE to encapsulate the nucleic acid resulted in an intermediary encapsulation efficiency of 38%.

Wan, Griffel, and Xu (2017) used the double emulsion solvent evaporation approach to encapsulate siRNA into hybrid nanoparticles composed of PLGA-PEG and a cationic lipid. The authors reached an encapsulation efficiency of 95% using a weight ratio of 20:1 (cationic lipid:siRNA); however, both increase and decrease of weight ratio (10:1 and 30:1) kept the encapsulation efficiency at the same level of 87%. In addition, the author reported that gene encapsulation could maintain the release level for 10 days.

#### **2.4.2 Batch (Dropwise Addition) and Continuous (Microfluidization) Self-Assembly**

Recent advancements in LNP formulations for mRNA encapsulation incorporate ionizable lipids and amino phospholipids, facilitating spontaneous self-assembly into higher order aggregates around the nucleic acid cargo (GUEVARA; PERSANO; PERSANO, 2020; RIPOLL et al., 2022). When this strategy is used, both techniques dropwise addition and microfluidization apply the nanoprecipitation principle, which involves the rapid solvent migration from an organic dispersed phase (e.g., lipids in ethanol) into the continuous phase, resulting in nanoparticle precipitation when the organic solution is introduced to the non-solvent (e.g., water) (SALATIN et al., 2017). In the presence of ionizable lipids and amino phospholipids in the organic phase and nucleic acid in the non-solvent phase, the LNPs precipitation is triggered by the electrostatic interaction between the cationic amino groups in the lipids molecules and the negatively charged phosphate groups of the nucleic acid chain (GUEVARA; PERSANO; PERSANO, 2020).

Traditionally, nucleic acid loading in LNPs through dropwise addition occurs in batch conditions (beakers or vials) using syringes or pipettes to slowly introduce the organic phase (lipids in ethanol) into the non-solvent phase (RNA in water) with vigorous stirring (DONG et al., 2022; LIU et al., 2022). The use of conventional batch processes for preparing LNPs has potential challenges such as inconsistent outcomes and scalability issues (ALI et al., 2021). This variability



poses difficulties when transitioning from discovery to animal testing, clinical trials, and commercial production (MAEKI et al., 2022). Techniques like ultrasound, nanoprecipitation, and quick mixing have been employed in batch operations to formulate LNPs and polymer nanoparticles, but these methods typically yield larger particles (>150 nm), which are suboptimal for tissue penetration and prolonged circulation (SHEPHERD; ISSADORE; MITCHELL, 2021).

Conversely, microfluidics represents a continuous manufacturing strategy, demonstrating enhanced reproducibility and smaller particle sizes compared to dropwise addition (GIMONDI et al., 2023). Microfluidics technology has emerged as a transformative tool, leveraging fluid dynamics principles at the microscale to precisely control nanoparticle production (MAEKI et al., 2022). In a microfluidic device, two solutions, one containing organic precursor materials (e.g., lipids and polymers) and the other a continuous aqueous phase with hydrophilic molecules (e.g., mRNA), are individually loaded and manipulated through microchannels. This approach offers meticulous control over process parameters, including continuous flow rate, precise process time, and temperature. This approach has several advantages compared to batch production such as precise size controllability with high reproducibility, high-throughput screening, reduced use of expensive samples, wearable sensing, rapid optimization of LNP-production conditions, and ease of scaling up, which enable a faster transition from laboratory-scale use to practical applications (ALI et al., 2021; MAEKI et al., 2022; RIPOLL et al., 2022; SHEPHERD; ISSADORE; MITCHELL, 2021).

## 2.5 MACROPHAGE-BASED IMMUNOTHERAPY

Cancer immunotherapies primarily aim to stimulate the host's anti-tumor immunity by regulating cellular immunological responses, particularly T-cell-mediated cytotoxicity aimed against tumor-specific antigens and tumor-associated antigens, which can lead to tumor depletion. (LAHIRI et al., 2023; MIAO; ZHANG; HUANG, 2021). By increasing the concentration of tumor-specific antibodies, natural killer cells, dendritic cells, macrophages, and cytokines in the blood plasma, immune-modulatory formulations can combat cancer cells. (LAHIRI et al., 2023).

Macrophages are essential elements of the immune system, serving a vital function in preserving tissue equilibrium and protecting the organism from external threats. Through a process known as phagocytosis, these adaptable cells are able to take up and break down cellular debris, foreign substances, and microorganisms (HIRAYAMA; IIDA; NAKASE, 2018; WATANABE et al., 2019). Although their positive contribution for the maintenance of body healthy conditions, macrophages can also significantly contribute to the pathogenesis and progression of various

inflammatory diseases when they unusually infiltrate and accumulate in tissues (MONDADORI et al., 2023).

In the cancer context, tumor-associated macrophages, which comprise almost half of the tumor mass, are found in cancerous areas and are considered one of the primary components of the tumor microenvironment. (CENDROWICZ et al., 2021; VINOGRADOV; WARREN; WEI, 2014). In the complex landscape of the tumor microenvironment, macrophages play a pivotal role by existing in a dynamic spectrum of phenotypes, notably as M0, M1, and M2 macrophages. The M0 phenotype represents macrophages in their resting state, possessing the unique ability to undergo differentiation into either M1 or M2 phenotypes, influenced by an intricate interplay of growth factors, chemokines, and cytokines emanating from both tumor cells and various microenvironmental cells. M1 macrophages are associated with the secretion of pro-inflammatory cytokines, and exhibit distinct antitumor properties, making them crucial components of the immune response against cancer. These macrophages are characterized by their ability to engage in antigen presentation, initiating a robust immune response, and demonstrating potent cytotoxicity to target cancer cells. On the other hand, M2 macrophages are generally considered immunosuppressive and have been implicated in fostering a microenvironment conducive to tumor growth, by reducing the immune response and promoting tissue repair and angiogenesis. M2 macrophages secrete anti-inflammatory cytokines, contributing to an environment that may facilitate tumor progression and metastasis. Additionally, they are involved in extracellular matrix remodeling and support the evasion of immune surveillance by cancer cells (LIN; XU; LAN, 2019; PAN et al., 2020). Thus, understanding the intricate balance and plasticity between these macrophage phenotypes in the tumor microenvironment is one promising approach for developing cancer immunotherapies. The modulation of macrophage polarization holds promise in harnessing the immune system to combat cancer effectively, either by enhancing the M1 antitumor response or by reprogramming M2 macrophages towards an antitumor phenotype (BOUTILIER; ELSAWA, 2021).

The regulation of tumor-associated macrophage differentiation has emerged as a promising strategy in cancer immunotherapy, and one of the most well-successful approaches for this involves the inhibition of the colony-stimulating factor 1 receptor (CSF1R) (NOY; POLLARD, 2014). CSF1R is a cell surface receptor that needs to bind to its respective ligands to guarantee the survival, proliferation, and differentiation of macrophages (STANLEY; CHITU, 2014). The inhibition of this receptor leads to the macrophage's repolarization (NOY; POLLARD, 2014). The role of CSF1R over macrophage's differentiation within the tumor microenvironment is well-documented, and in 2019 FDA approved the first CSF1R inhibitor, Pexidartinib (PLX3397), to be used as immunotherapy in tenosynovial giant cell tumor (HOU et al., 2021).

The application of mRNA loading nanoparticles as a macrophage-based immunotherapy tool is a promising strategy in the development of new therapeutic formulations. Zhang et al. (2019b) used poly( $\beta$ -amino ester), polyglutamic acid, and Di-mannose as an organic matrix to produce nanoparticles loaded with mRNA encoded with Interferon Regulatory Factor 5 (IRF5) and IKK $\beta$ . Using an *in vivo* model of ovarian cancer, metastatic melanoma, and glioblastoma, the researchers reported that the co-expression of IRF5/IKK $\beta$  upon nanoparticles delivery substantially reduced tumor progression and, in some animals, even cleared the disease.

The manipulation of the lipid mixture, regarding the chemical nature of the lipids (TRAFTON, 2023) and its molar ratio (FEI et al., 2023) in the formulation can drive the LNPs preferably to macrophages. Also, the use of LNPs has been reported as a promising tool for mRNA targeted delivery to macrophages, being able to even change the level of protein expression in M1 and M2 type macrophages according to the composition of the lipid matrix (TULI, 2023). Thus, there are opportunities to be explored for the design of mRNA loading LNPs formulations which target macrophages for immunotherapy.

## 2.6 OSTEOSARCOMA LUNG METASTASES

Cancer stands as the leading global cause of mortality, with approximately 90% of cancer-related deaths attributed to metastases (Seyfried & Huysentruyt, 2013). Osteosarcoma, the most prevalent form of bone cancer and the third most common cancer in children and adolescents, predominantly originates in long bones such as the femur, tibia, and humerus, and less frequently in the pelvis, jaws, and head and neck (Misaghi et al., 2018). The primary treatment for Osteosarcoma involves neoadjuvant chemotherapy followed by surgical resection and adjuvant chemotherapy, resulting in a commendable five-year survival rate of around 70% (Misaghi et al., 2018). Chemotherapy is normally given in combination, using agents such as methotrexate, doxorubicin, and cisplatin (Huang et al., 2019).

The lungs represent the primary and preferred site of metastasis in Osteosarcoma, with 80-90% of all metastases, which also include other bones, nest in lungs, and the pulmonary disease is the leading cause of death in Osteosarcoma (Han et al., 2019; Lussier et al., 2015). At the time of diagnosis, most individuals with Osteosarcoma harbor undetectable pulmonary micrometastases, while nearly 20% display clinically detectable tumors. In cases of advanced-stage Osteosarcoma, the survival rate drops dramatically to less than 30%, primarily due to metastases (Kleinerman et al., 2018; Lindsey et al., 2017; Zhang et al., 2018). The recommended treatment for metastatic Osteosarcoma involves neoadjuvant chemotherapy, identical to that used in localized cases, followed

by surgical resection if tumors are resectable, and subsequent adjuvant chemotherapy (Han et al., 2019; Huang et al., 2019; Isakoff et al., 2015). However, the survival rates for patients with Osteosarcoma lung metastases remain distressingly low, likely attributed to challenges associated with systemic chemotherapy (Alhudaithi et al., 2020; Kager et al., 2003; Mialou et al., 2005; Shaikh et al., 2016). These challenges include poor lung biodistribution of drugs and the emergence of drug resistance, highlighting the need for innovative approaches in the treatment of Osteosarcoma lung metastases (Alhudaithi et al., 2020).

## 2.7 LNPs PULMONARY LUNG DELIVERY

Pulmonary gene therapy has become an interesting approach for the treatment of different types of lung diseases, from hereditary conditions to cancer (KIM et al., 2022). mRNA exhibits significant promise as a therapeutic agent for a range of diseases. Delivering it to the appropriate area of the body without promoting side effects has proven to be a challenge in its deployment thus far (TRAFTON, 2023).

To further maximize the benefits of mRNA-based genomic medicines, they must be preferably delivered to specific cells, tissues, or organs (XU; XIA, 2023). While surface tissues such as muscles and eyes can be easily reached through local administration, deep organs (e.g., lungs) within the body require systemic administration for optimal delivery. However, traditional lipid nanoparticles that are commonly used for systemic administration tend to accumulate in the liver after intravenous injection, making targeted mRNA delivery beyond the liver difficult (WEI; TAO; CHENG, 2022). Platforms focused on lung drug delivery are becoming more attractive for being considered a non-invasive approach that offers the possibility of access to the alveoli and lung parenchyma for treating multiple lung disorders (e.g., asthma, idiopathic pulmonary fibrosis, and lung cancer). Moreover, this strategy also can take advantage of hundreds of square meters of well-perfused surface area for rapid drug absorption and distribution, and at the same time avoid metabolic alterations bypassing the liver, which has a remarkably high enzymatic activity compared to the lungs (SHAFFER, 2020). In addition, the pulmonary biodistribution of systemic administration drugs is poor, and typically only 2 - 4% of the administered dose reach to the lungs, which in turns demand a total dose over the therapeutic dose resulting in off-target side effects (SULAIMAN, 2021).

In 2018 FDA approved the first lipid-based inhalable formulation for *Mycobacterium avium* complex infections, using liposomes (LEONG; GE, 2022). However, the multiple obstacles associated with the pulmonary pathway, such as the respiratory mucosal layer, mucociliary clearance into the gastrointestinal tract, and phagocytic cells still demand the enhancement of lipid formulations

for mRNA lung delivery (SUBERI et al., 2023). According to literature reports the right lipid mixture, considering the chemical nature (KIM et al., 2022) of the lipids and molar proportion (CHENG et al., 2020) in the formulation, can significantly impact the mRNA delivery to the lungs. Nevertheless, the respiratory mucosa is particularly susceptible to immunopathology, and it has been demonstrated that the LNP delivery systems used in the two approved mRNA vaccines cause respiratory tract inflammation upon intranasal administration (SUBERI et al., 2023). These factors indicate that there are opportunities to be explored for the design of an optimized formulation to pulmonary mRNA administration.

## CHAPTER III

### 3 MATERIAL AND METHODS

#### 3.1 mRNA LOADED IN LECITHIN BASED LIPID NANOPARTICLES

This section describes the development of an encapsulation process, which combines the W/O/W double emulsion technique with an approach for soy lecithin protonation to promote the mRNA entrapment into LNPs. W/O/W double emulsion is one of the most used techniques for the encapsulation of hydrophilic molecules, by directly adding the loading molecule to the inner aqueous phase this method allows the incorporation of a larger amount of the hydrophilic drug within the aqueous core, minimizing drug loss during the emulsification process. The soy lecithin protonation by pH manipulation has the purpose of increasing the mRNA retention by the conjugation of the tertiary amine headgroup from soy lecithin and the anionic phosphate group from mRNA.

##### 3.1.1 Material

White Beeswax (GM ceras, Brazil) and a triacylglycerol composed of saturated medium-chain fatty acids (capric/caprylic acids) derived from coconut or palm oil (Crodamol GTCC, Chemical Alpha) were used respectively as solid and liquid lipids to form the lipid matrix. As nonionic surfactants, polyoxyethylene-20-sorbitan monooleate (Tween 80, Vetec) and zwitterionic soy lecithin (Alfa Aesar) were used. The nucleic acid Renilla-Luciferase mRNA (1500 nucleotides, Renilla-Luc-mRNA) used in this study was synthesized in the Laboratory of Immunobiology of the Federal University of Santa Catarina.

##### 3.1.2 Methods

###### 3.1.2.1 mRNA Encapsulation in Beeswax, Crodamol and Lecithin LNPs (B-mRNA-LNPs)

The composition of the lipid matrix, as well as the W/O/W double emulsion technique, were adapted from previous works by our research group (CORDEIRO et al., 2021; MAZUR et al., 2018).

Initially, white beeswax (72.5 mg) was melted at 70 °C in the presence of the surfactant soy lecithin (7.25 mg or 10% w/w) and 64 mg of Crodamol. Next, Renilla-mRNA was added as 65 µL of

0.1 M acetate buffer (pH 5.0) (0.3  $\mu\text{g}/\mu\text{L}$  of mRNA) and emulsified in the previously prepared lipid phase under magnetic stirring (500 rpm). The formed coarse emulsion was then sonicated at 40% amplitude for 30 s in a pulsed regime (15 s on, 10 s off) (Ultrasonic Dismembrator Model 500, Fischer Scientific) to form a W/O miniemulsion. Following, 1.45 mL of the aqueous solution with the second surfactant Tween 80 (14.5 mg or 1% w/v) was added to the first emulsion and kept under magnetic stirring (1000 rpm) for 10 min at 70 °C. The second emulsion was sonicated at 40% amplitude for 120 s in a pulsed regime (15 s on, 10 s off), forming a W/O/W double emulsion. To promote the rapid lipid solidification, the double emulsion was immediately transferred to a 50 mL Falcon tube immersed in a 200 mL cold bath of water:ethanol (1:1 v/v) at – 20 °C under magnetic stirring (1100 rpm) until reaching 10 °C.

The molar ratio of soy lecithin nitrogen/nucleic acid phosphate (N/P) of this formulation was equal to 80. Also, in this approach, the probe was dipped into the continuous phase of the emulsion, which results in a direct dispersion of ultrasonic energy to the system.

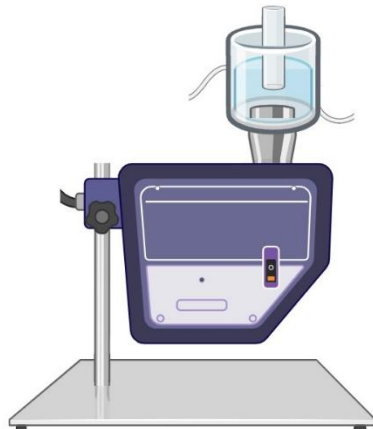
#### *3.1.2.2 mRNA Encapsulation in Crodamol and Lecithin LNPs (C-mRNA-LNPs)*

This formulation, as well as the W/O/W double emulsion technique, were adapted from previous works from our research group, which used beeswax, soy lecithin, and Crodamol as lipid matrix (CORDEIRO et al., 2021; MAZUR et al., 2018).

Initially, the stock solutions were prepared, Crodamol + Lecithin 30% (w/w) was made adding 4.0 g of the liquid lipid and 1.2 g of the surfactant, Water + Tween 80 0.5% (w/w) was made adding 10 g of water and 0.05 g of the surfactant. The procedure starts by aliquoting 18 mg of the organic phase in a 15 ml Falcon round bottom tube, and adding 10  $\mu\text{L}$  of the inner aqueous phase 0.1 M acetate buffer (pH 5.0) (0.81  $\mu\text{g}/\mu\text{L}$  of mRNA). The tube was briefly vortexed to form a coarse W/O emulsion and then placed in an inverted ultrasound probe apparatus to be sonicated at 18 °C using 90% amplitude for 3 min in a pulsed regime (30 s on, 15 s off). Following 190  $\mu\text{L}$  of the Water + Tween 80 0.5% (w/w) was added to the first emulsion, and the system was sonicated again at 18 °C using 90% amplitude for 5 min in pulsed regime (30 s on, 15 s off), forming the W/O/W double emulsion.

The molar ratio of soy lecithin nitrogen/nucleic acid phosphate (N/P) of 320. In this approach, the tube containing the emulsion was dipped into an inverted ultrasound probe apparatus, as shown in Figure 4, which results in an indirect dispersion of ultrasonic energy to the system.

Figure 4 – Schematical representation of the inverted ultrasound probe apparatus used to prepare the C-mRNA-LNPs



Source: Author (2023)

### 3.1.2.3 Encapsulation Efficiency (EE%)

Encapsulation efficiency (EE%) of C-mRNA-LNPs was measured using a fluorescence assay adapting the QuantiFluor® kit protocol (Promega, USA). Utilizing 0.5 mL tubes, 10  $\mu$ L of 1X TE buffer were added to wells designated for quantifying free mRNA in the formulation, and to quantify the total mRNA in the formulation 10  $\mu$ L of 2% Triton X-100 buffer (v/v) were added to wells, inducing the LNP lysis after 10 min incubation at 37 °C. Next, 10  $\mu$ L of the sample were carefully added to the corresponding Free and Total mRNA tubes. Finally, 200  $\mu$ L of the QuantiFluor® dye were added to each of the tubes, which were incubated for 5 min at room temperature, protected from light, and then analyzed using a Quantus™ Fluorometer (Promega, USA). The Equipment was calibrated using the kit recommendation for the high concentration standard, modified with 10  $\mu$ L of 2% Triton X-100 buffer. Encapsulation efficiency was calculated by Equation 1.

$$EE\% = \frac{\text{Sample Total}_{\text{Triton X-100}} - \text{Sample Free}_{\text{TE}}}{\text{Total Add}_{\text{Triton X-100}}} \times 100 \quad (1)$$

### 3.1.2.4 Morphology and Surface Characterization

The intensity average particle diameter and polydispersity index (PDI) were determined by dynamic light scattering (Zetasizer Nano S, Malvern Instruments, U. K.). The surface charge of dispersed LNPs was verified by zeta potential measurements (Zetasizer, Malvern Instruments, U. K.). The analyses were carried out in the Laboratory of Control and Polymerization Processes (LCP) and



in the Interdisciplinary Laboratory for the Development of Nanostructures (LINDEN), both situated in the Department of Chemical Engineering and Food Engineering of the Federal University of Santa Catarina.

Transmission electron microscopy analysis of C-mRNA-LNPs (TEM, JEM 2100F, 100Kv) was carried out by adding a 5 wt% uranyl acetate solution to the LNPs diluted dispersion (0.5 wt% solids content) at a 1:5 ratio (uranyl acetate: 0.5 wt% LNPs dispersion) and dropping on a carbon-coated copper grid (300 mesh). The samples were analyzed after drying for 48 h at room temperature. The analyses were carried out in the Central Electron Microscopy Laboratory (LCME) of the Federal University of Santa Catarina.

#### *3.1.2.5 Agarose Gel Electrophoresis*

The integrity of the nucleic acid added to the B-mRNA-LNPs formulation was verified by a 1.2% agarose gel electrophoresis assay. For this analysis, the formulation was separated into: (I) the nanoparticles and (II) the supernatant. For this, first, the LNPs were centrifuged at 13300 rpm (MiniSpin, Eppendorf, Germany) for 30 min; the supernatant was removed and centrifuged again under the same conditions to maximize nanoparticles removal. The RNA extraction from samples I and II was performed using Trizol LS Reagent® kit (Thermo Scientific™, USA) following the manufacturer's protocol. Non-manipulated RNA was used as the positive control.

#### *3.1.2.6 Cell Culture*

All cells were grown in T25 or T75 flasks at 37 °C in 5% CO<sub>2</sub>, humidified atmosphere, on HERACELL VIOS 160i incubators (Thermo-Fisher Scientific, Waltham, MA, USA). HEK 293T cells (human embryonic kidney cells, ATCC, USA) and Vero cells (monkey kidney epithelial cells) were cultured in DMEM media with 5% FBS and 1% antibiotic supplementation. These cell lines were chosen as *in vitro* models due to their well-established and effective transfection capabilities.

For maintenance, cells were passaged in T25 or T75 as necessary and kept incubated at 37 °C in 5% CO<sub>2</sub>, and humidified atmosphere. The passaging was performed by initially washing the cells with PBS solution pH 7.4 and subsequently incubating them with fresh trypsin/EDTA solution at 37 °C for 10 min. Subsequently, fresh media was added and trypsin/EDTA was removed by centrifugation of the cells. The cells were, then, resuspended in fresh media. Cells were counted using automated cell counters (Thermo-Fischer Scientific, Waltham, MA, USA).

### 3.1.2.7 *In vitro* Cell Viability

The *in vitro* effect of B-mRNA-LNPs and C-mRNA-LNPs over the cellular viability was investigated using HEK 293T, and Vero cells, respectively, adapting the protocol described by Patricio et al., (2022). Initially, utilizing a 96-well flat-bottom plate, the cells were seeded at  $2 \times 10^4$  cells/well and incubated at 37 °C in 5% CO<sub>2</sub> for 24 h. Next, the formulations were tested as follows: B-mRNA LNPs were added to the wells at the final LNPs concentration of 3.15, 6.3 and 9.45 µg/µL, which correspond to 0.3, 0.6 and 1% of total solids (w/v); C-mRNA LNPs were added to the wells at the final LNPs concentration of 0.49, 2.48, 4.97 and 24.85 µg/µL, which correspond to 0.05, 0.25, 0.5 and 2.5% of total solids (w/v). Untreated cells were used as a control group, and all the cells were kept at 37 °C in 5% CO<sub>2</sub> for 24 h. After the treatment period, the cells were washed with PBS, and cell viability was evaluated by the MTT method (3-(4,5-dimethylthiazol-2-yl)-2,5-diphenyltetrazolium bromide). For this, 100 µL of MTT solution (0.5 µg/mL) was added to each well, and the cells were incubated for 3 h. Next, the supernatant was discarded and Formazam crystals were dissolved in 100 µL of DMSO, and the staining intensity was determined by spectrophotometry, 550 - 600 nm.

### 3.1.2.8 *In Vitro* Luciferase Expression Promoted by mRNA-LNP Delivery

The utility of bioluminescence assays, both *in vitro* and *in vivo*, stems from their high specificity and sensitivity, particularly in luciferase reporting assays (LIU et al., 2021). Luminescence, in general, is characterized by light emission as a result of a chemical reaction without the production of heat or thermal changes. In this way, bioluminescence is when the light production is intermediate by biochemical reactions (THERMO FISHER SCIENTIFIC, 2023). The lack of intrinsic bioluminescence signal or luciferase activity in animals and most cell lines ensures high sensitivity and specificity, which coupled with the simplicity, and affordability make this assay indispensable in the exploration of several biological phenomena (LIU et al., 2021). The signal generated by firefly luciferase in these assays is a consequence of the ATP-catalyzed oxidation of D-luciferin into oxyluciferin, releasing light (BIOTIUM, 2023).

The *in vitro* Renilla-Luc expression promoted by the C-mRNA-LNP was quantified using the Dual-Glo luciferase assay system from Promega (USA), and adapting the protocol described by Ricciardi-Jorge et al., (2023) as follows. Initially, utilizing a 96-well flat-bottom plate, the HEK 293T cells were seeded at  $2 \times 10^4$  cells/well and incubated at 37 °C in 5% CO<sub>2</sub> overnight.

Following the incubation period, C-mRNA-LNPs were added to the wells at the final LNPs concentration of 0.49, 0.99, 1.49, 1.98, and 2.48  $\mu\text{g}/\mu\text{L}$ , which correspond to 37.2, 74.4, 111.6, 148.8 and 186 ng/well of Fluc-mRNA. Also, two groups of cells received 100 ng/well of Renilla-Luc-mRNA loaded in Lipofectamine 2000. The first group, which was the positive control for transfection received the mRNA loaded in Lipofectamine 2000 as prepared, the second group, which was the control for nucleic acid integrity, received the Renilla-Luc-mRNA loaded in Lipofectamine 2000 after exposition to the same ultrasonic conditions as C-mRNA-LNPs.

Finally, 24 h after the addition of C-mRNA-LNP and Lipofectamine 2000, cells were washed once with PBS and lysate with 20  $\mu\text{L}$  of Passive Lysis Buffer (Promega, USA). After this, 100  $\mu\text{L}$  of the Stop and Glo reagent from Dual-Glo luciferase assay kit were added to the lysate cells and the bioluminescence (400 – 850 nm) was immediately quantified using a SpectraMax® Paradigm® plate reader (Molecular Devices, USA).

### 3.2 MRNA LOADED IN IONIZABLE LIPID NANOPARTICLES

The following section was developed in *The da Rocha and Sweet Labs* at the Virginia Commonwealth University (Richmond, VA, USA) as part of the sandwich Ph.D. program financed by CAPES. The work conducted during the sandwich Ph.D. period was supervised by Prof. Dr. Sandro da Rocha which has a vast experience in pulmonary nanobiopharmaceutics filed, and in the last years has focused his work on the development of nanomaterials for biomedical applications, with particular focus on the aerosol formulation and delivery of nanomedicines to treat a variety of lung diseases, including cancer and others.

#### 3.2.1 Material

The ionizable lipids DLin-MC3-DMA (heptatriaconta-6,9,28,31-tetraen-19-yl-4-(dimethylamino)butanoate) and SM-102 (heptadecan-9-yl 8-((2-hydroxyethyl) (6-oxo-6-(undecyloxy) hexyl) amino) octanoate) were purchased from MedKoo Biosciences (United States) while DSPC (1,2-distearoyl-sn-glycero-3-phosphocholine), DOPE (1,2-dioleoyl-sn-glycero-3-phosphoethanolamine), Cholesterol,  $\beta$ -sitosterol and DMG-PEG (1,2-dimyristoyl-rac-glycero-3-methoxypolyethylene glycol-2000) were acquired from Avanti Polar Lipids (United States). The nucleic acid used in this study was CleanCap® Firefly Luciferase mRNA (1929 nucleotides, FLuc-mRNA) synthesized by Trylink BioTechnologies (United States).

### 3.2.2 Methods

#### 3.2.2.1 mRNA Encapsulation in LNP by Dropwise addition

The dropwise addition method was used to produce LNPs for screening how the lipid combination would impact the cellular uptake and mRNA transfection in different cell lines. The formulation design started from two main formulations: The first was the one already established by Onpattro™ composed by DLin-MC3-DMA/DSPC/Cholesterol/DMG-PEG and the second was a formulation purposed in The da Rocha and Sweet Labs at the Virginia Commonwealth University (VCU) for another project and composed by SM-102/DOPE/  $\beta$ -sitosterol/DMG-PEG which had already shown positive results in RAW 264.7 cells. So, based on these two formulations, six formulations were proposed to investigate. The formulations prepared by the dropwise addition method are displayed in Table 4.

Table 4 – Lipid composition of LNPs prepared by dropwise addition

Formulation	Lipids
F01	SM-102/CH/DOPE/ DMG-PEG
F02	SM-102/ $\beta$ /DOPE/ DMG-PEG
F03*	SM-102/CH+ $\beta$ /DOPE/ DMG-PEG
F04	SM-102/CH/DSPC/ DMG-PEG
F05	DLin-MC3-DMA /CH/DSPC/ DMG-PEG
F06	DLin-MC3-DMA /CH/DOPE/ DMG-PEG
F07	DLin-MC3-DMA / $\beta$ /DOPE/ DMG-PEG
F08	DLin-MC3-DMA / $\beta$ /DSPC/ DMG-PEG

Source: The Author (2023)

Notes:

Lipids molar ratio for all formulations except F03: 50/38.5/10/1.5

\*Lipids molar ratio for F03: 50/19.25+19.25/10/1.5

MC3 and SM102 = Ionizable Lipids

CH = Cholesterol

$\beta$  =  $\beta$ -Sitosterol

DMG-PEG = DMG-PEG2000

Before the LNP preparation, all the lipids were solubilized in ethanol, and stock solutions were prepared. In a typical formulation, in the first step, the lipids components are aliquoted from their respective stock solutions (Table A1) and mixed with ethanol to the final volume of 100  $\mu$ L. Subsequently, the aqueous phase was prepared by adding 5  $\mu$ g of mRNA (1  $\mu$ g/ $\mu$ L) to citrate buffer (pH 4) to the final volume of 300  $\mu$ L. The aqueous phase was placed in a vial with a magnetic stirring bar that was slowly set to 900 rpm at room temperature. After the stirring speed was achieved, using

a 200  $\mu\text{L}$  pipette set to 100  $\mu\text{L}$ , the lipid phase was loaded and added drop by drop to the aqueous phase (8 -11 drops), after the last drop dispersion was left for 5 min at 900 rpm and room temperature. At the end of the stirring time, the speed was slowly decreased until full stop of the magnetic bar, and the formulation was let to rest undisturbed for an additional 5 min on ice. All formulations had a final volume of 400  $\mu\text{L}$  and a theoretical mRNA concentration of 0.0125  $\mu\text{g}/\mu\text{L}$  using a molar ratio of ionizable lipid nitrogen/nucleic acid phosphate (N/P) of 6 and a mixing volume ratio of 3:1 (aqueous:lipid).

#### 3.2.2.2 Purification and Concentration of mRNA Loaded LNP Prepared by Dropwise Addition

The LNPs prepared by the dropwise addition method were purified and concentrated by the ultracentrifugation technique using the Amicon® Ultra centrifugal filter (Millipore, 10 kDa). For this, the whole formulation (400  $\mu\text{L}$ ) was placed in the 0.5 mL Amicon® Ultra centrifugal filter and centrifuged at 5000 rpm and 4 °C until the total volume on the retentate side of the filter reached 200  $\mu\text{L}$ . After, the filtrate was discarded from the tube and the filter was flipped upside down inside the same tube (Figure A1) to be centrifuged again at 5000 rpm and 4 °C for 15 min to collect the LNPs. In the last stage, after the LNPs were collected in the bottle of the Amicon® tube, 100  $\mu\text{L}$  of PBS buffer (pH 7) were added to the filter part of the Amicon®, and the filter was again flipped upside down inside the tube, and centrifuged at 5000 rpm and 4 °C for 15 min to maximize the LNPs recovery from the filter pores. At the end of this stage, it is expected that ethanol and any residual lipids will be removed from the formulation, as well as that the formulation will have a final volume of 300  $\mu\text{L}$  and a theoretical mRNA concentration of 0.017  $\mu\text{g}/\mu\text{L}$ .

#### 3.2.2.3 mRNA Encapsulation in LNP by Microfluidics

The microfluidics approach was used to produce LNP for *in vivo* experiments. Microfluidics is a continuous manufacturing strategy capable to produce LNP formulations with higher reproducibility and with a smaller size compared to the dropwise addition method (GIMONDI et al., 2023). Those two factors are crucial for *in vivo* LNPs tests, especially when the lungs are the target delivery route. The microfluidization method was explored using LNP formulation F05, which corresponds to the first commercial pharmaceutical formulation designed and approved by the FDA for siRNA delivery, named Onpatro® (FERRARESSO et al., 2022). Prior to the preparation for *in vivo* administration, the FLuc-mRNA encapsulation in F05 (DLin-MC3-DMA/DSPC/Cholesterol/DMG-PEG), using the microfluidic system was investigated for

understanding the protocols involved in the LNPs preparation, purification, and characterization, the results of these preliminary assays are described in the Appendix.

LNP formulations were prepared using a modified procedure (HASSETT et al., 2019; KIM et al., 2022). Briefly, lipids were individually dissolved in ethanol and mixed at molar ratios of 50:10:38.5:1.5 (DLin-MC3-DMA:DSPC:Cholesterol:DMG-PEG). The mRNA stock solution (1  $\mu\text{g}/\mu\text{L}$ ) was added to a 50 mM acetate buffer (pH 4.0) for acidification and mixed with the lipid mixture at a flow phase ratio (FFR) of 3:1 (acetate buffer:ethanol) using a microfluidic mixer (Precision Nanosystems, Vancouver, BC, Canada). The details of a typical formulation and conditions are described in Table 5:

**Table 5 – Details of formulation and operational conditions for LNPs preparation by microfluidics**

MC3-FLUC-05	
Ionizable Lipid	D-Lin-MC3-DMA
mRNA	CleanCap Fluc mRNA
Lipid Ratio	50:38.5:10:1.5 (MC3:DSPC:CH:PEG)
Total Lipid Concentration	5.5 mM
Aqueous Phase	50 mM Sodium Acetate Buffer pH 4.0
mRNA Concentration [mRNA]	0.23 mM or 76.77 $\mu\text{g}/\text{mL}$
Total Flow Ratio	12 mL/min
Flow Phase Ratio (FFR)	3:1 (acetate buffer:ethanol)
N/P Ratio	4

Source: The Author (2023)

For a formulation with a total volume of 1 mL, the following parameters were set according to Precision Nanosystems recommendations for iIgnite operation: both phases were loaded in 1 mL syringes, the start waste was set to 0.3 mL (0.22 mL from the aqueous phase and 0.07 mL from the lipid phase), and consequently, the sample volume was of 0.7 mL. The start waste is the volume discarded by the machine until reaches the liquid laminar flow, which is crucial for the manufacture of nanoparticles using microfluidic technology. Also, the mRNA concentration in the aqueous phase was calculated using the following Equation 2 provided by Precision Nanosystems, where X is the molar fraction of the ionizable lipid.

$$\left[ \begin{array}{c} \text{mRNA} \\ \text{Concentration} \end{array} \right] = \frac{[\text{Total Lipid Concentration}] \times X}{\text{FFR} \times \frac{N}{P}} \quad (2)$$

When necessary, DiD' (1,1'-Dioctadecyl-3,3,3',3'-Tetramethylindodicarbocyanine, 4-Chlorobenzenesulfonate Salt) was added to the formulation as lipophilic dye. DiD' is the lipophilic analogue of Cyanine 5 (TEXIER et al., 2009), which in turn is one most commonly used oligonucleotide labeling molecules (AGBAVWE; SOMOZA, 2011). The lipophilic dye was chosen aiming to label the lipid shell of the LNPs and DiD' labeled LNPs (DiD'-LNPs) were prepared by adding the dye as 0.2% of the total molar lipids content in the formulation.

#### *3.2.2.4 Purification and Concentration of mRNA Loaded LNP Prepared by Microfluidics*

The LNPs prepared by the microfluidics method were purified by dialysis. The formulation was dialyzed against sterile and RNase-Free PBS (pH 7.4) using a Slide-A-Lyzer G2 cassette with 10 kDa molecular-weight cutoff (Thermo Fisher, MA, USA) by 2 h changing the dialysis media every 30 min at 4 °C. The LNPs prepared by the microfluidics were concentrated by ultracentrifugation using the Amicon® Ultra centrifugal filter (Millipore, 10 kDa). For this, the formulation was aliquoted and centrifuged in a 0.5 mL Amicon® Ultra centrifugal filter at 5000 rpm and 4 °C until the total volume had been filtered. After, the filtrate was discarded from the tube and the filter was flipped upside down inside the same tube (Figure A1) to be centrifuged again at 5000 rpm and 4 °C for 15 min to collect the LNPs. In the last stage, the volume of the collected LNPs was measured and PBS buffer (pH 7.4) was added according to the desired mRNA concentration.

#### *3.2.2.5 Morphology and Surface Characterization*

The intensity average particle diameter, polydispersity index (PDI), and zeta potential were determined as described in Chapter III section 3.1.2.4.

#### *3.2.2.6 Encapsulation Efficiency (EE%)*

Encapsulation efficiency (EE%) was measured using a fluorescence plate-based assay adapting the Ribogreen kit protocol (Thermo Fisher, MA, USA) (CARRASCO et al., 2021). Utilizing a 96-well plate, initially, a sample stock solution was prepared by adding 15 µL of the LNPs formulation into assigned wells and 1X TE buffer was added to attain a final volume of 250 µL. Following, 50 µL of 1X TE buffer were added to wells designated for quantifying free mRNA in the formulation, marked as Free mRNA wells. Subsequently, 50 µL of 2% Triton X-100 buffer (v/v) were added to wells intended for quantifying total mRNA in the formulation, designated as Total

mRNA wells. Finally, 50  $\mu\text{L}$  of the sample stock solution was carefully added to all corresponding Free and Total mRNA wells. For the RNA standard curve, the well configuration specified in Table 6 below was employed within the standard curve-designated wells using the RNA Stock solution (20  $\mu\text{g}/\text{mL}$  RNA), 1X TE Buffer, and 2% Triton X-100 buffer. Following the arrangement of solutions and the standard curve, an incubation step at 37  $^{\circ}\text{C}$  was performed for 10 min, to induce the LNP lysis in the presence of 2% Triton X-100 buffer. After the incubation period, 100  $\mu\text{L}$  of the Quant-iT Ribogreen solution were added to each well of the plate, which was then left to stand for 20 min. In the last step, a fluorescent microplate reader (Synergy H1, Biotek, USA) was utilized at an excitation wavelength of 485 nm, an emission wavelength of 528 nm, in the top read optics mode, with a gain of 55x, and an adjusted read height of 8 mm. The formulations were analyzed in duplicate at room temperature.

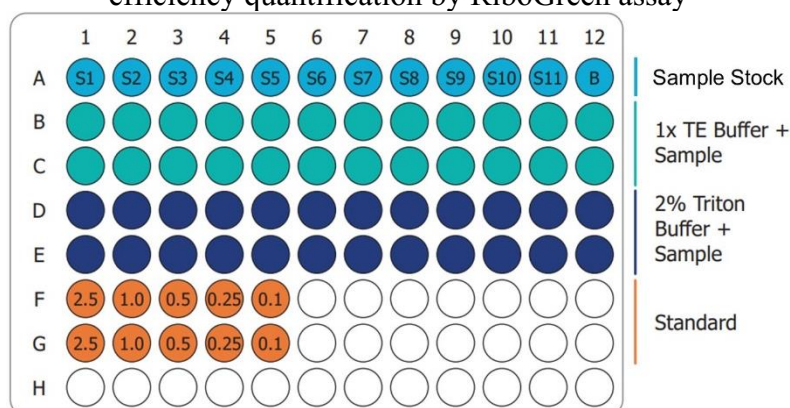
Table 6 – RNA standard curve preparation for encapsulation efficiency quantification by the RiboGreen assay

Final RNA ( $\mu\text{g}/\text{mL}$ )	RNA Stock Required ( $\mu\text{L}$ )	TE Buffer Required ( $\mu\text{L}$ )	Triton Buffer Required ( $\mu\text{L}$ )
2.5	25	25	50
1	10	40	50
0.5	5	45	50
0.25	2.5	47.5	50
0.1	1	49	50
0	0	50	50

Source: The Author (2023)

Figure 5 presents a schematic example of a typical 96-well plate used for this assay, and encapsulation efficiency (EE%) was calculated by Equation 3.

Figure 5 – Schematical representation of a 96 well plate configuration used for encapsulation efficiency quantification by RiboGreen assay



Source: Adapted from Precision Nanosystem (2023)



$$EE\% = \frac{\text{Sample Total}_{\text{Triton X-100}} - \text{Sample Free}_{\text{TE}}}{\text{Total Add}_{\text{Triton X-100}}} \times 100 \quad (3)$$

### 3.2.2.7 Cell Culture

All cells were grown in T25 or T75 flasks at 37 °C in 5% CO<sub>2</sub>, humidified atmosphere, on HERACELL VIOS 160i incubators (Thermo-Fisher Scientific, Waltham, MA, USA). K7M2, murine osteosarcoma lung metastasis cells, (ATCC, Manassas, VA, USA) and NIH-3T3 (ATCC, Manassas, VA, USA), mouse embryonic fibroblast cells, were grown in DMEM media, supplemented with 10% FBS, and 1% antibiotic. RAW 264.7, murine macrophage cells, were grown in DMEM media with sodium pyruvate (DMEM-SP), supplemented with 10% FBS, and 1% antibiotic.

For maintenance, cells were passaged in T25 or T75 as necessary and kept incubated at 37 °C in 5% CO<sub>2</sub>, and humidified atmosphere. The passaging was performed by initially washing the cells with PBS solution pH 7.4 and subsequently incubating them with fresh trypsin/EDTA solution at 37 °C for 10 min. Subsequently, fresh media was added and trypsin/EDTA was removed by centrifugation of the cells at 1200 rpm for 7 min. The cells were, then, resuspended in fresh medium. Cells were counted using automated cell counters (Thermo-Fischer Scientific, Waltham, MA, USA).

### 3.2.2.8 In Vitro Luciferase Expression promoted by mRNA-LNP Delivery

The *in vitro* luciferase expression promoted by the mRNA-LNP was quantified using the One-Glo luciferase assay system from Promega (USA), and adapting the protocol described by Kim, Jozic & Sahay (2020) as follows. Initially, utilizing a 96-well flat-bottom plate, the K7M2, and RAW 264.7 cells were seeded at 10<sup>4</sup> cells/well and incubated at 37 °C in 5% CO<sub>2</sub> for 24 h. After this period, cell media was removed, cells were briefly washed with 100 μL of sterile PBS and then treated with 100 ng of Fluc-mRNA by adding 100 μL of mRNA-LNP formulation diluted in cell media to each well. 24 h after adding the mRNA-LNP formulation to the cells, 100 μL of the One-Glo Luciferase reagent were added to the wells already containing 100 μL of the mRNA-LNP formulation diluted in culture media. After an incubation period of 20 min at room temperature, luminescence was quantified using a microplate reader (Synergy H1, Biotek, USA).

### 3.2.2.9 Co-Culture of Spheroids Using K7M2, RAW 264.7 and NIH-3T3 Cells

Tumor spheroids were chosen as *in vitro* model for tracking the *in vitro* LNPs delivery as well the luciferase expression profile promoted by mRNA-LNP in a more complex environment. This model serves as a more powerful tool for investigating the interaction and effects of new cancer therapies in the tumor microenvironment, being able to mimic tumor behavior more effectively than conventional 2D culture systems (GALATEANU et al., 2016). To prepare the tumor spheroids, K7M2 tumor cells were co-cultured with RAW 264.7, once that almost half of the tumor mass are tumor-associated macrophages, and with NIH-3T3 fibroblast cells due to its key functions in the tumor microenvironment such as production growth factors, chemokines, adhesion molecules and in the deposition of extracellular matrix. The studies regarding the production of K7M2, RAW 264.7, and NIH-3T3 co-culture spheroids, and the respective results are reported in the Appendix.

### 3.2.2.10 *In Vivo* Luciferase Expression Profile promoted by mRNA-LNP Delivery

For tracking the *in vivo* luciferase expression profile promoted by mRNA-LNP delivery, five healthy BALB/c mice were used. The LNP treatment (25  $\mu$ L LNPs containing 2  $\mu$ g of Fluc-mRNA solution per mouse) was pulmonary administered (P.A.) intratracheally. At different preset time points (0.5, 2, 3, 4, 5, 6, and 12 h) post mRNA-LNPs administration, mice were anesthetized with isoflurane and injected with 200  $\mu$ L of 15 mg/mL D-Luciferin potassium solution subcutaneously, then 10 min after injection, mice were kept under isoflurane anesthesia and imaged using IVIS Spectrum instrument (Xenogen, USA) to obtain *in vivo* bioluminescence intensity produced by luciferase expression. As control and baseline for this assay, one day before being treated with LNPs, each mouse received the D-Luciferin dose and was imaged using an IVIS Spectrum instrument to quantify the natural bioluminescence intensity produced by the mice.

### 3.2.2.11 Luciferase Expression *In Vivo*, *Ex Vivo*, and in BALF's Macrophages promoted by mRNA-LNP Delivery

To further investigate the *in vivo* P.A. administration of LNP loaded with mRNA, mice's lungs were analyzed *ex vivo* and to address the proposal of delivering the designed LNP to macrophages, the bronchoalveolar lavage fluid (BALF) was collected for analysis, once more than

90% of Balb/c bronchoalveolar lavage cells are macrophages (BEDORET et al., 2009). BALF is obtained by a minimally invasive procedure that involves the instillation of sterile fluid (e.g., saline, PBS) into a subsegment of the lung, followed by suction and collection of it for analysis.

To quantify the luciferase expression promoted by mRNA-LNP delivery *in vivo*, *ex vivo*, and in BALF's macrophage, 9 healthy BALB/c mice were used. The LNP treatment (25  $\mu$ L LNPs containing 1  $\mu$ g of Fluc-mRNA per mouse) was P.A. intratracheally. At 2, 6, and 12 h post mRNA-LNPs administration, three mice were anesthetized with isoflurane and injected with 200  $\mu$ L of 15 mg/mL D-Luciferin potassium solution subcutaneously, after 10 min of injection mice were kept under isoflurane anesthesia and imaged, then the mice were sacrificed for BALF and lungs collection. BALF was collected by washing the lungs three times with 1 mL of PBS (3 mL total). After BALF total recovery, the lungs were harvested, and finally, the fluid and the lungs were imaged *ex vivo*. All the images were acquired using the IVIS Spectrum instrument in the bioluminescence mode to obtain luciferase expression signal (Xenogen, USA). The control group and baseline of this assay were composed of non-treat mice (n=3) that received the same D-Luciferin dose and were manipulated and imaged as the treatment groups.

#### 3.2.2.12 Luciferase Expression and DiD'-LNPs Tracking In Vivo, Ex Vivo, and in BALF's Macrophages promoted by mRNA-LNP Delivery

To simultaneously quantify the luciferase expression and track the LNP *in vivo*, *ex vivo*, and in BALF's macrophage, a specific formulation containing both FLuc-mRNA and DiD' lyophilic dye was prepared and identified as DiD'-LNPs.

The FLuc-mRNA dosing, LNPs administration, group arrangements, animals, and tissue handling were performed as described in Chapter III section 3.2.2.11. All the images were acquired using the IVIS Spectrum instrument (Xenogen, USA), first in the bioluminescence mode to obtain luciferase expression signal, and subsequently in the fluorescence mode with Cy5 filter, to identify DiD'-LNPs presence.

#### 3.2.2.13 Statistical Analyses

Significant differences were determined by ANOVA or *t*-test, followed by Tukey's test for multiple comparisons, when necessary, at a 95.0% confidence level ( $p \leq 0.05$ ).

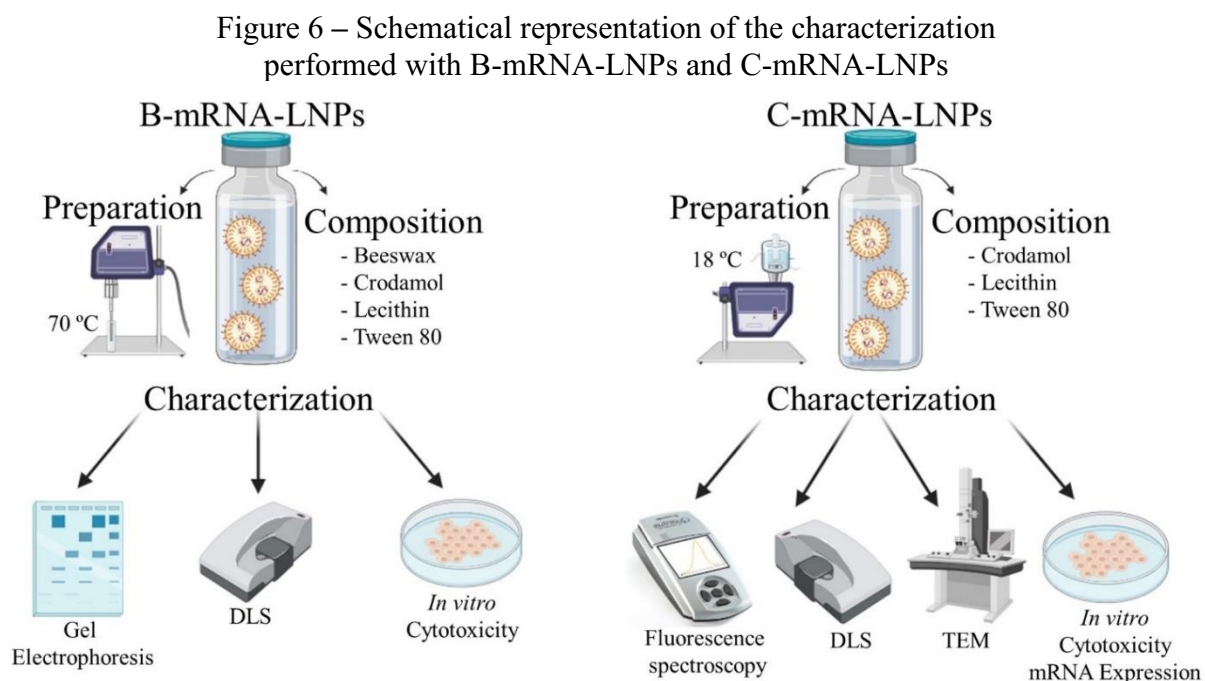
## CHAPTER IV

### 4 RESULTS AND DISCUSSION

#### 4.1 LECITHIN BASED LIPID NANOPARTICLES PREPARED BY W/O/W DOUBLE EMULSION

##### 4.1.1 Nanoparticle characterization

Two W/O/W double emulsion formulations focusing on exploring soy lecithin amine head group for mRNA encapsulation were proposed based on previous studies of our research group about hydrophilic molecules loading in lipid nanoparticles (BECKER PERES et al., 2016; CORDEIRO et al., 2021; MAZUR et al., 2018), the schematical representation of the characterization performed with each formulation is displayed in Figure 6. Besides the adjustments of the operational conditions to promote the ultrasonic double emulsification, two main adaptations were proposed: I – the use of acid aqueous inner phase, in this case, acetate buffer (pH 5.0), to promote the protonation of the lecithin amino head group (PÉREZ et al., 2012); II – the removal of beeswax from the lipid matrix, aiming to decrease the viscosity and increase the lecithin content in the formulation. Table 7 shows how these modifications impacted the size, dispersity, and zeta potential of the mRNA-LNPs.



Source: Author (2023)

Table 7 - Intensity mean diameter of nanoparticles (Dp), polydispersity index (PDI), and Zeta potential ( $\xi$ ) of B-mRNA-LNP and C-mRNA-LNP

Formulation	Size (nm)*	PDI	$\xi$ (mV)
B-mRNA-LNP <sup>pH 8</sup>	283 ± 5	0.224 ± 0.026	-58 ± 1
B-mRNA-LNP <sup>pH 5</sup>	255 ± 4	0.221 ± 0.032	-43 ± 2
C-mRNA-LNP <sup>pH 5</sup>	166 ± 4	0.248 ± 0.073	-39 ± 1

\* Statistical difference in the column  $p \leq 0.05$

B-mRNA-LNP: Beeswax, Crodamol, Lecithin, and Tween 80

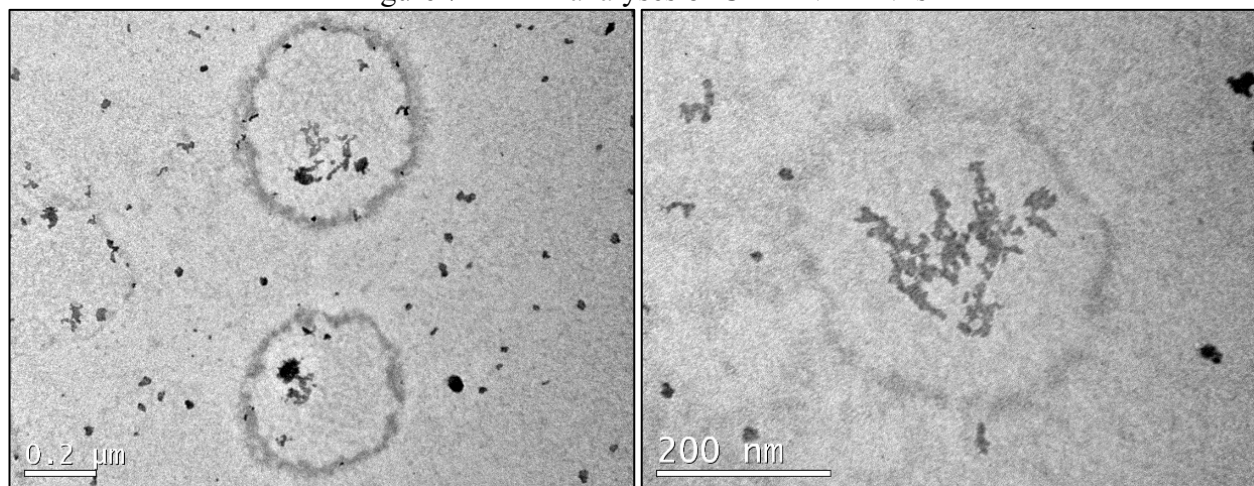
C-mRNA-LNP: Crodamol, Lecithin, and Tween 80

The characterization of LNP formulations shows that all systems presented a submicrometric average size and PDI values close to 0.2, indicating that the ultrasonic double emulsion approaches are capable of generating a relatively monodisperse system (DANA EI et al., 2018). The pH changing from 8.0 to 5.0 in B-mRNA-LNP formulation promoted a decrease in the LNPs average size. According to Pérez et al. (2012), who used lecithin-based nanoparticles to encapsulate siRNA, the nanoparticles formed at pH 5.0 have a small size and spherical shape, while at pH 7.0, the system forms more elongated and cylindrical structures. Also, C-mRNA-LNPs had a significantly smaller average size compared to B-mRNA-LNPs, this could be attributed to the reduction in the system viscosity upon the beeswax removal. The lower viscosity of C-mRNA-LNPs could favor the formation of smaller nanoparticles in two ways: First by the better distribution of the ultrasonic energy throughout the emulsion; Second, droplets with a lower viscosity require less energy to be deformed and broken (GREENWOOD; BAMBERGER, 2002). In addition, all formulations presented a zeta potential value below -30, indicating their desirable colloidal stability and being less susceptible to form aggregates or increase in particle size (SAMIMI et al., 2019).

From Figure 7, it is possible to observe that C-mRNA-LNPs have semi-spherical morphology and submicrometric size, corroborating DLS analysis data. The size enlargement of the nanostructures in Figure 7 in comparison to the DLS data could be related to the heating of the lipid caused by the exposition to the electron beam, which can lead to the deformation of the LNPs structure. Thus, the negative staining with uranyl acetate was used to improve LNPs observation and preserve the nanoparticle contour (CAMPANI; GIARRA; DE ROSA, 2018; SHI et al., 2011). Also, inside the LNPs it is possible to observe the existence of structures that could be associated with the encapsulated mRNA. Brader et al. (2021) performed the mRNA encapsulation using DLin-MC3-DMA/CH/DSPC/DMG-PEG as a lipid matrix and observed similar structures inside the LNPs, which were identified and attributed to the mRNA loading due to the use of thionine dye. So, even with W/O/W double emulsion being broadly used for the encapsulation of hydrophilic molecules, the mRNA's large size is an obstacle that needs to be overcome by the encapsulation method used (ZENG et al., 2020). The combination of this method with an approach capable of promoting the protonation

of the amine headgroup from lecithin to complex with the tail phosphate group from mRNA is an interesting strategy to enhance the nucleic acid trapping and retention inside the LNPs.

Figure 7 – TEM analyses of C-mRNA-LNPs



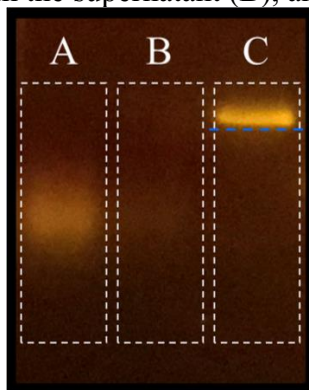
Finally, the quantification of Renilla-Luc-mRNA loaded in the LNPs revealed an encapsulation efficiency of 31.6% for formulation C-mRNA-LNPs. This EE% is considered low, and few hypotheses could explain it. First, the N/P of 320 used on this formulation may not be sufficient to promote adequate binding between the amino head groups of lecithin and the phosphate group from the mRNA. Pérez et al. (2012) reported that using lecithin for siRNA encapsulation at N/P below 1000, the association tends to be weak. The ionizable lipids approved by the FDA for mRNA encapsulation have only an amine head group that is charged at the encapsulation pH, and the formulations based on this molecule use an N/P ratio of about 6 (YANG et al., 2022). The demand for a higher N/P ratio using lecithin could be related to the zwitterionic nature of the molecule, which in addition to the amine head group also has a negative phosphate group in the structure, and both of them are charged at pH 5.0 (PÉREZ et al., 2012). Second, the removal of the beeswax from the formulation could have affected the LNPs structure, once the presence of a solid lipid tends to form a more stable shell for cargo retention compared to the Crodamol liquid droplet (KHOSA; REDDI; SAHA, 2018).

#### 4.1.2 Agarose Gel Electrophoresis

The agarose gel electrophoresis assay was used to verify the integrity of the Renilla-Luc-mRNA encapsulated in the B-mRNA-LNPs. Two samples were prepared to individually analyze the LNPs and the supernatant, which could have non-encapsulated mRNA. Pure Renilla-Luc-mRNA

without manipulation was used as control. Figure 8 shows the agarose gel obtained from the electrophoresis assay with Renilla-Luc-mRNA.

Figure 8 – Agarose gel electrophoresis from Renilla-Luc-mRNA extracted from LNPs (A), extracted from the supernatant (B), and control (C).



The fluorescent signal observed in the Renilla-Luc-mRNA sample extracted from LNPs (column A) indicates that the encapsulated RNA was degraded during the encapsulation process. This can be inferred from the less clean and defined sign of the mRNA band, and from the position of the band in the gel, once that nucleic acid fragments have a smaller size compared to the original molecule, being able to migrate further through the gel, getting closer to the positive pole (DAVIS; DIBNER; BATTEY, 1986). In column B, no signal of Renilla-Luc-mRNA was detected, indicating that there was no mRNA in the supernatant, which indicates that all the mRNA added to the formulation was loaded into the LNPs. Column C, which is the control sample, shows the specific band of Renilla-Luc-mRNA indicating no signs of degradation on the nucleic acid before being exposed to the LNPs preparation conditions. This indicates that degradation could have occurred during the double emulsion process. Also, another factor that must be considered, is that the encapsulation process was not conducted under completely sterile conditions, so mRNA degradation may be related to the presence of ribonuclease enzymes, which catalyze RNA degradation (EUN, 1996).

### 4.1.3 Cell Viability

Initially, we investigated the tolerability of HEK cells to B-mRNA-LNPs. Cells were treated with different concentrations of B-mRNA-LNPs for 24 h and the results are shown in Table 8.

Table 8 – HEK cellular viability (n=3) after 24h treatment with B-mRNA-LNPs

LNPs [ $\mu\text{g}/\mu\text{L}$ ]	mRNA [ng]*	Solids% (w/v)	Viability (%)
3.15	157	0.3	0
6.30	314	0.6	0
9.45	472	0.9	0

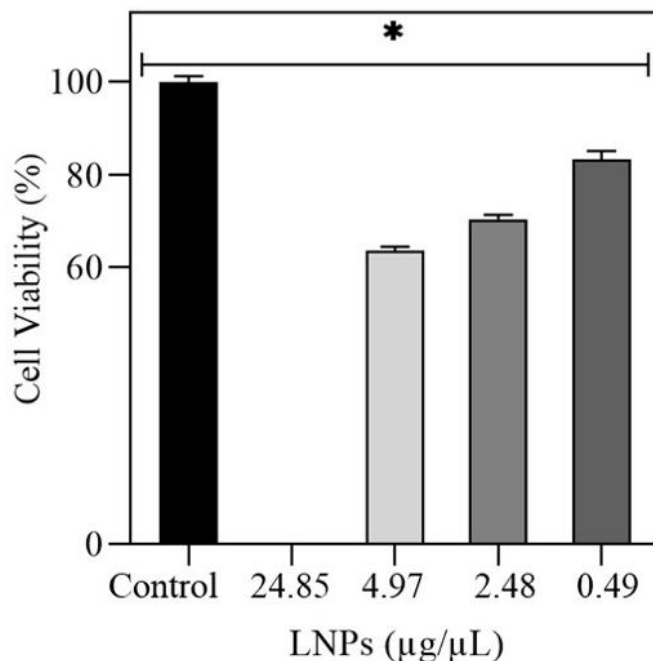
\* Considering hypothetical encapsulation efficiency of 100%

As can be observed, after 24 h of treatment, HEK cells presented no cell viability under all tested conditions. Based on our previous experience with this formulation and literature reports, we hypothesized that this high cellular cytotoxicity could be related to LNPs composition or dosage (STRACHAN et al., 2020). The possibility of decreasing the LNPs dosage of this formulation was limited by the mRNA concentration, which in turn was restricted by the N/P ratio. B-mRNA-LNPs had an N/P ratio of 80, which could not be enough to promote a strong binding between mRNA and lecithin (PÉREZ et al., 2012). Thus, the LNPs composition was manipulated by removing the beeswax from the formulation to increase the Crodamol and lecithin content, and by decreasing the Tween 80 percentage. The removal of beeswax and decrease of the Tween 80 content aimed to decrease the viscosity of the emulsion.

The modifications in the formulation resulted in an increase of the lecithin content from 10% to 30% in the organic phase, and a decrease of Tween 80 amount from 1% to 0.5% in the continuous aqueous phase. This C-mRNA-LNP formulation raised the N/P ratio to 320, and the lower viscosity of the system positively impacted the *in vitro* cellular tolerance to the formulation. The effect of C-mRNA-LNPs on Vero cell viability is shown in Figure 9.



Figure 9 – Cellular viability of Vero cells (n=3) after 24 h treatment with different concentrations of C-mRNA-LNPs



\* Statistical difference between the columns  $p \leq 0.05$

As can be observed, the modifications in the formulation enhanced lecithin-based LNPs *in vitro* tolerability, increasing the concentration required to promote cytotoxic effects on Vero cells with a dose-dependent profile. At the lower concentration, the viability of Vero cells was 83%, and remained above 60% when the two intermediate doses were used. According to ISO 10993-5:2009 (2009), values above 80% for cell viability are considered as non-cytotoxicity and within 80% – 60% indicating weak cytotoxicity effect. At the highest concentration, no cellular viability was detected.

#### 4.1.4 *In Vitro* Luciferase Expression

Based on the gel electrophoresis results obtained with B-mRNA-LNPs (section 4.1.2) and cell viability studies promoted with C-mRNA-LNPs (section 4.1.3), the *in vitro* luciferase expression promoted by Renilla-Luc-mRNA delivery on HEK 293T was investigated using two different carriers: I – C-mRNA-LNPs was tested at five different concentrations of LNPs to verify the capacity of the proposed formulation of generating *in vitro* mRNA expression; II – Lipofectamine 2000 was used to investigate the possibility of degradation of the mRNA chain after being exposed to ultrasonic processing. The C-mRNA-LNPs concentrations tested, and the corresponding mRNA mass are presented in Table 9.

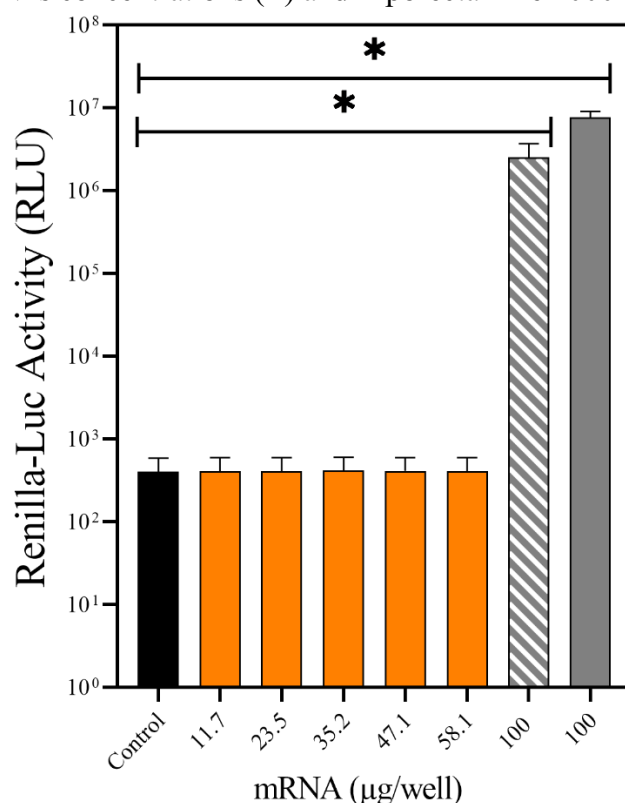
Table 9 – C-mRNA-LNPs and Renilla-Luc-mRNA concentrations used in the *in vitro* luciferase expression assay

LNPs ( $\mu\text{g}/\mu\text{L}$ )	mRNA (ng)*	Solids% (w/v)
0.49	11.7	0.05
0.99	23.5	0.10
1.49	35.2	0.15
1.98	47.1	0.20
2.48	58.1	0.25

\* Considering quantified encapsulation efficiency of 31.6%

Figure 10, presents the results for the *in vitro* quantification of Renilla-Luc expression, using five different concentrations of C-mRNA-LNPs and two conditions of Lipofectamine 2000.

Figure 10 – Renilla-Luc activity on HEK 293T cells (n=3) after 24 h treatment with five C-mRNA-LNPs concentrations (■) and Lipofectamine 2000 (■)#



\* Statistical difference between the columns  $p \leq 0.05$

# Hatched column represents Lipofectamine 2000 exposed to ultrasound conditions

As can be observed, the treatments with C-mRNA-LNPs had no signal of Renilla-Luc activity in any of the concentrations tested. However, using Lipofectamine 2000 as a carrier the Renilla-Luc activity was significantly higher compared to the control group and C-mRNA-LNPs treatments. This could be related to the low encapsulated concentration of Renilla-Luc-mRNA obtained by C-mRNA-LNPs. Also, the exposure to ultrasound conditions led to a significant decrease in the Renilla-Luc signal but didn't extinguish its activity on HEK 293T cells. This result indicates

that using the appropriate operational conditions (applied energy and temperature) the inverse ultrasonic probe could be able to prepare nanoparticles loaded with mRNA. Moreover, considering both results the EE% efficiency obtained by C-mRNA-LNPs (31.6%) and the Renilla-Luc activity obtained by Lipofectamine 2000, the W/O/W double emulsion technique associated with ultrasonic shear could be used to encapsulate mRNA molecules without causing critical damages in the amino acid chain structure, which could compromise its *in vitro* activity.

The process of protein expression resulting from the delivery of mRNA-LNPs is complex, with several essential steps along the pathway from administration to the actual expression of the protein (SCHLICH et al., 2021). Lipofectamine 2000 is a cationic liposome-based transfection agent, and as Moderna and Pfizer mRNA LNP formulations, it has a lipid mixture designed focusing on the delivery of nucleic acids (DALBY, 2004; FERRARESSO et al., 2022). Thus, further studies are necessary to completely understand the reason for the absence of Renilla-Luc expression using formulation C-mRNA-LNPs, more specifically how soy lecithin and Crodamol could interfere in the extracellular mRNA-based protein expression pathway

## 4.2 IONIZABLE LNPs PREPARED BY DROPWISE ADDITION

### 4.2.1 Nanoparticle characterization

To date, the most advanced system for *in vivo* extracellular mRNA delivery are LNPs composed of four lipid compounds, being: an ionizable lipid, a helper phospholipid, a sterol lipid, and a pegylated lipid. Different lipids can be employed in the LNPs formulation aiming to suppress specific necessities such as target organs, route of administration, type of nucleic acid to be used, and loading capacity (CHENG et al., 2020; SWETHA et al., 2023; XU; XIA, 2023).

The formulations proposed in Table 4 (Chapter III, section 3.2.2.1) were based on the first FDA approved and the most broadly studied formulation for nucleic acid delivery (F05), composed of DLin-MC3-DMA/DSPC/Cholesterol/DMG-PEG in the molar proportion of 50/10/38.5/1.5. However, this formulation was developed and optimized specifically for siRNA delivery, which has inherent chemical and structural differences from mRNA in terms of length, stability, and charge density (KAUFFMAN et al., 2015). The mentioned formulation was adapted by Moderna and Pfizer-BioNTech to incorporate mRNA encoding spike proteins for COVID-19 immunization, which are the only FDA approved LNP formulations for mRNA administration. However, even with both of them showing promising results, there is still significant room for improvement in the field (KAUFFMAN et al., 2015; XU; XIA, 2023).

In this study, DOPE (HOU et al., 2021; ZHANG et al., 2021),  $\beta$ -sitosterol (KIM et al., 2022; MEDJMEDJ et al., 2022) and SM-102 (ESCALONA-RAYO et al., 2023; SNOW et al., 2022) were chosen to be incorporated into the LNPs formulation due to reported evidences about its positive effect over key mRNA therapy aspects such as biosafety, endosomal escape, loading and transfection efficiency. In this way, LNP formulations were first characterized for size distribution, zeta potential, and mRNA encapsulation efficiency, as presented in Table 10.

Table 10 – LNPs Intensity mean diameter of nanoparticles (Dp), polydispersity index (PDI), Zeta potential ( $\xi$ ), and Encapsulation Efficiency (EE%) achieved with different lipid formulation (n=2)

Formulation	Lipids	Size (nm)	PDI	$\xi$ (mV)	EE (%)
F01	SM-102/CH/DOPE/DMG-PEG	105 $\pm$ 23	0.118 $\pm$ 0.025	-3.9 $\pm$ 1.2	85.7 $\pm$ 6.4
F02	SM-102/ $\beta$ /DOPE/DMG-PEG	116 $\pm$ 13	0.167 $\pm$ 0.077	-3.7 $\pm$ 0.2	82.7 $\pm$ 21.9
F03	SM-102/CH+ $\beta$ /DOPE/DMG-PEG	107 $\pm$ 18	0.155 $\pm$ 0.045	-3.1 $\pm$ 0.3	90.7 $\pm$ 11.2
F04	SM-102/CH/DSPC/DMG-PEG	104 $\pm$ 27	0.116 $\pm$ 0.019	-2.6 $\pm$ 0.4	88.6 $\pm$ 5.6
F05	DLin-MC3-DMA/CH/DSPC/DMG-PEG	126 $\pm$ 32	0.154 $\pm$ 0.062	-5.0 $\pm$ 1.3	82.8 $\pm$ 0.8
F06	DLin-MC3-DMA/CH/DOPE/DMG-PEG	120 $\pm$ 26	0.113 $\pm$ 0.017	-3.8 $\pm$ 0.6	87.2 $\pm$ 1.4
F07	DLin-MC3-DMA/ $\beta$ /DOPE/DMG-PEG	155 $\pm$ 18	0.193 $\pm$ 0.116	-4.3 $\pm$ 1.9	83.9 $\pm$ 6.3
F08	DLin-MC3-DMA/ $\beta$ /DSPC/DMG-PEG	123 $\pm$ 26	0.168 $\pm$ 0.019	-7.7 $\pm$ 3.3	86.4 $\pm$ 7.6

All the formulations presented a submicrometric average diameter below 200 nm, narrow size distribution, and high EE% level above 80%. The zeta potential values are in agreement with the literature for this kind of LNP formulation (CARRASCO et al., 2021; LY et al., 2022; YAVUZ et al., 2023), with the colloidal stability being provided by the PEGylated layer on the LNP surface, independent of the system charge (JU et al., 2023).

As can be observed in Table 10, the LNP formulations (n=2) prepared by the dropwise addition method didn't present significant differences in any of the physicochemical characteristics. However, there is evidence in the literature that not only the type of lipid used but also the lipid molar ratio can impact on LNP's properties (KIM et al., 2022).

Geng et al. (2023) tested both hypotheses: I - how the combination of different types of lipids and II – how the change in the molar lipid ratio would impact the physicochemical characteristics of LNP. The authors reported that by changing the helper phospholipid, the size and PDI are slightly affected, but using PEGylated lipids with a long anchor tail, larger LNPs were obtained. Regarding changing the molar ratio of lipids, the authors showed that by increasing the PEG content from 0.5% to 3% the LNPs size can be decreased about 2-fold. It's important to highlight that the EE% was not affected by any of the variables tested in the study.

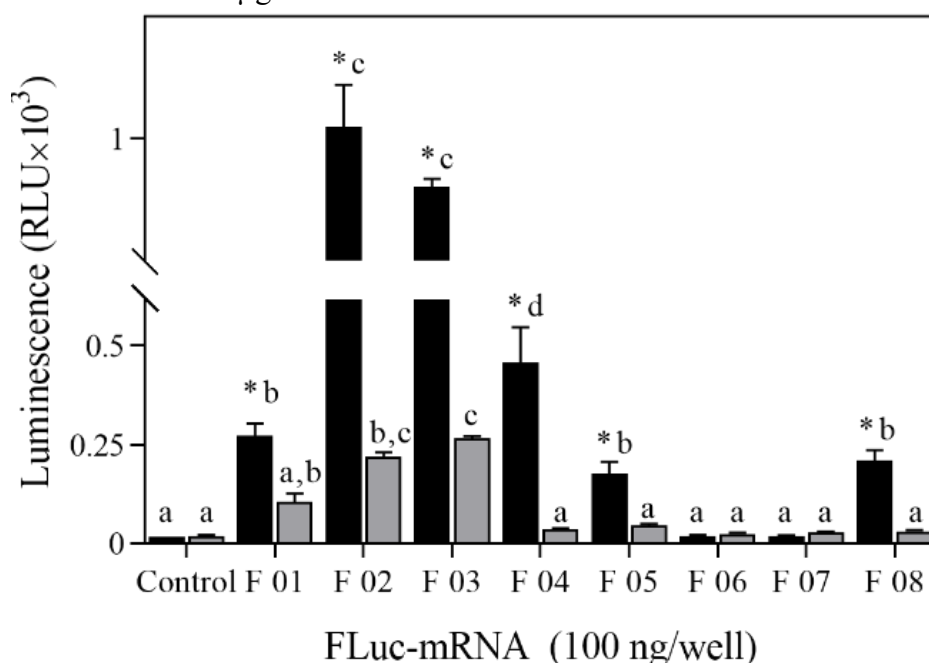
The absence of a difference in the properties of the formulations presented in Table 10 could be related to the high variability associated with the manual dropwise addition method used to make the LNPs (MARES et al., 2021; MEEWAN et al., 2022). Nevertheless, considering that the cellular

uptake of nanoparticles is size dependent (GENG et al., 2023; JI et al., 2023), this result is advantageous once that the aim of this assay was only to investigate how the chemical and structural differences of the lipids in the LNPs composition could impact the *in vitro* uptake by RAW 264.7 and K7M2 cells.

#### 4.2.2 *In Vitro* Formulation Screening on RAW 264.7 and K7M2 cells

The *in vitro* screening of the eight formulations mentioned in the prior section was performed, looking to investigate how the lipid combination in the formulation would impact on the *in vitro* bioluminescence generation mediated by FLuc-mRNA delivery. Figure 11 shows the bioluminescence signal on RAW 264.7 and K7M2 cells after 24 h treatment with LNPs loaded with Fluc-mRNA.

Figure 11 – Bioluminescence signal on RAW 264.7 (■) and K7M2 (▒) cells (n=3) after 24 h treatment with 100 µg of Fluc-mRNA loaded in different LNPs formulations



Notes:

\* Statistical difference  $p \leq 0.05$  between cell lines treated with the same LNPs formulation;  
 Different letters within the same color columns indicate difference  $p \leq 0.05$  among LNP formulations in the same cell line.

Observing Figure 11 for RAW 264.7 cells results allows to conclude that the replacement of the ionizable lipid DLin-MC3-DMA by SM-102 had a positive impact in all formulations, with F01-F04 promoting the FLuc expression and being statistically different from control and from

K7M2. However, using DLin-MC3-DMA only F05 and F08 promoted FLuc expression and were statistically different from the control and from K7M2 cells.

The results obtained for K7M2 cells in Figure 11 indicate that only when SM-102 was used in association with  $\beta$ -sitosterol, combined (F03) or not with cholesterol (F02), the bioluminescence signal generated was statistically different from the control. LNPs that used DLin-MC3-DMA (F05-F08) as ionizable lipid were not able to promote FLuc expression on K7M2 cells.

As could be observed, while F02, F03, and F04 were able to stimulate both RAW 264.7 and K7M2 cells, F1, F05, and F08 were able to generate a significant level of bioluminescence only in RAW 264.7. Also, F04 and F05, which have the same lipid mixture except for the ionizable lipid, presented a statistical difference in the bioluminescence signal with the SM-102 formulation promoting a Fluc expression about 2.5-fold higher.

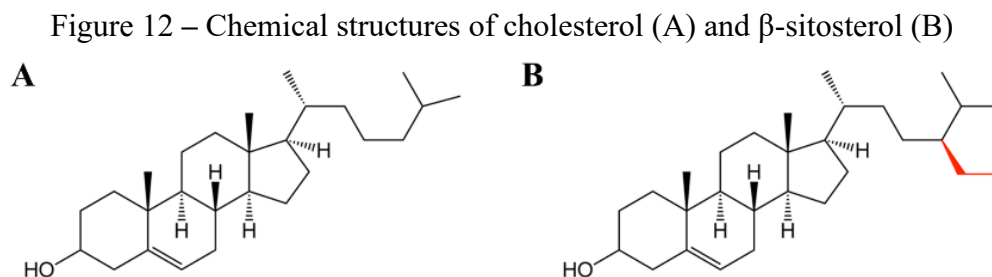
The enhanced results using SM-102 regarding DLin-MC3-DMA are rational since DLin-MC3-DMA was optimized for siRNA delivery, while SM-102 was designed focusing on mRNA. The best performance obtained by SM-102 formulations could be associated with two important aspects of the mRNA endosomal escape mechanism. First, the capacity to be back to the protonated state, and SM-102 (pKa 6.75) has a higher pKa than DLin-MC3-DMA (pKa 6.4), which can increase the number of SM-102 molecules in the protonated form found in the endosomal lumen (HALD ALBERTSEN et al., 2022; LY et al., 2022; MELAMED et al., 2023). In the endosome to lysosome pathway the pH ranges from 6.5 to 4.5, so as earlier the mRNA endosomal escape starts, lower the LNPs concentration that reach to the lysosomes, which are responsible for digest the LNPs and degrade the mRNA (HU et al., 2015; SCHLICH et al., 2021). Second, the SM-102 molecule was designed with a higher number of branches in ionizable lipid molecule than Dlin-MCE-DMA, which are associated to higher capacity of ionization of the amino headgroups, increasing the mRNA endosomal escape (FANG et al., 2022; HASHIBA et al., 2023).

Using SM-102, the presence of  $\beta$ -sitosterol promoted positive effects over the bioluminescence signal generated by the RAW 264.7 and K7M2 cells. F02 and F03, which had respectively  $\beta$ -sitosterol and  $\beta$ -sitosterol+cholesterol incorporated into the formulation presented the highest FLuc expression level among all the formulations and in both cell lines. While keeping DLin-MC3-DMA and changing cholesterol by  $\beta$ -sitosterol didn't have a significant impact over the FLuc expression in RAW 264.7.

Overall, cholesterol plays a crucial role in the development of lipid-based drug delivery systems, and its effects on the stability, size, and delivery efficacy of LNPs have been extensively studied (KAWAGUCHI et al., 2023; TENCHOV et al., 2021). Cholesterol influences the biophysical characteristics of unsaturated lipid membranes, increasing the rigidity of the bilayer (KIM et al.,

2022). When incorporated into ionizable LNP formulations, due to its poor solubility cholesterol is no longer liquid and is found as a microcrystal, which in turns influences the LNPs morphology and potentially contributes to the endosomal fusion (YANEZ ARTETA et al., 2018; YANG et al., 2022). Thus, the use of different types of sterols directly impacts mRNA release (PATEL et al., 2020). The substitution of cholesterol by  $\beta$ -sitosterol is documented as a promising strategy for enhancing nucleic acid delivery using lipid-based nanoparticles (EYGERIS et al., 2020; KIM et al., 2022; PATEL et al., 2020).

$\beta$ -sitosterol is a type of phytosterol molecule widely found in plants, being very similar in composition to cholesterol, with basically two extra carbons in the side chain (Figure 12) (KOHLMIEIER, 2013; RAKEL, 2018). The use of  $\beta$ -sitosterol promotes changes in the LNPs morphology and structure. Kim et al. (2022) tested how the switch from cholesterol to  $\beta$ -sitosterol impacts the LNPs morphology and reported that, using cholesterol the system is spherical and has uni-lamellar shapes, while using  $\beta$ -sitosterol it is polymorphic with polyhedral multi-lamellar shapes. These changes may increase the LNPs surface defects, which might contribute to the improvement of fusogenic properties with the endosome, where the nucleic acid release occurs (EYGERIS et al., 2020; PATEL et al., 2020).

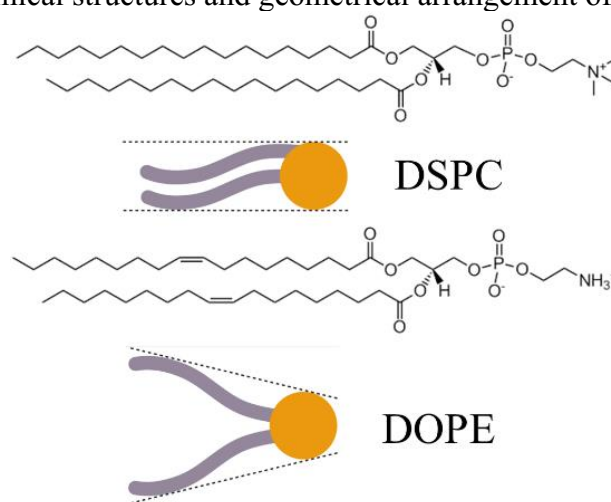


Source: (Author, 2023)

About the changes in the helper phospholipid, using SM-102 and cholesterol, the substitution of DSPC (F04) by DOPE (F01) didn't promote a statical change in the Fluc expression of K7M2 cells and promoted a decrease in the FLuc expression level in RAW 264.7. The combination of SM-102,  $\beta$ -sitosterol and DSPC was not tested. When using DLin-MC3-DMA as ionizable lipid, the treatment of Raw 264.7 cells with formulations containing DSPC (F05 and F08) promoted a statistically higher level of FLuc expression from control and from the other two formulations that used DLin-MC3-DMA (F06-F07). Also, the substitution of DSPC by DOPE apparently was harmful in association with DLin-MC3-DMA, independently of the sterol used, once no bioluminescence signal was generated by RAW 264.7 after being treated with F06 and F07.

The results presenting DSPC as a better helper lipid than DOPE in terms of FLuc expression in RAW 264.7 and K7M2 were unexpected. According to the literature, the use of DOPE as a helper phospholipid would be beneficial for the mRNA delivery efficacy of ionizable-based LNPs (GENG et al., 2023). DSPC is classified as a saturated phosphatidylcholine with a cylindrical molecular structure and, DOPE in turns is a cone shape unsaturated phosphatidylethanolamine (Figure 13) (HALD ALBERTSEN et al., 2022). The molecular structure of phosphatidylcholine is more associated with the formation of more stable lipid bilayers; while the enhanced fusogenic properties of DOPE are attributed to its conical geometry, which has a small head group, and to its capacity to be arranged as an inverted lipid phase (ÁLVAREZ-BENEDICTO et al., 2022; LONEZ et al., 2010).

Figure 13 – Chemical structures and geometrical arrangement of DSPC and DOPE

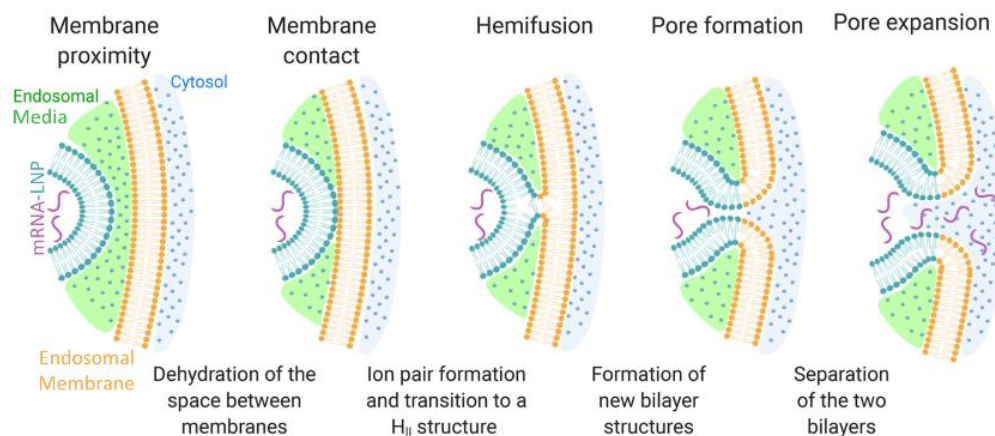


Source: (Author, 2023)

In the most accepted mRNA release mechanism (Figure 14), when the endocytosis pathway maturation initiates for the LNPs, the heads of the ionizable lipids become positively charged and begin to interact with the negatively charged lipids of the endosomal membrane. This interaction disorganizes the original conformation of the endosomal membrane and starts the formation of non-bilayer hexagonal ( $H_{II}$ ) structures, which, in turn, induce membranes fusion and disrupts the endosome, causing the mRNA release into the cytosol (ÁLVAREZ-BENEDICTO et al., 2022; SCHLICH et al., 2021).



Figure 14 – Proposed mechanism for mRNA-LNP endosomal escape



Source: Adapted from Schlich et al., (2021)

Nevertheless, it is important to highlight that the optimization of LNPs lipid composition is related to the target cell, tissue, or organ (CHENG et al., 2020; OKUDA et al., 2022). As shown by F02 and F03, which had the best performances in both cell lines, but in RAW 264.7 the Fluc expression was 4.5 and 3.5 times higher, respectively.

Medjmedj et al. (2022) tested how using DLin-MC3-DMA with different combinations of the helper phospholipid and sterol would impact the transfection of eGFP mRNA. The authors reported that in HEK cells there was no statistical difference in the transfection level promoted by DSPC+cholesterol, DOPE+cholesterol, or DOPE+ $\beta$ -sitosterol. But, in DC 2.4 cells and using the same combinations both formulations containing DOPE presented a transfection level at least 4-fold higher than the one with DSPC. Even though, the average transfected cells by the three formulations also were affected by cell line type, being 60 - 80% for HEK and 40 - 70% for DC 2.4.

Tuli (2023) investigated how the helper phospholipid interferes in the uptake of LNPs made of Dlin-MC3-DMA/cholesterol/DMG-PEG by RAW 264.7 cells. The author stimulated the macrophage cells from M0 to M1 or M2 and observed that the uptake level by M0 was statistically the same using DSPC, DOPC, or DOPE. However, in the M1 macrophages, DSPC had an uptake performance about 4-fold lower than DOPC and DOPE, which presented the same level. For M2 macrophages DSPC still presented the lowest uptake percentage, but this time DOPC had a statistically better performance than DOPE.

Cheng et al. (2020) proposed a LNPs formulation for nucleic acid delivery with the addition of a fifth lipid molecule, exclusively for selective organ targeting. The strategy named SORT had results suggesting that the use of the extra lipid to shift the charge of the delivery system, can drive the LNPs specifically to a target tissue using the same route of administration. The authors reported

that using the original DLin-MC3-DMA/Cholesterol/DSPC/DMG-PEG formulation the delivery occurs preferably in the liver with some LNP signal in the spleen. However, adding a fifth lipid as 30% of the negatively charged 1,2-dioleoyl-*sn*-glycero-3-phosphate the nanoparticles accumulate exclusively in the spleen, and using the extra lipid as 50% of the positively charged 1,2-dioleoyl-3-trimethylammonium-propane leads the formulation to be delivered exclusively to the lungs.

Thus, to the best of our knowledge, at least until date there is no mRNA LNP formulation able to have an optimized performance in all delivering sites. The success of mRNA delivery is intricately linked to the lipid components within the delivery system and the unique attributes of the intended delivery site. Therefore, specific and optimized LNP stands as a critical factor for advancing the field of the design of efficient mRNA delivery systems.

### 4.3 IONIZBLE LNPs PREPARED BY MICROFLUIDIC

#### 4.3.1 Nanoparticle characterization

Microfluidics have been extensively used for producing organic nanoparticles such as liposomes and polymeric nanoparticles, and this technique has been recently explored for the production of ionizable self-assembled lipid nanoparticles (KHOO et al., 2011; LIU et al., 2022). Microfluidic formulation of LNPs for mRNA loading allows controlled, rapid mixing of lipids (usually solubilized in ethanol) the nucleic acid cargo (typically in a low pH buffer) to generate particles with high encapsulation efficiency (frequently close to 100%), narrow size distribution and reproducible physicochemical properties (PILKINGTON et al., 2021). Also, microfluidics have the capability to generate a nanostructured system with higher performance characteristics, regarding conventional methods, such as dropwise addition (GIMONDI et al., 2023).

In this work, F05 was chosen for the studying of the microfluidics manufacture because the DLin-MC3-DMA:DSPC:cholesterol:DMG-PEG formulation was the first one approved for nucleic acid delivery by FDA, which made this formulation to be widely set as a benchmark of several research studies involving self-assembly ionizable LNPs and nucleic acid delivery (MENDONÇA et al., 2023). Consequently, the amount of data available to be used as guidance about physicochemical characteristics of this formulation is much higher than for formulations using SM-102.

Table 11, presents size, PDI, zeta potential, and mRNA encapsulation efficiency of F05 using the microfluidics and the dropwise addition approach.

Table 11 – Intensity mean diameter of nanoparticles (Dp), polydispersity index (PDI), Zeta potential ( $\xi$ ), and Encapsulation Efficiency (EE%) of F05 achieved with different manufacturing methods (n=4)

Dlin-MC3-DMA:DSCP:cholesterol:DMG-PEG		
Characteristic	Microfluidics	Dropwise*
Dp (nm)**	71 $\pm$ 7	116 $\pm$ 15
PDI	0.175 $\pm$ 0.049	0.132 $\pm$ 0.045
$\xi$ (mV)	-3.6 $\pm$ 1.3	-5.4 $\pm$ 2.6
EE (%)	90.3 $\pm$ 4.7	76.9 $\pm$ 17.6

Notes:

\*Two more replicates were added to the values presented previously in Table 10 for Dropwise results, totaling n=4 for both manufacture methods

\*\* Statistical difference in the row  $p \leq 0.05$

The use of microfluidics impacted the manufacture of the ionizable LNPs, producing nanoparticles significantly smaller than the dropwise addition method. The lower nanoparticle size obtained using microfluidics was also observed by Gimondi et al. (2022) and Mares et al. (2021) who reported that using this strategy the nanoparticles can reach sizes 0.5 and 2 times smaller compared to the manual dropwise addition technique. The PDI, zeta potential, and EE% were not significantly affected by the manufacture method used. However, microfluidics proved to be more reproducible compared to dropwise addition, as can be observed by the smaller deviation in size and EE% results. Zeta potential presented average results in agreement with the literature for this kind of formulation (CARRASCO et al., 2021; LY et al., 2022; YAVUZ et al., 2023), which has its colloidal stability provided by the PEGylated layer on the surface (JU et al., 2023).

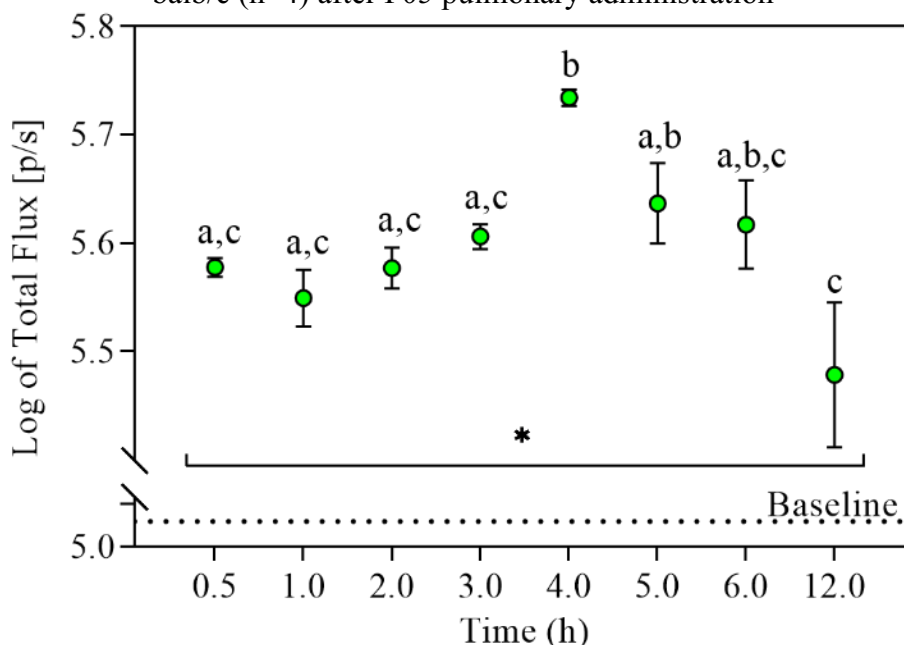
#### 4.3.2 *In Vivo* Lung Fluc Expression Profile

LNP formulation F05(DLin-MC3-DMA:DSCP:cholesterol:DMG-PEG) corresponds to the formulation of Onpattro®, which is a commercial pharmaceutical formulation designed and approved by the FDA to deliver siRNA into the liver, being clinically administered by intravenous route (FERRARESSO et al., 2022). However, the LNPs biodistribution is highly dependent on the route of administration (HAJJ et al., 2020), and looking for the lung as the drug target site, only 2 - 4% of the total drug dosage reaches the lungs when systemically administered (SULAIMAN, 2021). The pulmonary administration is the most efficient way to perform drug delivery into the lungs, but at the same time, the route also has multiple protective bio-barriers such as mucus, ciliated cells, and resident macrophages that limit drug's localization, penetration, and adsorption (LEE et al., 2015).

Thus, the FLuc-mRNA expression profile after pulmonary administration of F05 by the trachea was investigated. Figure 15 presents the *in vivo* FLuc expression profile in the lungs after

local administration of F05, containing 2  $\mu\text{g}$  of FLuc-mRNA. The bioluminescence signal was obtained from the thoracic area in BALB/c mice.

Figure 15 – *In vivo* bioluminescence signal profile obtained from FLuc mRNA (2  $\mu\text{g}$ ) expression on balb/c (n=4) after F05 pulmonary administration



Notes:

\* Statistical different from baseline  $p \leq 0.05$

Different letters mean Statistical difference within time points  $p \leq 0.05$

As can be observed in Figure 15, F05 was successfully delivered to the lungs. Fluc expression starts half an hour after F05 intratracheal administration, showing a bioluminescence peak at 4 h with the protein expression decreasing afterwards and reaching a lower level at 12 h than the first signal. All points presented a statistically significant increase in the bioluminescence signal regarding baseline, which corresponds to the natural bioluminescence signal from the animal. Except for 5 h and 6 h, at 4 h the bioluminescence signal was statistically higher than all the other time points. This bioluminescence profile agrees with the literature, which reports that the *in vivo* peak for encapsulated Fluc-mRNA is at 6 h post administration, with the signal starting to decrease around 12 h (DI et al., 2022; KAMIYA et al., 2022; MELAMED et al., 2022).

#### 4.3.3 Lung Fluc Expression and mRNA-LNP's Uptake Quantification *In Vivo*, *Ex Vivo*, and in BALF

Knowing that the LNPs could be delivered and detected in the lungs, LNPs biodistribution and FLuc expression on different sites of the respiratory tract after pulmonary administration of the

formulation was investigated. So, besides the *in vivo* analysis, the *ex vivo* and BALF quantification of FLuc expression and DiD' presence was performed, using two formulations: F05 and DiD'-F05. The second has incorporated DiD' as lipophilic fluorescent dye into formulation F05. The addition of DiD' was tested in an independent formulation to verify if the dye would affect F05 physicochemical properties (Table 12) and FLuc expression.

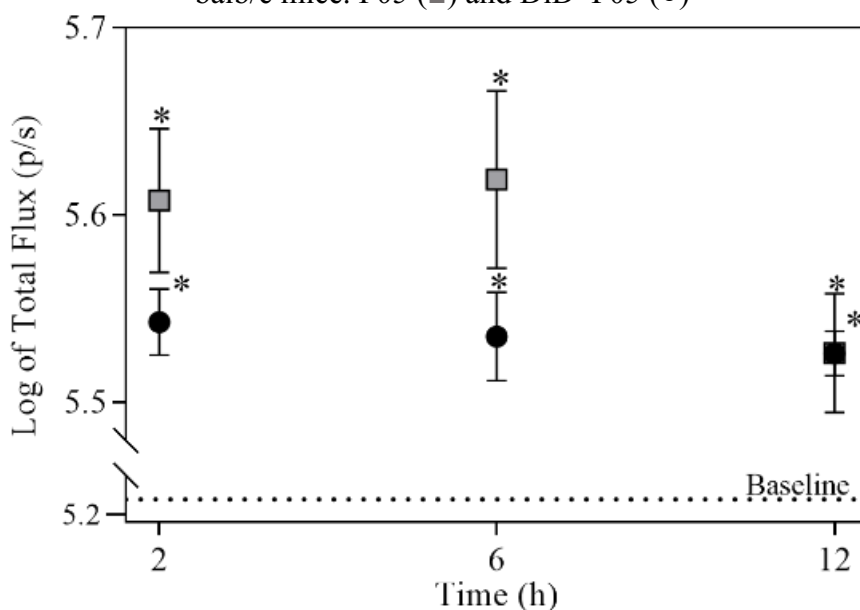
Table 12 – Intensity mean diameter of nanoparticles (Dp), polydispersity index (PDI), Zeta potential ( $\xi$ ), and Encapsulation Efficiency (EE%) of F05 and DiD'-F05

Formulation	Dp (nm)	PDI	$\xi$ (mV)	EE (%)
F05	71 $\pm$ 7	0.175 $\pm$ 0.049	-3.6 $\pm$ 1.3	90.3 $\pm$ 4.7
DiD'-F05	73	0.348	-1,2	88,7

As observed in Table 12, the incorporation of DiD' to F05 formulation affected only the polydispersity of the LNPs.

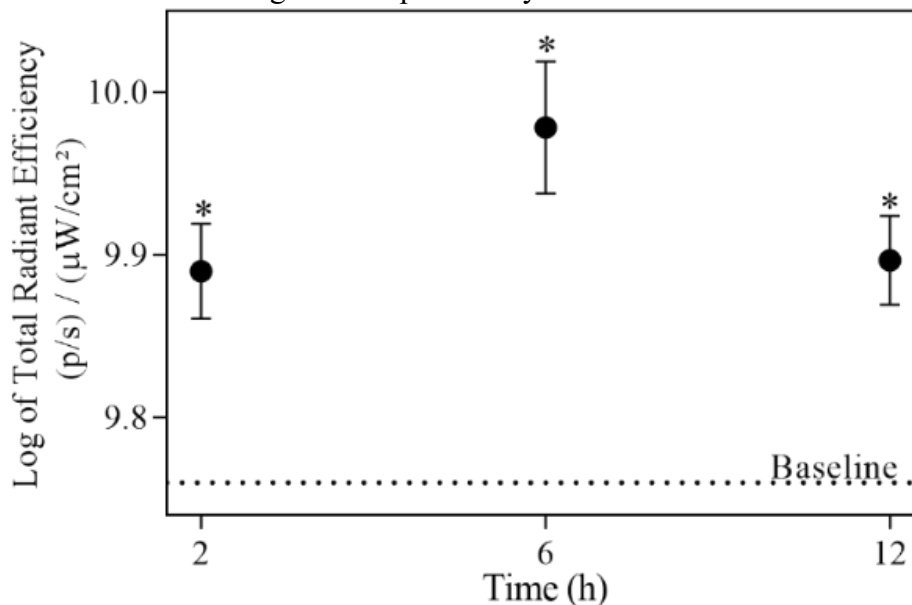
Figure 16 presents the *in vivo* quantification of Fluc expression in the lungs stimulated by F05 and DiD'-F05 containing 1  $\mu$ g of FLuc-mRNA on balb/c mice followed by Figure 17, which displays the fluorescent intensity of DiD' promoted by DiD'-F05 presence in the lungs, both measures were made at 2, 6 and 12 h post administration.

Figure 16 – *In vivo* bioluminescence signal after pulmonary administration of 1  $\mu$ g FLuc-mRNA on balb/c mice. F05 (■) and DiD'-F05 (●)



Notes:

\* Statistical different from baseline  $p \leq 0.05$   
2h and Baseline (n=9), 6 h (n=6), 12 h (n=3)

Figure 17 – *In vivo* fluorescent signal after pulmonary administration of DiD'-F05 on balb/c mice

Notes:

\* Statistical different from baseline  $p \leq 0.05$   
 2 h and Baseline (n=9), 6 h (n=6), 12 h (n=3)

As can be observed in Figure 16, the lung bioluminescence signal was statistically increased by both formulations compared to baseline at all the evaluated times. The incorporation of DiD' to the formulation didn't affect the *in vivo* bioluminescence signal, indicating that the fluorescent dye didn't affect the FLuc expression, even with DiD'-F05 presenting a higher polydispersity. This result is corroborated by Figure 17, which shows a significant increase in the animal's fluorescent signal after the administration of DiD'-F05, indicating the presence and uptake of DiD'-F05 in the lungs.

Figure 18 presents the *ex vivo* quantification of Fluc expression in the lungs stimulated by F05 and DiD'-F05 containing 1 μg of FLuc-mRNA on balb/c mice followed by Figure 19, which displays the fluorescent intensity of DiD' promoted by DiD'-F05 presence in the lungs, both measures were made at 2, 6 and 12 h post administration.

Figure 18 – *Ex vivo* bioluminescence signal after pulmonary administration of 1  $\mu\text{g}$  FLuc-mRNA on balb/c (n=3) mice. F05 (■) and DiD'-F05 (●)

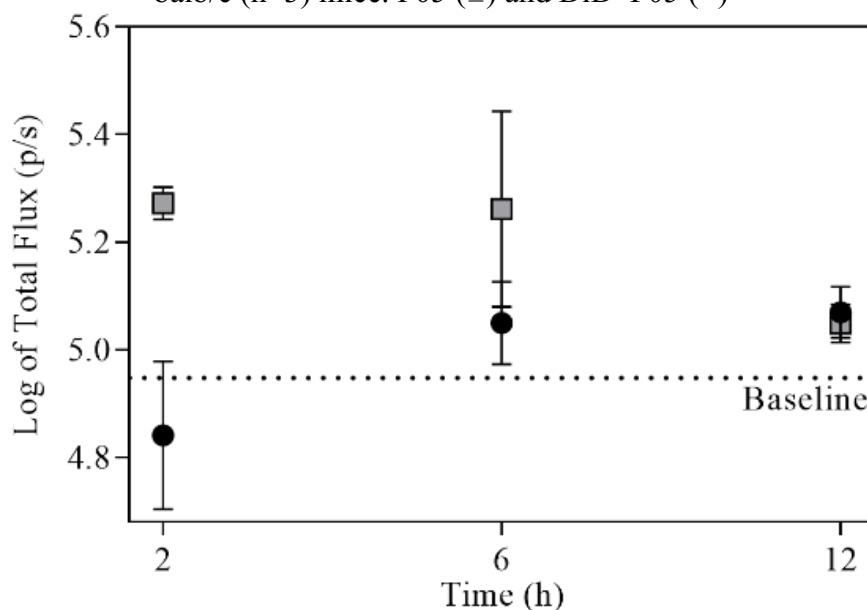
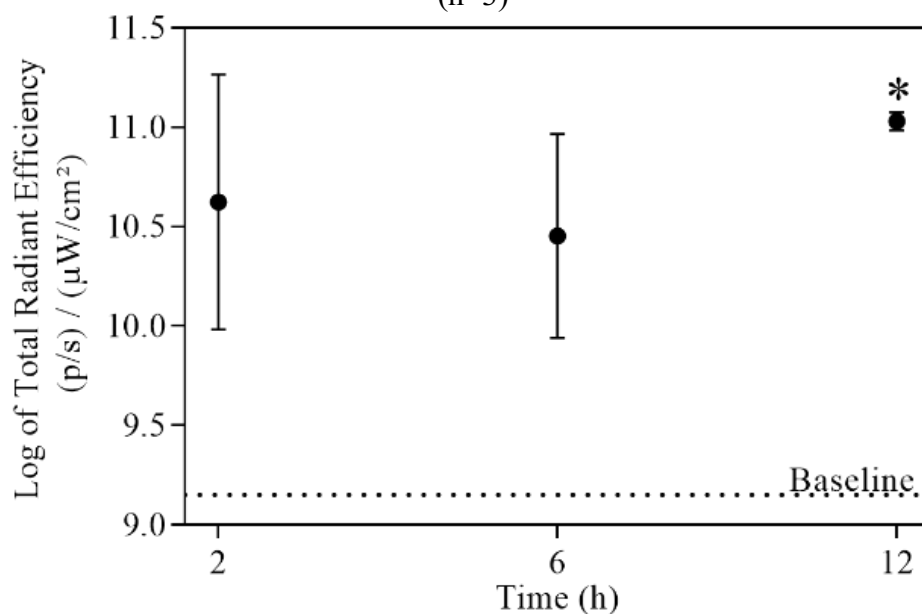


Figure 19 – *Ex vivo* fluorescent signal after pulmonary administration of DiD'-F05 on balb/c mice (n=3)



Notes:

\* Statistical different from baseline  $p \leq 0.05$

As can be observed in Figure 18, the lung bioluminescence signal was slightly higher than baseline 2 and 6 h after F05 administration but had a value close to baseline at 12 h. Fluc expression induced by F05 observed *ex vivo*, agrees with the results of Zhang et al. (2020), who reported the generation of a similar *ex vivo* bioluminescence level in the lungs 6 h after P.A. of 1.5  $\mu\text{g}/\text{mouse}$  of Fluc-mRNA using a similar ionizable LNPs composition.

The signal coming from DiD'-F05 administration was close to baseline values at all times. Yet, even without presenting a clear sign of FLuc expression, Figure 19 shows that the administration of DiD'-F05 increased the fluorescent signal coming from the lungs, with a significant difference from baseline at 12 h, indicating that LNPs were uptaken in the lungs tissue.

The FLuc-mRNA dose reduction from 2  $\mu\text{g}/\text{mouse}$  to 1  $\mu\text{g}/\text{mouse}$  promoted a slight decrease in the bioluminescence intensity. However, both formulations presented an unexpected decrease in the *ex vivo* bioluminescence signal compared to *in vivo*. The removal of animal fur, skin, and muscle should lead to a more powerful and accurate detection of bioluminescence signal (ZHANG et al., 2017). This could be related to the delay between the *in vivo* and *ex vivo* imaging. According to Pan et al. (2018) and Luker & Luker (2008), the bioluminescence detection of Fluc using D-luciferin as substrate has its peak around 10 min post substrate administration, which is the waiting time between D-luciferin injection and the first *in vivo* imaging. Also, D-luciferin suppliers suggest that protocols for the quantification of the enzymatic reaction of Fluc and D-luciferin should be done within 10 min (ANTIBODIES-ONLINE, 2023; BIO-CONNECT, 2022; MERCK, 2023).

Figure 20 presents the quantification of Fluc expression in the BALF stimulated by F05 and DiD'-F05 containing 1  $\mu\text{g}$  of FLuc-mRNA, followed by Figure 21, which displays the fluorescent intensity of DiD' promoted by DiD'-F05 presence in BALF, both measures were made at 2, 6 and 12 h post administration.

Figure 20 – BALF bioluminescence signal after pulmonary administration of 1  $\mu\text{g}$  FLuc-mRNA on balb/c (n=3) mice. F05 (■) and DiD'-F05 (●)

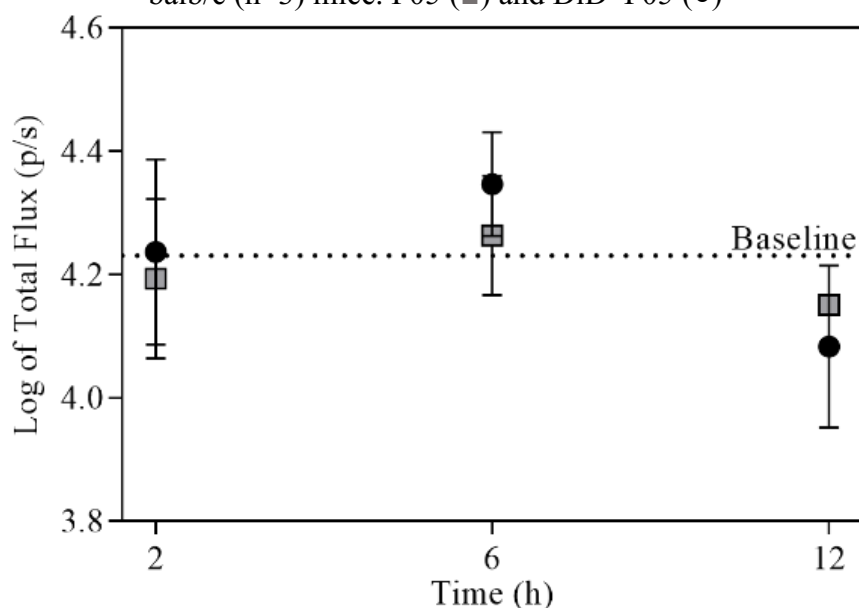
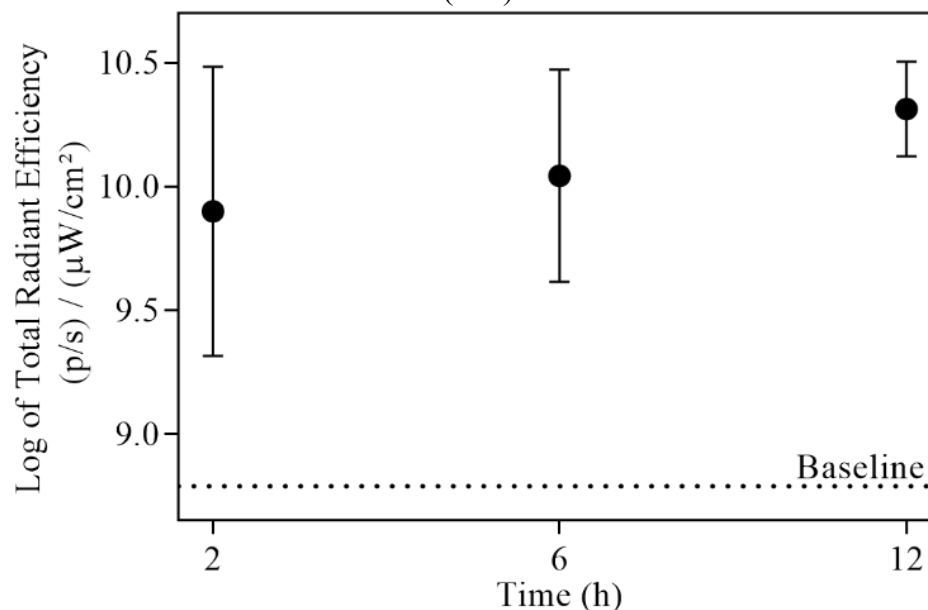




Figure 21 – BALF fluorescent signal after pulmonary administration of DiD'-F05 on balb/c mice (n=3)



As shown in Figure 20, both formulations presented a bioluminescence signal close to the baseline, indicating no FLuc expression on the BALF. However, Figure 21 indicates the presence of DiD'-F05 in the BALF, as seen by the increase in the fluorescent signal coming from the BALF, which also presents an increasing tendency until reaching the highest value at 12 h. Again, the absence of bioluminescence from FLuc expression could be related to the delay between the *in vivo* D-Luciferin administration and the BALF collection and imaging.

## CHAPTER V

### 5 CONCLUSION

The production of lipid nanoparticles for macrophage-based immunotherapy and pulmonary lung delivery was explored using different approaches. Initially, Renilla-Luc-mRNA was encapsulated in LNPs prepared using the W/O/W double emulsion approach associated with melt dispersion. However, two drawbacks were observed: 1) the encapsulation of Renilla-Luc-mRNA was compromised, because the gel electrophoresis analysis indicated the presence of Renilla-Luc-mRNA inside the LNPs, but with some signals of degradation; and 2) this formulation proved to be cytotoxic to HEK 293T cells, promoting the total inhibition of the cells at all tested concentrations. Thus, the use of beeswax, soy lecithin, and Crodamol for mRNA encapsulation by the W/O/W double emulsion approach associated with melt dispersion using an ultrasonic probe to promote the emulsification is not appropriate for the intended application, considering the proposed formulations.

Following, Renilla-Luc-mRNA was encapsulated in LNPs prepared using the W/O/W double emulsion approach, but this time the lipid matrix was made only of soy lecithin and a liquid lipid (Crodamol), and an inverted ultrasound probe apparatus was used to promote the emulsification under milder temperature conditions. The modifications made in the formulation and emulsification conditions positively affected the LNPs formation and Renilla-Luc-mRNA loading. The lower viscosity enhanced the cellular tolerance to the formulation, but no protein expression was detected, which could be related to the low encapsulation efficiency and to the ability of soy lecithin and Crodamol to properly promote the mRNA endosomal escape. Therefore, this formulation is promising for mRNA encapsulation using the W/O/W double emulsion technique with an inverted ultrasound probe apparatus to promote the emulsification, but further work needs to be done in order to increase the mRNA encapsulation efficiency and to promote the *in vitro* mRNA expression.

Changing the focus from proposing an alternative LNPs formulation and approach for mRNA encapsulation, two types of ionizable lipids, helper phospholipids and sterol lipids were screened *in vitro* for macrophages targeting using the self-assembly dropwise addition approach. The LNP formulations containing SM-102 as ionizable lipid presented a higher protein expression, and the use and  $\beta$ -sitosterol enhanced its performance compared to Cholesterol. The combination of SM-102, DOPE, and  $\beta$ -sitosterol had the highest overall transfection in RAW 264.7 cells. Thus, the higher branching of SM-102, the conical molecular geometry of DOPE, and the incorporation of  $\beta$ -sitosterol to the LNPs shell proved to have a positive effect over the LNPs capability to promote FLuc-mRNA

expression. However, the effect of the addition of DOPE to the LNPs formulation needs to be further investigated, as a function of the lipid's mixture.

Finally, the pulmonary administration of the self-assembly LNPs was investigated *in vivo* using DLin-MC3-DMA/DSPC/Cholesterol/DMG-PEG formulation loaded with FLuc-mRNA and prepared using a microfluidic system, which positively affected the LNPs formation and encapsulation efficiency. The LNPs successfully delivered the mRNA to the lungs and the protein expression profile revealed a bioluminescence peak in the mice's lung at 6 h.

Last, mRNA expression and LNPs presence were identified in the *in vivo* and *ex vivo* lung tissues, but only the LNPs fluorescence signal was detected in the BALF of the animals. So, further studies need to be done to investigate and precisely identify the site of LNPs delivery and FLuc-mRNA expression after intratracheal administration. Therefore, LNPs are a promising strategy to promote the direct delivery of mRNA to the lungs, and focusing on anticancer medicines the adjustment of the lipid formulation can be used as an advantage to target deliver the LNPs, exploring the vast macrophage population in the tumor microenvironment as immunotherapy tool.

## 6 FURTHER SUGGESTIONS

The use of soy lecithin as an ionizable molecule for mRNA encapsulation could be explored in a different lipid matrix. The addition of a second amino holder lipid, such as DSPC or DOPE could benefit the formulation regarding the encapsulation efficiency level and mRNA transfection. Also, using a helper phospholipid associated with soy lecithin could impact the N/P range necessary to use soy lecithin as an ionizable lipid. The production of lipid nanoparticles using soy lecithin and Crodamol using the dropwise addition and microfluidic approach would be interesting to verify the capability of these lipids to be used in a self-assembly formulation as well for continuous manufacturing.

The screening of ionizable lipid-based formulations could be expanded to other cells that are found in the tumor microenvironment, to deeply understand the effectiveness of targeting the macrophages. In addition to the mRNA expression, the cellular viability of the cells after being treated with the screened LNPs also should be quantified, searching for possible cytotoxic combinations of lipids. The *in vivo* mRNA transfection could be further explored using a 3D co-culture cell model, using multiple cells founded in the tumor microenvironment. This approach would be able to explore the LNPs uptake, infiltration, cell targeting delivery, and mRNA expression in a more realistic system, increasing the translation level of *in vitro* results to *in vivo*. The DiD' could be incorporated

into the nucleic acid chain, making it possible to track the LNPs during the delivery, the mRNA transfection, and expression.

Other ionizable lipids-based formulations should be screened specifically for pulmonary administration due to the challenges associated with the singularity of the pulmonary obstacles. Biodistribution could be further investigated using flowcytometry in the BALF, indicating in which cells the LNPs are preferably being delivered. Also, moving forward for an *in vivo* tumor model study, the *ex vivo* study of the LNPs biodistribution and mRNA expression would be helpful to understand how deeply inside the lungs the LNPs could be deposited and absorbed. The resection and flowcytometry processing of the tumor nodules could be used to investigate the targeting delivery of mRNA loading LNPs to tumor-associated macrophages.

## REFERENCES

AGBAVWE, C.; SOMOZA, M. M. Sequence-Dependent Fluorescence of Cyanine Dyes on Microarrays. **PLoS ONE**, v. 6, n. 7, p. e22177, 25 jul. 2011.

AKINC, A. et al. **The Onpattro story and the clinical translation of nanomedicines containing nucleic acid-based drugs**. **Nature Nanotechnology** Nature Research, , 1 dez. 2019. Disponível em: <[www.nature.com/naturenanotechnology](http://www.nature.com/naturenanotechnology)>. Acesso em: 29 mar. 2021

ALI, M. S. et al. Microfluidics for Development of Lipid Nanoparticles: Paving the Way for Nucleic Acids to the Clinic. **ACS Applied Bio Materials**, 18 set. 2021.

ALMUQBIL, R. M. **Overcoming Mechanisms of Acquired and Innate Doxorubicin Resistance Using Nanomedicine and Tumor-Associated Macrophage Immunotherapy**. [s.l.] Virginia Commonwealth University, 2021.

ÁLVAREZ-BENEDICTO, E. et al. Optimization of phospholipid chemistry for improved lipid nanoparticle (LNP) delivery of messenger RNA (mRNA). **Biomaterials Science**, v. 10, n. 2, p. 549–559, 2022.

AMIN, M. et al. Thermal properties of beeswax/graphene phase change material as energy storage for building applications. **Applied Thermal Engineering**, v. 112, p. 273–280, fev. 2017.

ANGELINI, G. et al. Neutral liposomes containing crown ether-lipids as potential DNA vectors. **Biochimica et Biophysica Acta (BBA) - Biomembranes**, v. 1828, n. 11, p. 2506–2512, nov. 2013.

ANTIBODIES-ONLINE. **Luciferase Reporter Gene Assay Kit**. Disponível em: <<https://www.antibodies-online.com/kit/1000341/Luciferase+Reporter+Gene+Assay+Kit/>>.

AZMI, N. A. N. et al. Nanoemulsions: Factory for Food, Pharmaceutical and Cosmetics. **Processes**, v. 7, n. 9, p. 617, 11 set. 2019.

BANCOS, S.; TYNER, K. M. Evaluating the effect of assay preparation on the uptake of gold nanoparticles by RAW264.7 cells. **Journal of Nanobiotechnology**, v. 12, n. 1, p. 45, 26 nov. 2014.

BARBA, A. A. et al. Lipid Delivery Systems for Nucleic-Acid-Based-Drugs: From Production to Clinical Applications. **Pharmaceutics**, v. 11, n. 8, p. 360, 24 jul. 2019.

BATTAGLIA, L. et al. Application of lipid nanoparticles to ocular drug delivery. **Expert Opinion on Drug Delivery**, v. 13, n. 12, p. 1743–1757, 1 dez. 2016.

BECKER PERES, L. **SÍNTESE DE POLÍMEROS A PARTIR DE AMINOÁCIDOS E O DESENVOLVIMENTO DE SISTEMAS NANOPARTICULADOS PARA**

**ENCAPSULAÇÃO DE FÁRMACOS.** [s.l.] Universidade Federal de Santa Catarina, 2016.

BECKER PERES, L. et al. Solid lipid nanoparticles for encapsulation of hydrophilic drugs by an organic solvent free double emulsion technique. **Colloids and Surfaces B: Biointerfaces**, v. 140, p. 317–323, 1 abr. 2016.

BEDORET, D. et al. Lung interstitial macrophages alter dendritic cell functions to prevent airway allergy in mice. **Journal of Clinical Investigation**, v. 119, n. 12, p. 3723–3738, 1 dez. 2009.

BIO-CONNECT. **Thermostable luciferase for sensitive microbiology assays.** Disponível em: <<https://www.bio-connect.nl/news/thermostable-luciferase-for-sensitive-microbiology-assays/>>.

BIOTIUM. **Technology - Luciferase Assays.** Disponível em: <<https://biotium.com/technology/luciferase-assays/>>.

BLAKNEY, A. K. et al. The Skin You Are In: Design-of-Experiments Optimization of Lipid Nanoparticle Self-Amplifying RNA Formulations in Human Skin Explants. **ACS Nano**, v. 13, n. 5, p. 5920–5930, 28 maio 2019.

BOUTILIER, A. J.; ELSAWA, S. F. Macrophage Polarization States in the Tumor Microenvironment. **International Journal of Molecular Sciences**, v. 22, n. 13, 1 jul. 2021.

BRADER, M. L. et al. Encapsulation state of messenger RNA inside lipid nanoparticles. **Biophysical Journal**, v. 120, n. 14, p. 2766–2770, jul. 2021.

BUSCHMANN, M. D. et al. Nanomaterial Delivery Systems for mRNA Vaccines. **Vaccines**, v. 9, n. 1, p. 65, 19 jan. 2021.

CAMPANI, V.; GIARRA, S.; DE ROSA, G. Lipid-based core-shell nanoparticles: Evolution and potentialities in drug delivery. **OpenNano**, v. 3, p. 5–17, 1 jan. 2018.

CARRASCO, M. J. et al. Ionization and structural properties of mRNA lipid nanoparticles influence expression in intramuscular and intravascular administration. **Communications Biology**, v. 4, n. 1, p. 956, 11 ago. 2021.

CENDROWICZ, E. et al. The Role of Macrophages in Cancer Development and Therapy. **Cancers**, v. 13, n. 8, 2 abr. 2021.

CHENG, Q. et al. Selective organ targeting (SORT) nanoparticles for tissue-specific mRNA delivery and CRISPR–Cas gene editing. **Nature Nanotechnology**, v. 15, n. 4, p. 313–320, 1 abr. 2020.

CLEMENTINO, A. R. et al. Structure and Fate of Nanoparticles Designed for the Nasal Delivery of Poorly Soluble Drugs. **Molecular Pharmaceutics**, v. 18, n. 8, p. 3132–3146, 2 ago. 2021.

COFFEY, J. W.; GAIHA, G. DAS; TRAVERSO, G. Oral Biologic Delivery: Advances Toward Oral Subunit, DNA, and mRNA Vaccines and the Potential for Mass Vaccination During Pandemics. **Annual Review of Pharmacology and Toxicology**, v. 61, n. 1, p. 517–540, 6 jan. 2021.

CORDEIRO, A. P. et al. In vitro synergic activity of diethyldithiocarbamate and 4-nitrochalcone loaded in beeswax nanoparticles against melanoma (B16F10) cells. **Materials Science and Engineering: C**, v. 120, p. 111651, jan. 2021.

CROMBEZ, L. et al. Peptide-Based Nanoparticle for Ex Vivo and In Vivo Drug Delivery. 2008.

DALBY, B. Advanced transfection with Lipofectamine 2000 reagent: primary neurons, siRNA, and high-throughput applications. **Methods**, v. 33, n. 2, p. 95–103, jun. 2004.

DANAEI, M. et al. Impact of Particle Size and Polydispersity Index on the Clinical Applications of Lipidic Nanocarrier Systems. **Pharmaceutics**, v. 10, n. 2, p. 57, 18 maio 2018.

DATE, T. et al. Lipid-polymer hybrid nanocarriers for delivering cancer therapeutics. **Journal of Controlled Release**, v. 271, p. 60–73, fev. 2018.

DAVIS, L. G.; DIBNER, M. D.; BATTEY, J. F. Agarose Gel Electrophoresis. In: **Basic Methods in Molecular Biology.** [s.l.] Elsevier, 1986. p. 58–61.

DE GROOT, A. M. et al. Immunogenicity Testing of Lipidoids In Vitro and In Silico: Modulating Lipidoid-Mediated TLR4 Activation by Nanoparticle Design. **Molecular Therapy -**

**Nucleic Acids**, v. 11, p. 159–169, 1 jun. 2018.

DI, J. et al. Biodistribution and Non-linear Gene Expression of mRNA LNPs Affected by Delivery Route and Particle Size. **Pharmaceutical Research**, v. 39, n. 1, p. 105–114, 26 jan. 2022.

DOKTOROVOVA, S.; SOUTO, E. B.; SILVA, A. M. Nanotoxicology applied to solid lipid nanoparticles and nanostructured lipid carriers – A systematic review of in vitro data. **European Journal of Pharmaceutics and Biopharmaceutics**, v. 87, n. 1, p. 1–18, maio 2014.

DONG, H. et al. Preparation and characterization of nanoparticles from field pea starch by batch versus continuous nanoprecipitation techniques. **Food Hydrocolloids**, v. 122, p. 107098, 1 jan. 2022.

DOS SANTOS, P. C. M. et al. Antitumor activity associated with hyperthermia and 4-nitrochalcone loaded in superparamagnetic poly(thioether-ester) nanoparticles. **Journal of Biomaterials Science, Polymer Edition**, v. 31, n. 15, p. 1895–1911, 12 out. 2020.

DUAN, Q. et al. How far are the new wave of mRNA drugs from us? mRNA product current perspective and future development. **Frontiers in Immunology**, v. 13, 12 set. 2022.

EKAMBARAM, P.; SATHALI, A. A. H.; PRIYANKA, K. Solid Lipid Nanoparticles : a Review. **Scientific Reviews & Chemical Communications**, 2012.

ERASMUS, J. H. et al. A Nanostructured Lipid Carrier for Delivery of a Replicating Viral RNA Provides Single, Low-Dose Protection against Zika. **Molecular Therapy**, v. 26, n. 10, p. 2507–2522, out. 2018.

ESCALONA-RAYO, O. et al. In vitro and in vivo evaluation of clinically-approved ionizable cationic lipids shows divergent results between mRNA transfection and vaccine efficacy. **Biomedicine & Pharmacotherapy**, v. 165, p. 115065, set. 2023.

EUN, H.-M. Nucleases. In: **Enzymology Primer for Recombinant DNA Technology**. [s.l.] Elsevier, 1996. p. 145–232.

EYGERIS, Y. et al. Deconvoluting Lipid Nanoparticle Structure for Messenger RNA Delivery. **Nano Letters**, v. 20, n. 6, p. 4543–4549, 10 jun. 2020.

FANG, E. et al. Advances in COVID-19 mRNA vaccine development. **Signal Transduction and Targeted Therapy**, v. 7, n. 1, p. 94, 23 mar. 2022.

FEI, Q. et al. Macrophage-Targeted Lipid Nanoparticle Delivery of microRNA-146a to Mitigate Hemorrhagic Shock-Induced Acute Respiratory Distress Syndrome. **ACS Nano**, v. 17, n. 17, p. 16539–16552, 12 set. 2023.

FERNANDES, F. et al. Critical Review of Lipid-Based Nanoparticles as Carriers of Neuroprotective Drugs and Extracts. **Nanomaterials**, v. 11, n. 3, p. 563, 24 fev. 2021.

FERRARESSO, F. et al. Comparison of DLin-MC3-DMA and ALC-0315 for siRNA Delivery to Hepatocytes and Hepatic Stellate Cells. **Molecular Pharmaceutics**, v. 19, n. 7, p. 2175–2182, 4 jul. 2022.

FRATINI, F. et al. Beeswax: A minireview of its antimicrobial activity and its application in medicine. **Asian Pacific Journal of Tropical Medicine**, v. 9, n. 9, p. 839–843, 1 set. 2016.

GALATEANU, B. et al. Impact of multicellular tumor spheroids as an in vivo-like tumor model on anticancer drug response. **International Journal of Oncology**, v. 48, n. 6, p. 2295–2302, jun. 2016.

GANESAN, P.; NARAYANASAMY, D. Lipid nanoparticles: Different preparation techniques, characterization, hurdles, and strategies for the production of solid lipid nanoparticles and nanostructured lipid carriers for oral drug delivery. **Sustainable Chemistry and Pharmacy**, v. 6, p. 37–56, 1 dez. 2017.

GARCÊS, A. et al. **Formulations based on solid lipid nanoparticles (SLN) and nanostructured lipid carriers (NLC) for cutaneous use: A review**. **European Journal of Pharmaceutical Sciences** Elsevier B.V., , 15 jan. 2018. Disponível em: <<https://pubmed.ncbi.nlm.nih.gov/29183800/>>. Acesso em: 17 mar. 2021

GASPAR, R.; COELHO, F.; SILVA, B. F. B. Lipid-Nucleic Acid Complexes:

Physicochemical Aspects and Prospects for Cancer Treatment. **Molecules**, v. 25, n. 21, p. 5006, 28 out. 2020.

GEBRE, M. S. et al. Novel approaches for vaccine development. **Cell**, v. 184, n. 6, p. 1589–1603, mar. 2021.

GENG, L. et al. Influence of lipid composition of messenger RNA-loaded lipid nanoparticles on the protein expression via intratracheal administration in mice. **International Journal of Pharmaceutics**, v. 637, p. 122896, abr. 2023.

GHASEMIYEH, P.; MOHAMMADI-SAMANI, S. Solid lipid nanoparticles and nanostructured lipid carriers as novel drug delivery systems: applications, advantages and disadvantages. **Research in Pharmaceutical Sciences**, v. 13, n. 4, p. 288, 1 ago. 2018.

GIMONDI, S. et al. Microfluidic-driven mixing of high molecular weight polymeric complexes for precise nanoparticle downsizing. **Nanomedicine: Nanotechnology, Biology and Medicine**, v. 43, p. 102560, jul. 2022.

GIMONDI, S. et al. Microfluidic Devices: A Tool for Nanoparticle Synthesis and Performance Evaluation. **ACS Nano**, v. 17, n. 15, p. 14205–14228, 8 ago. 2023.

GORDILLO-GALEANO, A.; MORA-HUERTAS, C. E. Solid lipid nanoparticles and nanostructured lipid carriers: A review emphasizing on particle structure and drug release. **European Journal of Pharmaceutics and Biopharmaceutics**, v. 133, p. 285–308, 1 dez. 2018.

GOTTESMAN, M. M.; FOJO, T.; BATES, S. E. Multidrug resistance in cancer: role of ATP-dependent transporters. **Nature Reviews Cancer**, 2002.

GOUDAR, V. S. et al. Impact of a Desmoplastic Tumor Microenvironment for Colon Cancer Drug Sensitivity: A Study with 3D Chimeric Tumor Spheroids. **ACS Applied Materials & Interfaces**, v. 13, n. 41, p. 48478–48491, 20 out. 2021.

GREENWOOD, M. S.; BAMBERGER, J. A. Measurement of viscosity and shear wave velocity of a liquid or slurry for on-line process control. **Ultrasonics**, v. 39, n. 9, p. 623–630, ago. 2002.

GUEVARA, M. L.; PERSANO, F.; PERSANO, S. Advances in Lipid Nanoparticles for mRNA-Based Cancer Immunotherapy. **Frontiers in Chemistry**, v. 8, p. 589959, 23 out. 2020.

HAIDER, M. et al. Nanostructured Lipid Carriers for Delivery of Chemotherapeutics: A Review. **Pharmaceutics**, v. 12, n. 3, p. 288, 23 mar. 2020.

HAJJ, K. A. et al. A Potent Branched-Tail Lipid Nanoparticle Enables Multiplexed mRNA Delivery and Gene Editing In Vivo. **Nano Letters**, v. 20, n. 7, p. 5167–5175, 8 jul. 2020.

HAJJ, K. A.; WHITEHEAD, K. A. Tools for translation: non-viral materials for therapeutic mRNA delivery. **Nature Reviews Materials**, v. 2, n. 10, p. 17056, 12 out. 2017.

HALD ALBERTSEN, C. et al. The role of lipid components in lipid nanoparticles for vaccines and gene therapy. **Advanced Drug Delivery Reviews**, v. 188, p. 114416, set. 2022.

HAN, X. et al. An ionizable lipid toolbox for RNA delivery. . 13 dez. 2021, p. 1–6.

HASHIBA, K. et al. Branching Ionizable Lipids Can Enhance the Stability, Fusogenicity, and Functional Delivery of mRNA. **Small Science**, v. 3, n. 1, 9 jan. 2023.

HASSETT, K. J. et al. Optimization of Lipid Nanoparticles for Intramuscular Administration of mRNA Vaccines. **Molecular Therapy - Nucleic Acids**, v. 15, p. 1–11, abr. 2019.

HEINE, A.; JURANEK, S.; BROSSART, P. **Clinical and immunological effects of mRNA vaccines in malignant diseases**. **Molecular CancerBioMed Central Ltd**, , 1 dez. 2021. Disponível em: <<https://doi.org/10.1186/s12943-021-01339-1>>. Acesso em: 2 jun. 2021

HIRAYAMA, D.; IIDA, T.; NAKASE, H. The Phagocytic Function of Macrophage-Enforcing Innate Immunity and Tissue Homeostasis. **International Journal of Molecular Sciences**, v. 19, n. 1, 1 jan. 2018.

HONG, S. et al. Protein-Based Nanoparticles as Drug Delivery Systems. **Pharmaceutics**, v. 12, n. 7, p. 604, 29 jun. 2020.

HOU, X. et al. Lipid nanoparticles for mRNA delivery. **Nature Reviews Materials 2021**

6:12, v. 6, n. 12, p. 1078–1094, 10 ago. 2021.

HU, Y.-B. et al. The endosomal-lysosomal system: from acidification and cargo sorting to neurodegeneration. **Translational Neurodegeneration**, v. 4, n. 1, p. 18, 30 dez. 2015.

IBBA, M. L. et al. Advances in mRNA non-viral delivery approaches. **Advanced Drug Delivery Reviews**, v. 177, p. 113930, out. 2021.

INC, M. **Moderna and Merck Announce mRNA-4157/V940, an Investigational Personalized mRNA Cancer Vaccine, in Combination With KEYTRUDA(R) (pembrolizumab), was Granted Breakthrough Therapy Designation by the FDA for Adjuvant Treatment of Patients With High-Risk Mela.** Disponível em: <<https://www.accesswire.com/740413/Moderna-and-Merck-Announce-mRNA-4157V940-an-Investigational-Personalized-mRNA-Cancer-Vaccine-in-Combination-With-KEYTRUDAR-pembrolizumab-was-Granted-Breakthrough-Therapy-Designation-by-the-FDA-for-Adjuvant-Treatment-of-Pa>>. Acesso em: 12 jun. 2023.

ISLAM, M. A. et al. Biomaterials for mRNA delivery. **Biomaterials Science**, v. 3, n. 12, p. 1519–1533, 1 dez. 2015.

ISO 10993-5:2009. **Biological Evaluation of Medical Devices. Part 5: Tests for In Vitro Cytotoxicity.** Geneva, Switzerland: [s.n.].

JAIN, K. K. An Overview of Drug Delivery Systems. In: [s.l: s.n.]. p. 1–54.

Jl, A. et al. Lipid Microparticles Show Similar Efficacy With Lipid Nanoparticles in Delivering mRNA and Preventing Cancer. **Pharmaceutical Research**, v. 40, n. 1, p. 265–279, 30 jan. 2023.

JU, Y. et al. Impact of anti-PEG antibodies induced by SARS-CoV-2 mRNA vaccines. **Nature Reviews Immunology**, v. 23, n. 3, p. 135–136, 20 mar. 2023.

KACZMAREK, J. C.; KOWALSKI, P. S.; ANDERSON, D. G. Advances in the delivery of RNA therapeutics: from concept to clinical reality. **Genome Medicine**, v. 9, n. 1, p. 60, 27 dez. 2017.

KAHRAMAN, E.; GÜNGÖR, S.; ÖZSOY, Y. Potential enhancement and targeting strategies of polymeric and lipid-based nanocarriers in dermal drug delivery. **Therapeutic Delivery**, v. 8, n. 11, p. 967–985, nov. 2017.

KAMIYA, M. et al. Stability Study of mRNA-Lipid Nanoparticles Exposed to Various Conditions Based on the Evaluation between Physicochemical Properties and Their Relation with Protein Expression Ability. **Pharmaceutics**, v. 14, n. 11, p. 2357, 31 out. 2022.

KANG, Z.; MENG, Q.; LIU, K. **Peptide-based gene delivery vectors.** **Journal of Materials Chemistry B** Royal Society of Chemistry, , 13 mar. 2019. Disponível em: <<https://pubs-rsc-org.ez46.periodicos.capes.gov.br/en/content/articlehtml/2019/tb/c8tb03124j>>. Acesso em: 23 mar. 2021

KAUFFMAN, K. J. et al. Optimization of Lipid Nanoparticle Formulations for mRNA Delivery in Vivo with Fractional Factorial and Definitive Screening Designs. **Nano Letters**, v. 15, n. 11, p. 7300–7306, 11 nov. 2015.

KAWAGUCHI, M. et al. Effect of Cholesterol Content of Lipid Composition in mRNA-LNPs on the Protein Expression in the Injected Site and Liver After Local Administration in Mice. **Journal of Pharmaceutical Sciences**, v. 112, n. 5, p. 1401–1410, maio 2023.

KHOO, H. S. et al. Self-Assembly in Micro- and Nanofluidic Devices: A Review of Recent Efforts. **Micromachines**, v. 2, n. 1, p. 17–48, 11 fev. 2011.

KHOSA, A.; REDDI, S.; SAHA, R. N. Nanostructured lipid carriers for site-specific drug delivery. **Biomedicine & Pharmacotherapy**, v. 103, p. 598–613, jul. 2018.

KIAIE, S. H. et al. Recent advances in mRNA-LNP therapeutics: immunological and pharmacological aspects. **Journal of Nanobiotechnology**, v. 20, n. 1, p. 276, 14 jun. 2022.

KIANFAR, E. Protein nanoparticles in drug delivery: animal protein, plant proteins and protein cages, albumin nanoparticles. **Journal of Nanobiotechnology**, v. 19, n. 1, p. 159, 29 dez. 2021.

KIM, J. et al. Engineering Lipid Nanoparticles for Enhanced Intracellular Delivery of mRNA



through Inhalation. **ACS Nano**, v. 16, n. 9, p. 14792–14806, 27 set. 2022.

KIM, J.; JOZIC, A.; SAHAY, G. Naturally Derived Membrane Lipids Impact Nanoparticle-Based Messenger RNA Delivery. **Cellular and Molecular Bioengineering**, v. 13, n. 5, p. 463–474, 26 out. 2020.

KOHLMEIER, M. How Nutrients are Affected by Genetics. In: **Nutrigenetics**. [s.l.] Elsevier, 2013. p. 103–221.

KONATE, K. et al. Peptide-Based Nanoparticles to Rapidly and Efficiently “Wrap ’n Roll” siRNA into Cells. **Bioconjugate Chemistry**, v. 30, n. 3, p. 592–603, 20 mar. 2019.

KULKARNI, J. A. et al. On the role of helper lipids in lipid nanoparticle formulations of siRNA. **Nanoscale**, v. 11, n. 45, p. 21733–21739, 2019.

KUMARI, A.; KUMAR, V.; YADAV, S. K. Nanotechnology: A Tool to Enhance Therapeutic Values of Natural Plant Products. **Trends in Medical Research**, v. 7, n. 2, p. 34–42, 1 fev. 2012.

KYOBULA, M. et al. 3D inkjet printing of tablets exploiting bespoke complex geometries for controlled and tuneable drug release. **Journal of Controlled Release**, v. 261, p. 207–215, 10 set. 2017.

LAGE, H. **An overview of cancer multidrug resistance: A still unsolved problem. Cellular and Molecular Life Sciences**, 2008.

LAHIRI, A. et al. Lung cancer immunotherapy: progress, pitfalls, and promises. **Molecular Cancer** **2023 22:1**, v. 22, n. 1, p. 1–37, 21 fev. 2023.

LAMBA, H.; SATHISH, K.; SABIKHI, L. Double Emulsions: Emerging Delivery System for Plant Bioactives. **Food and Bioprocess Technology**, v. 8, n. 4, p. 709–728, 15 abr. 2015.

LANGER, R.; TIRRELL, D. A. Designing materials for biology and medicine. **Nature** **2004 428:6982**, v. 428, n. 6982, p. 487–492, 1 abr. 2004.

LE BARS, G. et al. Oral toxicity of Miglyol 812® in the Göttingen® minipig. **Regulatory Toxicology and Pharmacology**, v. 73, n. 3, p. 930–937, 1 dez. 2015.

LEANER, V. D. et al. Inhibition of AP-1 Transcriptional Activity Blocks the Migration, Invasion, and Experimental Metastasis of Murine Osteosarcoma. **The American Journal of Pathology**, v. 174, n. 1, p. 265–275, jan. 2009.

LEE, W.-H. et al. Inhalation of nanoparticle-based drug for lung cancer treatment: Advantages and challenges. **Asian Journal of Pharmaceutical Sciences**, v. 10, n. 6, p. 481–489, dez. 2015.

LEHNER, R. et al. A comparison of plasmid DNA delivery efficiency and cytotoxicity of two cationic diblock polyoxazoline copolymers. **Nanotechnology**, v. 28, n. 17, p. 175602, 28 abr. 2017.

LEONG, E. W. X.; GE, R. Lipid Nanoparticles as Delivery Vehicles for Inhaled Therapeutics. **Biomedicines**, v. 10, n. 9, 1 set. 2022.

LETCHFORD, K.; BURT, H. A review of the formation and classification of amphiphilic block copolymer nanoparticulate structures: micelles, nanospheres, nanocapsules and polymersomes. **European Journal of Pharmaceutics and Biopharmaceutics**, v. 65, n. 3, p. 259–269, mar. 2007.

LI, Z. et al. Nanoparticle depots for controlled and sustained gene delivery. **Journal of Controlled Release**, v. 322, p. 622–631, jun. 2020.

LIN, Y.; XU, J.; LAN, H. Tumor-associated macrophages in tumor metastasis: biological roles and clinical therapeutic applications. **Journal of Hematology & Oncology** **2019 12:1**, v. 12, n. 1, p. 1–16, 12 jul. 2019.

LIST, G. R. Soybean Lecithin: Food, Industrial Uses, and Other Applications. In: **Polar Lipids**. [s.l.] Elsevier, 2015. p. 1–33.

LIU, S. et al. Brightening up Biology: Advances in Luciferase Systems for in Vivo Imaging. **ACS Chemical Biology**, v. 16, n. 12, p. 2707–2718, 17 dez. 2021.

LIU, Y. et al. Microfluidic Nanoparticles for Drug Delivery. **Small**, v. 18, n. 36, 9 set. 2022.

LONEZ, C. et al. Fusogenic activity of cationic lipids and lipid shape distribution. **Cellular and Molecular Life Sciences**, v. 67, n. 3, p. 483–494, 19 fev. 2010.

LOPES, C. et al. Microfluidic production of mRNA-loaded lipid nanoparticles for vaccine applications. **Expert opinion on drug delivery**, v. 19, n. 10, p. 1381–1395, 2022.

LUKER, K. E.; LUKER, G. D. Applications of bioluminescence imaging to antiviral research and therapy: Multiple luciferase enzymes and quantitation. **Antiviral Research**, v. 78, n. 3, p. 179–187, jun. 2008.

LY, H. H. et al. Optimization of Lipid Nanoparticles for saRNA Expression and Cellular Activation Using a Design-of-Experiment Approach. **Molecular Pharmaceutics**, v. 19, n. 6, p. 1892–1905, 6 jun. 2022.

MACLACHLAN, I. Liposomal formulations for nucleic acid delivery. In: **Antisense drug technology: principles, strategies, and applications 2**. [s.l.: s.n.]. p. 237–270.

MAEKI, M. et al. Microfluidic technologies and devices for lipid nanoparticle-based RNA delivery. **Journal of Controlled Release**, v. 344, p. 80–96, 1 abr. 2022.

MAHMOUD, K. et al. Lipid based nanoparticles as a novel treatment modality for hepatocellular carcinoma: a comprehensive review on targeting and recent advances. **Journal of Nanobiotechnology**, v. 20, n. 1, p. 109, 5 mar. 2022.

MANTOVANI, A. et al. Macrophages as tools and targets in cancer therapy. **Nature Reviews Drug Discovery** 2022 21:11, v. 21, n. 11, p. 799–820, 16 ago. 2022.

MARES, A. G. et al. Formulation of tunable size PLGA-PEG nanoparticles for drug delivery using microfluidic technology. **PLOS ONE**, v. 16, n. 6, p. e0251821, 18 jun. 2021.

MAZUR, K. L. et al. Diethyldithiocarbamate loaded in beeswax-copaiba oil nanoparticles obtained by solventless double emulsion technique promote promastigote death in vitro. **Colloids and Surfaces B: Biointerfaces**, v. 176, p. 507–512, abr. 2018.

MEDJMEDJ, A. et al. In Cellulo and In Vivo Comparison of Cholesterol, Beta-Sitosterol and Diolelyphosphatidylethanolamine for Lipid Nanoparticle Formulation of mRNA. **Nanomaterials**, v. 12, n. 14, p. 2446, 17 jul. 2022.

MEEWAN, J. et al. Preparation of Zein-Based Nanoparticles: Nanoprecipitation versus Microfluidic-Assisted Manufacture, Effects of PEGylation on Nanoparticle Characteristics and Cellular Uptake by Melanoma Cells. **International Journal of Nanomedicine**, v. Volume 17, p. 2809–2822, jun. 2022.

MEHTA, M. et al. Lipid-Based Nanoparticles for Drug/Gene Delivery: An Overview of the Production Techniques and Difficulties Encountered in Their Industrial Development. **ACS Materials Au**, 2023.

MELAMED, J. R. et al. Lipid nanoparticle chemistry determines how nucleoside base modifications alter mRNA delivery. **Journal of Controlled Release**, v. 341, p. 206–214, jan. 2022.

MELAMED, J. R. et al. Ionizable lipid nanoparticles deliver mRNA to pancreatic  $\beta$  cells via macrophage-mediated gene transfer. **Science Advances**, v. 9, n. 4, 27 jan. 2023.

MENDONÇA, M. C. P. et al. Design of lipid-based nanoparticles for delivery of therapeutic nucleic acids. **Drug Discovery Today**, v. 28, n. 3, p. 103505, mar. 2023.

MENESES, A. C. DE. **ENCAPSULAÇÃO DE ÓLEO DE CRAVO EM NANOPARTÍCULAS LIPÍDICAS E POLIMÉRICAS EM SISTEMA LIVRE DE SOLVENTE**. [s.l.: s.n.].

MERCK. **Bioluminescent Firefly Luciferase Assays**. Disponível em: <<https://www.sigmaaldrich.com/BR/pt/technical-documents/technical-article/cell-culture-and-cell-culture-analysis/imaging-analysis-and-live-cell-imaging/firefly-luciferase-assays>>.

MERZ, J. et al. Pro- and anti-inflammatory macrophages express a sub-type specific purinergic receptor profile. **Purinergic Signalling**, v. 17, n. 3, p. 481, 1 set. 2021.

MIAO, L.; ZHANG, Y.; HUANG, L. mRNA vaccine for cancer immunotherapy. **Molecular Cancer**, v. 20, n. 1, p. 41, 25 dez. 2021.

MILANOVIĆ, J. et al. Blend of natural waxes as a matrix for aroma encapsulation. **Facta universitatis - series: Physics, Chemistry and Technology**, v. 15, n. 2, p. 103–111, 2017.

MIRZA, A. Z.; SIDDIQUI, F. A. Nanomedicine and drug delivery: a mini review. **International Nano Letters**, v. 4, n. 1, p. 94, 20 mar. 2014.

MONDADORI, C. et al. Assessing the response of human primary macrophages to defined fibrous architectures fabricated by melt electrowriting. **Bioactive Materials**, v. 21, p. 209–222, 1 mar. 2023.

MÜLLER, R. H. et al. Solid lipid nanoparticles (SLN) for controlled drug delivery – a review of the state of the art. **European Journal of Pharmaceutics and Biopharmaceutics**, v. 50, n. 1, p. 161–177, 3 jul. 2000.

MURPHY, R. J. et al. Formation and growth of co-culture tumour spheroids: new mathematical models and experiments. **bioRxiv**, p. 2022.12.21.521515, 14 mar. 2023.

NASIRIZADEH, S.; MALAEKEH-NIKOUEI, B. Solid lipid nanoparticles and nanostructured lipid carriers in oral cancer drug delivery. **Journal of Drug Delivery Science and Technology**, v. 55, n. July 2019, p. 101458, fev. 2020.

NATIONAL NANOTECHNOLOGY INITIATIVE, U. S. **Nanotechnology: What It Is and How It Works**. Disponível em: <<https://www.nano.gov/nanotech-101/what>>. Acesso em: 15 mar. 2021.

NAYEK, S.; VENKATACHALAM, A.; CHOUDHURY, S. RECENT NANOCOCHLEATE DRUG DELIVERY SYSTEM FOR CANCER TREATMENT: A REVIEW. **International Journal of Current Pharmaceutical Research**, p. 28–32, 15 nov. 2019.

NOY, R.; POLLARD, J. W. Tumor-associated macrophages: from mechanisms to therapy. **Immunity**, v. 41, n. 1, p. 49, 7 jul. 2014.

OBEID, M. A. et al. Delivering natural products and biotherapeutics to improve drug efficacy. **Therapeutic Delivery**, v. 8, n. 11, p. 947–956, 1 nov. 2017.

OKUDA, K. et al. On the size-regulation of RNA-loaded lipid nanoparticles synthesized by microfluidic device. **Journal of Controlled Release**, v. 348, p. 648–659, ago. 2022.

ORLANDINI VON NIESSEN, A. G. et al. Improving mRNA-Based Therapeutic Gene Delivery by Expression-Augmenting 3' UTRs Identified by Cellular Library Screening. **Molecular Therapy**, v. 27, n. 4, p. 824–836, abr. 2019.

ORTIZ, A. C. et al. Development of a nanostructured lipid carrier (NLC) by a low-energy method, comparison of release kinetics and molecular dynamics simulation. **Pharmaceutics**, v. 13, n. 4, 1 abr. 2021.

PALIWAL, R. et al. Solid lipid nanoparticles: a review on recent perspectives and patents. **Expert Opinion on Therapeutic Patents**, v. 30, n. 3, p. 179–194, 3 mar. 2020.

PAN, W. et al. Development and application of bioluminescence imaging for the influenza A virus. **Journal of Thoracic Disease**, v. 10, n. S9, p. S2230–S2237, jul. 2018.

PAN, Y. et al. Tumor-Associated Macrophages in Tumor Immunity. **Frontiers in Immunology**, v. 11, p. 583084, 3 dez. 2020.

PARDI, N. et al. mRNA vaccines — a new era in vaccinology. **Nature Reviews Drug Discovery**, v. 17, n. 4, p. 261–279, 12 abr. 2018.

PATEL, S. et al. Naturally-occurring cholesterol analogues in lipid nanoparticles induce polymorphic shape and enhance intracellular delivery of mRNA. **Nature Communications**, v. 11, n. 1, p. 983, 20 fev. 2020.

PATIL, T. S. et al. Targeting pulmonary tuberculosis using nanocarrier-based dry powder inhalation: current status and futuristic need. **Journal of Drug Targeting**, v. 27, n. 1, p. 12–27, 2 jan. 2019.

PATRA, J. K. et al. Nano based drug delivery systems: recent developments and future prospects. **Journal of Nanobiotechnology**, v. 16, n. 1, p. 71, 19 dez. 2018.

PATRICIO, D. DE O. et al. DNA-PKcs restricts Zika virus spreading and is required for

effective antiviral response. **Frontiers in Immunology**, v. 13, 13 out. 2022.

PÉREZ, S. E. et al. Formulation Strategies, Characterization, and In Vitro Evaluation of Lecithin-Based Nanoparticles for siRNA Delivery. **Journal of Drug Delivery**, v. 2012, p. 1–9, 5 abr. 2012.

PHUA, K. K. L.; NAIR, S. K.; LEONG, K. W. Messenger RNA (mRNA) nanoparticle tumour vaccination. **Nanoscale**, v. 6, n. 14, p. 7715–7729, 2014.

PILKINGTON, E. H. et al. From influenza to COVID-19: Lipid nanoparticle mRNA vaccines at the frontiers of infectious diseases. **Acta Biomaterialia**, v. 131, p. 16–40, set. 2021.

PINTO REIS, C. et al. Nanoencapsulation I. Methods for preparation of drug-loaded polymeric nanoparticles. **Nanomedicine : nanotechnology, biology, and medicine**, v. 2, n. 1, p. 8–21, 1 mar. 2006.

POLLARD, C. et al. Type I IFN counteracts the induction of antigen-specific immune responses by lipid-based delivery of mRNA vaccines. **Molecular Therapy**, v. 21, n. 1, p. 251–259, 1 jan. 2013.

POPE-HARMAN, A. et al. Biomedical Nanotechnology for Cancer. **Medical Clinics of North America**, v. 91, n. 5, p. 899–927, set. 2007.

QI, X.-R.; ZHAO; ZHUANG. Comparative study of the in vitro and in vivo characteristics of cationic and neutral liposomes. **International Journal of Nanomedicine**, p. 3087, dez. 2011.

RAKEL, D. Benign Prostatic Hyperplasia. In: **Integrative Medicine**. [s.l.] Elsevier, 2018. p. 601-607.e1.

RAKINA, M. et al. Spheroid Formation and Peritoneal Metastasis in Ovarian Cancer: The Role of Stromal and Immune Components. **International Journal of Molecular Sciences**, v. 23, n. 11, p. 6215, 1 jun. 2022.

RATEMI, E. et al. Alternative approaches for the treatment of airway diseases: focus on nanoparticle medicine. **Clinical & Experimental Allergy**, v. 46, n. 8, p. 1033–1042, ago. 2016.

RICCIARDI-JORGE, T. et al. PKR-mediated stress response enhances dengue and Zika virus replication. **mBio**, v. 14, n. 5, 31 out. 2023.

RIPOLL, M. et al. Optimal self-assembly of lipid nanoparticles (LNP) in a ring micromixer. **Scientific Reports 2022 12:1**, v. 12, n. 1, p. 1–12, 8 jun. 2022.

ROMANELLI, C. et al. **Connecting global priorities: biodiversity and human health: a state of knowledge review**. [s.l.] WHO/CBD, 2015.

S, K. Sustained drug delivery of capecitabine using natural (bee wax) and synthetic polymer (PLGA). **MOJ Drug Design Development & Therapy**, v. 2, n. 3, 21 jun. 2018.

SADARANGANI, M.; MARCHANT, A.; KOLLMANN, T. R. Immunological mechanisms of vaccine-induced protection against COVID-19 in humans. **Nature Reviews Immunology**, v. 21, n. 8, p. 475–484, 1 ago. 2021.

SALATIN, S. et al. Development of a nanoprecipitation method for the entrapment of a very water soluble drug into Eudragit RL nanoparticles. **Research in Pharmaceutical Sciences**, v. 12, n. 1, p. 1, 1 fev. 2017.

SALEEM, K. et al. Applications of Nanomaterials in Leishmaniasis: A Focus on Recent Advances and Challenges. **Nanomaterials**, v. 9, n. 12, p. 1749, 9 dez. 2019.

SAMIMI, S. et al. Lipid-Based Nanoparticles for Drug Delivery Systems. **Characterization and Biology of Nanomaterials for Drug Delivery: Nanoscience and Nanotechnology in Drug Delivery**, p. 47–76, 1 jan. 2019.

SARMENTO, B. et al. Oral insulin delivery by means of solid lipid nanoparticles. **International Journal of Nanomedicine**, v. 2, n. 4, p. 743–9, 2007.

SCHAFFAZICK, S. R. et al. Caracterização e estabilidade físico-química de sistemas poliméricos nanoparticulados para administração de fármacos. **Química Nova**, v. 26, n. 5, p. 726–737, out. 2003.

SCHLICH, M. et al. Cytosolic delivery of nucleic acids: The case of ionizable lipid

nanoparticles. **Bioengineering & Translational Medicine**, v. 6, n. 2, p. e10213, 20 maio 2021.

SCHOLFIELD, C. R. Composition of soybean lecithin. **Journal of the American Oil Chemists' Society**, v. 58, n. 10, out. 1981.

SHAFFER, C. Mist begins to clear for lung delivery of RNA. **Nature Biotechnology**, v. 38, n. 10, p. 1110–1112, 5 out. 2020.

SHEPHERD, S. J.; ISSADORE, D.; MITCHELL, M. J. Microfluidic formulation of nanoparticles for biomedical applications. **Biomaterials**, v. 274, p. 120826, 1 jul. 2021.

SHI, J. et al. Differentially charged hollow core/shell lipid-polymer-lipid hybrid nanoparticles for small interfering rna delivery. **Angewandte Chemie - International Edition**, 2011.

SINGH, N. et al. Drug delivery: advancements and challenges. In: **Nanostructures for Drug Delivery**. [s.l.] Elsevier, 2017. p. 865–886.

SNOW, A. et al. Development of a mRNA Lipid Nanoparticle (mRNA-LNP) Cancer Vaccine to Prevent Leukemia Relapse after Stem Cell Transplant. **Blood**, v. 140, n. Supplement 1, p. 7382–7383, 15 nov. 2022.

SOLEIMANIAN, Y. et al. Formulation and characterization of novel nanostructured lipid carriers made from beeswax, propolis wax and pomegranate seed oil. **Food Chemistry**, v. 244, p. 83–92, abr. 2018.

SOUTO, E. B. et al. SLN and NLC for topical, dermal, and transdermal drug delivery. **Expert Opinion on Drug Delivery**, v. 17, n. 3, p. 357–377, 3 mar. 2020.

SOUZA, C.; DE FREITAS, L. A. P.; MAIA CAMPOS, P. M. B. G. Topical Formulation Containing Beeswax-Based Nanoparticles Improved In Vivo Skin Barrier Function. **AAPS PharmSciTech**, v. 18, n. 7, p. 2505–2516, 17 out. 2017.

STANLEY, E. R.; CHITU, V. CSF-1 Receptor Signaling in Myeloid Cells. **Cold Spring Harbor Perspectives in Biology**, v. 6, n. 6, 2014.

STRACHAN, J. B. et al. Toxicity and cellular uptake of lipid nanoparticles of different structure and composition. **Journal of Colloid and Interface Science**, v. 576, p. 241–251, set. 2020.

SUBERI, A. et al. Polymer nanoparticles deliver mRNA to the lung for mucosal vaccination. **Science Translational Medicine**, v. 15, n. 709, 16 ago. 2023.

SUGAWARA, E.; NIKAIDO, H. Properties of AdeABC and AdeIJK efflux systems of *Acinetobacter baumannii* compared with those of the AcrAB-TolC system of *Escherichia coli*. **Antimicrobial agents and chemotherapy**, v. 58, n. 12, p. 7250–7, dez. 2014.

SULAIMAN, A. **Local delivery of tumor associated macrophage immunotherapy for the treatment of metastases to the lungs**. [s.l.] Virginia Commonwealth University, 2021.

SUN, D.; LU, Z.-R. R. Structure and Function of Cationic and Ionizable Lipids for Nucleic Acid Delivery. **Pharmaceutical Research**, v. 40, n. 1, p. 27–46, 4 jan. 2023.

SUR, S. et al. Recent developments in functionalized polymer nanoparticles for efficient drug delivery system. **Nano-Structures & Nano-Objects**, v. 20, p. 100397, 1 out. 2019.

SWETHA, K. et al. Recent Advances in the Lipid Nanoparticle-Mediated Delivery of mRNA Vaccines. **Vaccines**, v. 11, n. 3, p. 658, 14 mar. 2023.

TENCHOV, R. et al. Lipid Nanoparticles—From Liposomes to mRNA Vaccine Delivery, a Landscape of Research Diversity and Advancement. **ACS Nano**, v. 15, n. 11, p. 16982–17015, 23 nov. 2021.

TEXIER, I. et al. Cyanine-loaded lipid nanoparticles for improved in vivo fluorescence imaging. **Journal of Biomedical Optics**, v. 14, n. 5, p. 054005, 2009.

THERMO FISHER SCIENTIFIC. **Luciferase Reporters**. Disponível em: <<https://www.thermofisher.com/br/en/home/life-science/protein-biology/protein-biology-learning-center/protein-biology-resource-library/pierce-protein-methods/luciferase-reporters.html>>.

THILAKARATHNA, S. H.; VASANTHA RUPASINGHE, H. P. **Flavonoid bioavailability and attempts for bioavailability enhancement**. **Nutrients** MDPI AG, , 28 ago. 2013. Disponível em: <<https://pubmed.ncbi.nlm.nih.gov/23989753/>>. Acesso em: 16 mar. 2021

TRAFTON, A. New nanoparticles can perform gene editing in the lungs. **MIT News**, mar. 2023.

TRUCILLO, P.; CAMPARDELLI, R.; REVERCHON, E. Liposomes: From Bangham to Supercritical Fluids. **Processes**, v. 8, n. 9, p. 1022, 21 ago. 2020.

TULI, V. **Targeting Inflammation And Fibrosis In Liver Injury Mouse Models By Modulating Microrna-155 Expression Using Passive Liver Targeting Lipid Nanoparticles**. [s.l.] University Of Twente, 2023.

VAN HOECKE, L. et al. **mRNA in cancer immunotherapy: beyond a source of antigen**. **Molecular CancerBioMed Central Ltd**, , 1 dez. 2021. Disponível em: <<https://doi.org/10.1186/s12943-021-01329-3>>. Acesso em: 2 jun. 2021

VAUTHIER, C.; BOUCHEMAL, K. Methods for the Preparation and Manufacture of Polymeric Nanoparticles. **Pharmaceutical Research**, v. 26, n. 5, p. 1025–1058, 24 maio 2009.

VEGA-VÁSQUEZ, P.; MOSIER, N. S.; IRUDAYARAJ, J. Nanoscale Drug Delivery Systems: From Medicine to Agriculture. **Frontiers in Bioengineering and Biotechnology**, v. 8, 18 fev. 2020.

VINOGRADOV, S.; WARREN, G.; WEI, X. Macrophages associated with tumors as potential targets and therapeutic intermediates. **Nanomedicine (London, England)**, v. 9, n. 5, p. 695, 2014.

VISHWESHWARAIAH, Y. L.; DOKHOLYAN, N. V. mRNA vaccines for cancer immunotherapy. **Frontiers in Immunology**, v. 13, 14 dez. 2022.

WADHWA, A. et al. Opportunities and Challenges in the Delivery of mRNA-Based Vaccines. **Pharmaceutics**, v. 12, n. 2, p. 102, 28 jan. 2020.

WANG, H. et al. Nanostructured lipid carriers for MicroRNA delivery in tumor gene therapy. **Cancer Cell International**, v. 18, n. 1, p. 101, 13 dez. 2018.

WANG, L.; GRIFFEL, B.; XU, X. Synthesis of PLGA–Lipid Hybrid Nanoparticles for siRNA Delivery Using the Emulsion Method PLGA-PEG–Lipid Nanoparticles for siRNA Delivery. In: [s.l.: s.n.]. p. 231–240.

WANG, Y. et al. **mRNA vaccine: a potential therapeutic strategy**. **Molecular CancerBioMed Central Ltd**, , 1 dez. 2021. Disponível em: <<https://doi.org/10.1186/s12943-021-01311-z>>. Acesso em: 15 abr. 2021

WATANABE, S. et al. The role of macrophages in the resolution of inflammation. **The Journal of Clinical Investigation**, v. 129, n. 7, p. 2619, 5 maio 2019.

WEI, T.; TAO, W.; CHENG, Q. Lipid nanoparticles for mRNA therapy: recent advances in targeted delivery. **Life Medicine**, v. 1, n. 1, p. 21–23, 1 ago. 2022.

WHEELER, J. J. et al. Stabilized plasmid-lipid particles: construction and characterization. **Gene Therapy**, v. 6, n. 2, p. 271–281, 1 fev. 1999.

WISSING, S. A.; KAYSER, O.; MÜLLER, R. H. **Solid lipid nanoparticles for parenteral drug delivery**. **Advanced Drug Delivery Reviews**, 2004.

XU, L. et al. Lipid Nanoparticles for Drug Delivery. **Advanced NanoBiomed Research**, v. 2, n. 2, p. 2100109, 25 fev. 2022.

XU, X.; XIA, T. Recent Advances in Site-Specific Lipid Nanoparticles for mRNA Delivery. **ACS Nanoscience Au**, v. 3, n. 3, p. 192–203, 21 jun. 2023.

YAMADA, Y. Nucleic Acid Drugs—Current Status, Issues, and Expectations for Exosomes. **Cancers**, v. 13, n. 19, 1 out. 2021.

YANEZ ARTETA, M. et al. Successful reprogramming of cellular protein production through mRNA delivered by functionalized lipid nanoparticles. **Proceedings of the National Academy of Sciences**, v. 115, n. 15, 10 abr. 2018.

YANG, L. et al. Recent Advances in Lipid Nanoparticles for Delivery of mRNA. **Pharmaceutics**, v. 14, n. 12, p. 2682, 1 dez. 2022.

YAVUZ, A. et al. DLin-MC3-Containing mRNA Lipid Nanoparticles Induce an Antibody

Th2-Biased Immune Response Polarization in a Delivery Route-Dependent Manner in Mice. **Pharmaceutics**, v. 15, n. 3, p. 1009, 21 mar. 2023.

YETISGIN, A. A. et al. Therapeutic Nanoparticles and Their Targeted Delivery Applications. **Molecules**, v. 25, n. 9, p. 2193, 8 maio 2020.

ZAMBRANO-ZARAGOZA, M. L. et al. Effect of Nano-Edible Coating Based on Beeswax Solid Lipid Nanoparticles on Strawberry's Preservation. **Coatings**, v. 10, n. 3, p. 253, 9 mar. 2020.

ZENG, C. et al. Formulation and Delivery Technologies for mRNA Vaccines. In: [s.l: s.n.].

ZHANG, C. et al. Advances in mRNA Vaccines for Infectious Diseases. **Frontiers in Immunology**, v. 10, n. MAR, p. 594, 27 mar. 2019a.

ZHANG, F. et al. Genetic programming of macrophages to perform anti-tumor functions using targeted mRNA nanocarriers. **Nature Communications**, v. 10, n. 1, 1 dez. 2019b.

ZHANG, H. et al. Aerosolizable Lipid Nanoparticles for Pulmonary Delivery of mRNA through Design of Experiments. **Pharmaceutics**, v. 12, n. 11, p. 1042, 30 out. 2020.

ZHANG, R. et al. Helper lipid structure influences protein adsorption and delivery of lipid nanoparticles to spleen and liver. **Biomaterials Science**, v. 9, n. 4, p. 1449–1463, 2021.

ZHANG, X. et al. Sodium cholate-enhanced polymeric micelle system for tumor-targeting delivery of paclitaxel. **International Journal of Nanomedicine**, v. Volume 12, p. 8779–8799, dez. 2017.

## APPENDIX

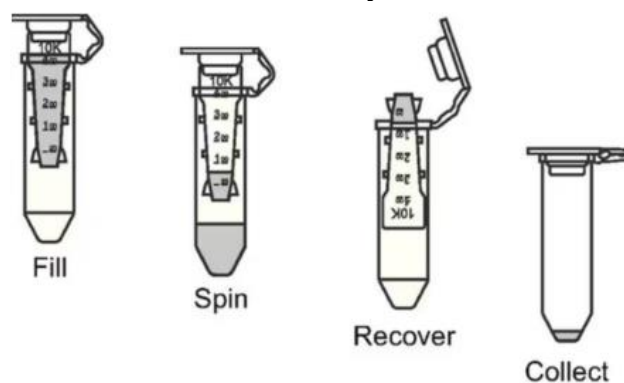
### mRNA LOADING IN IONIZABLE LIPID NANOPARTICLES

Table A1– Lipids stock solutions used in the Dropwise Addition method

Lipid	Concentration ( $\mu\text{g}/\mu\text{L}$ )
SM-102	25
DLin-MC3-DMA	7.04
Cholesterol	10
$\beta$ -sitosterol	10
DOPE	10
DSPC	10
DMG-PEG-2000	10

Source: The Author (2023)

Figure A1 – Schematical representation of how to use the Amicon® ultra centrifugal filter for LNP recovery



Source: Merck-Millipore (2023)

Prior to the preparation of DLin-MC3-DMA/DSPC/Cholesterol/DMG-PEG LNPs for *in vivo* administration, encapsulation of FLuc-mRNA in this formulation using the microfluidic system was investigated for understanding the protocols involved in the LNPs preparation, purification, and characterization described in the section 3.2.2.1 from Chapter III. Table A2 shows the results obtained from the preliminary assays of FLuc-mRNA encapsulation in DLin-MC3-DMA/DSPC/Cholesterol/DMG-PEG LNPs using the microfluidics system.



Table A2 – Intensity mean diameter of nanoparticles (Dp), polydispersity index (PDI), Zeta potential ( $\xi$ ), and Encapsulation Efficiency (EE%) of DLin-MC3-DMA/DSPC/Cholesterol/DMG-PEG LNPs prepared by microfluidics

Formulation	Condition	Dp (nm)	PDI	$\xi$ (mV)	EE (%)
MC3-FLUC-01	Before Dialysis	69.3 ± 0.3	0.148±0.007	-4.7 ± 0.7	-
	After Dialysis	85.8 ± 1.2	0.199 ±0.027	-	-
MC3-FLUC-02	Before Dialysis	69.86 ± 0.7	0.176 ± 0.005	- 1.1 ± 0.22	-
	After Dialysis	73.65 ± 0.3	0.113 ± 0.010	- 3.43 ± 0.22	85.58
	Start Waste	86.51 ± 0.5	0.235 ± 0.007	- 2.42 ± 0.37	88.91
MC3-FLUC-03	After Dialysis	63.06 ± 0.3	0.160 ± 0.006	- 5.33 ± 2.10	92.06
MC3-FLUC-04 With DiD'	Before Dialysis	56.2 ± 0.6	0.215 ± 0.007	-1.34 ± 0.1	-
	After Dialysis	72.86 ± 3.7	0.348 ± 0.033	-	88.76

Source: The Author (2023)

As can be observed, all the formulations presented submicrometric size, narrow PDI, negative zeta potential, and EE% close to 90% in agreement with the results presented in section 4.3.1 from Chapter IV. Also, is possible to observe that all the formulations had an increase in the LNPs size values after the purification step, and except MC3-FLUC-02, the same tendency is observed in the PDI values of the other formulations. This result could be explained by the LNPs coalescence during the solvent removal in the dialysis process (VAUTHIER; BOUCHEMAL, 2009). The zeta potential results indicated that all the formulations remained in the expected range for the DLin-MC3-DMA/DSPC/Cholesterol/DMG-PEG formulations before and after purification, thus MC3-FLUC-01 and MC3-FLUC-04 were not analyzed after dialysis (CARRASCO et al., 2021; LY et al., 2022; YAVUZ et al., 2023).

The MC3-FLUC-02 presents the characterization of the *Start Waste*, which are the first drops formed in the microfluidization process. According to the microfluidics equipment manufacturer, discarding this initial volume is required to establish the laminar flow of the fluids through the microfluidics cartridge. It is important to highlight that the LNPs formed in the *Start Waste* are in the same range as the LNPs formed in the laminar flow for all the properties analyzed. This could indicate a possibility for process optimization through the decrease of the *Start Waste* volume, leading to a better use of resources.

The MC3-FLUC-04 with DiD' formulation had the highest PDI value, an increase already reported in the results presented in section 4.3.3 from Chapter IV. The increase of PDI in this formulation could be related to the addition of DiD'. The lipophilic dye was added as solid crystals to the formulation, which may not have been completely solubilized in the ethanol phase due to lipid saturation, and consequently were not incorporated into the LNPs matrix and remained in suspension in the aqueous phase. This could explain the reason for the notable increase in PDI but the maintenance of the size in the level as the other formulations.

## CO-CULTURE OF SPHEROIDS USING K7M2, RAW 264.7, AND NIH-3T3

### **Methods**

#### ***Passaging and 2D Culture***

All cells were passaged in T25 or T75 flasks at 37 °C in 5% CO<sub>2</sub>, humidified atmosphere, on HERACELL VIOS 160i incubators (Thermo-Fisher Scientific, Waltham, MA, USA). K7M2, murine osteosarcoma lung metastasis cells (ATCC, Manassas, VA, USA) and NIH-3T3, mouse embryonic fibroblast cells (ATCC, Manassas, VA, USA) were grown in DMEM media, supplemented with 10% FBS, and 1% antibiotic. RAW 264.7, murine macrophage cells, were grown in DMEM media with sodium pyruvate (DMEM-SP), supplemented with 10% FBS, and 1% antibiotic. The cells were then shortly washed with PBS solution pH 7.4 and subsequently incubated with fresh trypsin/EDTA solution at 37 °C for 10 min. Fresh media was added and EDTA was removed by centrifugation of the cells at 1200 rpm for 7 min. The cells were, then, resuspended in fresh medium. Cells were counted using an automated cell counters (Thermo-Fischer Scientific, Waltham, MA, USA).

#### ***Preparation of Plates for Culturing Spheroids***

In order to make spheroids, wells of 96-well plates were firstly coated with PolyHEMA. The coating was achieved by adding 100 µL of a 1.2% w:v solution of PolyHEMA in absolute ethanol and allowing the ethanol to evaporate in an oven (Thermo-Fischer Scientific, Waltham, MA, USA) at 60 °C for 12 h. Once ethanol was completely evaporated, the plates were placed under UV light for 30 min for sterilization.

#### ***Culturing Single Cell Culture and Co-Culture Spheroids (3D culture)***

The ability to form single, tight spheroids was investigated using different ratios of K7M2, NIH-3T3, and RAW 264.7 cells. The total cell number was 220 or 250, and the following ratios were investigated as shown in Table A3:

Table A3 – Spheroids composition and percentage of NIH-3T3 cells over the total amount of K7M2 or K7M2+RAW 264.7

Cells	Number of Seeded Cells	Percentage of NIH-3T3
K7M2:NIH-3T3	200:20	10%
	132:68:20	10%
	100:100:20	10%
	68:132:20	10%
	132:68:50	25%
K7M2:NIH-3T3:RAW 264.7	100:100:50	25%
	68:132:50	25%
	110:55:55	33.3%
	92:45:83	60.6%
	74:36:110	100%

Source: The Author (2023)

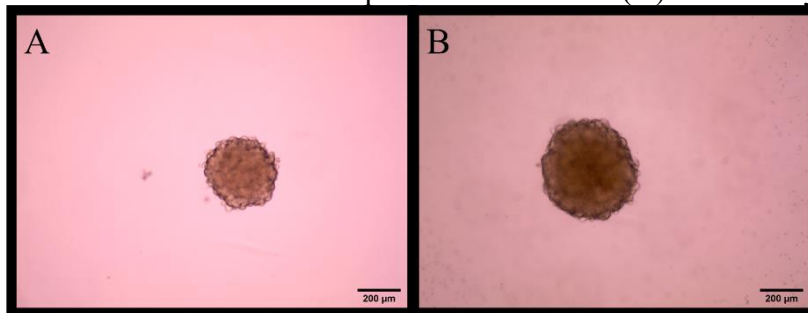
The cells were mixed in the appropriate media (DMEM or DMEM-SP, supplemented with 10% FBS and 1% AB) and seeded onto the coated wells and the plates were centrifuged (Plate Swing Bucket, Thermo-Fisher Scientific, Waltham, MA, USA) at 2000 rpm for 60 min at 4 °C. The size and morphology of the spheroids as a function of days after seeding were followed within 6 days with bright field microscopy using an EVOS™ XL Core Imaging System Olympus Microscope (Thermo-Fischer Scientific, Waltham, MA, USA). The morphology and Feret's diameter of the spheres formed were calculated using ImageJ (version 1.53a). The formed spheroids were classified as tight and loose according to their capability of being manipulated without being easily disrupted.

## Results and Discussion

Tumor spheroids serve as a more complex tool for investigating cancer progression and are essential for advancing cancer therapies. Additionally, they provide a more accurate link between *in vitro* studies and *in vivo* experiments (MURPHY et al., 2023). The spheroids formation from the co-culture of two cell lines was previously investigated in The da Rocha and Sweet Labs at VCU by Almuqbil (2021) who investigated the effect of the cells ratio on the spheroid's formation using A459 (Lung Adenocarcinoma) and NIH-3T3 cells and concluded that starting with 10% NIH-3T3 regarding the total number of A549 cells was the best condition for the regular formation of tight and singular spheroids. The incorporation of NIH-3T3 cells into the spheroid culture was established since fibroblasts play an essential role in the tumor microenvironment, including the production of different growth factors, chemokines, adhesion molecules, and in the deposition of the extracellular matrix,

which also helps in the spheroid formation process (ALMUQBIL, 2021; RAKINA et al., 2022). Thus, once that the goal of the present work was to investigate the delivery of the LNPs in the osteosarcoma lung metastasis tumor microenvironment, A549 cells were substituted by K7M2 cells and experimental conditions used by Almuqbil (2021) were adapted as needed. As can be seen in Figures A2(A) and A2(B), starting with 200 K7M2 cells and 20 NIH-3T3 cells led to the formation of tight and singular spheroids. The cells were concentrated in one single spot by centrifugation on day 0 to promote easier spheroids formation and at day 3 (Figure A2(A)) it was already possible to observe the formation of an initial spheroid structure with an average Feret's diameter of  $379 \pm 22 \mu\text{m}$  that kept growing evenly as sphere until reaching the average diameter of  $489 \pm 41 \mu\text{m}$  on day 6 (Figure A2(B)).

Figure A2 – K7M2 + NIH-3T3 Spheroids after three (A) and six days (B)



Source: The Author (2023)

After, RAW 264.7 cells were incorporated to the spheroids microenvironment because the idea was to use the macrophages as immunotherapy target tool and because tumor-associated macrophages form approximately 50% of tumor mass (VINOGRADOV; WARREN; WEI, 2014). Thus, the first trial maintained the initial total number of cells in 220 cells with 10% of NIH-3T3 and divided the initial 200 cells in three ways: I - K7M2:RAW 264.7 ratio equal to 2:1, II - K7M2:RAW 264.7 ratio equal to 1:1, and III - K7M2:RAW 264.7 ratio equal to 1:2. The cell proportion were chosen to check how the doubling time would interfere with the spheroid formation, once that it is already known that RAW 264.7 have a shorter doubling time compared to K7M2 (BANCOS; TYNER, 2014; LEANER et al., 2009) and to investigate how the presence of RAW 264.7 in the environment would interfere in the shape and tightness of the spheroids, because as previously observed (data not shown) using the same cell proportion of RAW 264.7 and NIH-3T3 (200:20) as used in the K7M2+NIH-3T3 assay, there was no spheroid formation after 6 days. As can be seen in Figure A3(A - F) after the incorporation of RAW 264.7 no tight spheroids were formed in any of the ratios tested, being possible to identify individual cells in the edges of the structure after 6 days which

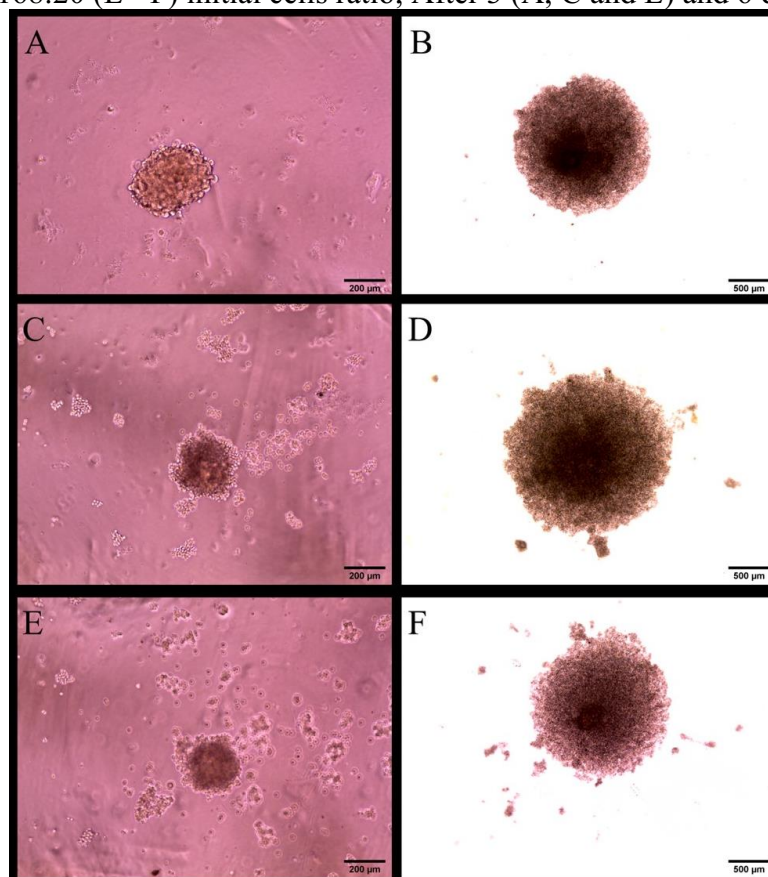
indicates that the structures formed were loose. Also, the addition of RAW 264.7 changed the environment and the cells grew irregularly, and the population reached a bigger size compared to the spheroids made only by K7M2+NIH-3T3. The average Feret's diameter obtained by each condition is shown in Table A4.

Table A4 – K7M2+RAW 264.7 spheroids average Feret's diameter for each cell ratio using 10% of NIH-3T3 after 3 and 6 days

Number of Seeded Cells (K7M2:RAW:NIH-3T3)	Days After Seeding	Feret's Diameter ( $\mu\text{m}$ )
132:68:20	3	$417 \pm 35$
	6	$1693 \pm 134$
100:100:20	3	$338 \pm 20$
	6	$2027 \pm 88$
68:132:20	3	$264 \pm 52$
	6	$1863 \pm 157$

Source: The Author (2023)

Figure A3 – K7M2+RAW 264.7+NIH-3T3 spheroids using 168:32:20 (A - B), 100:100:20 (C - D) and 32:168:20 (E - F) initial cells ratio; After 3 (A, C and E) and 6 days (B, D and F)



Source: The Author (2023)

In the subsequent trial, the initial total number of cells was increased to 250 cells and the content of NIH-3T3 to 25%, aiming that the presence of the higher fibroblast could enhance the

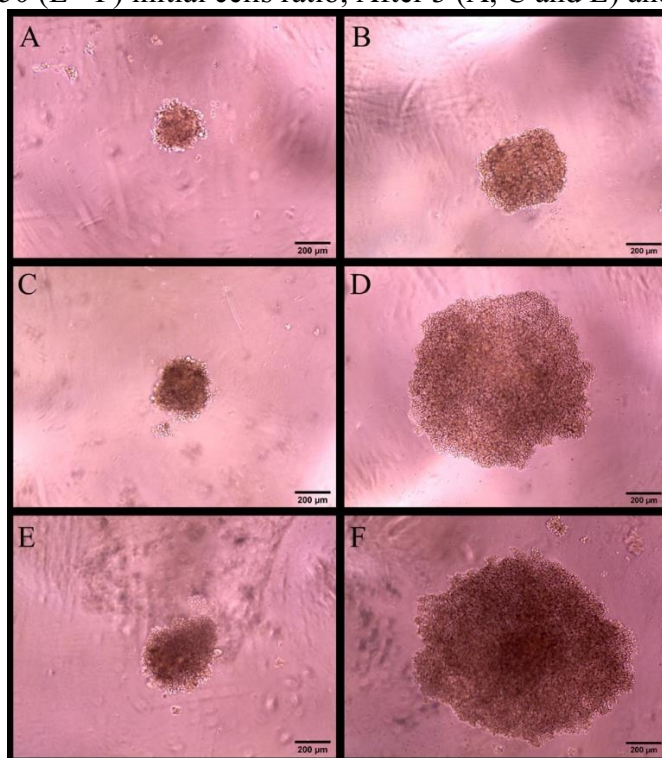
spheroid organization once that fibroblasts form pre-metastatic niches, and promote the peritoneal adhesion and the implantation of tumor cells (RAKINA et al., 2022). The other initial 200 cells were divided in the same three ratios as in the previous assay. As can be seen in Figure A4 (A – F) after increasing the NIH-3T3 content no tight spheroids were formed in any of the ratios tested, being possible to identify individual cells at the edges of the structure after 6 days which indicates that the structures formed were loose. The cells grew irregularly, and the population reached a bigger size compared to the spheroids made only by K7M2+NIH-3T3, however after increasing the total number of cells and the content of NIH-3T3 to 25%, the cell population showed a smaller average diameter of 867  $\mu\text{m}$  compared to the assay using 10% of NIH-3T3, which had an average of 1867  $\mu\text{m}$ . This could be explained by the capability of NIH-3T3 to promote the kinetics of tumor organoid formation (GOUDAR et al., 2021). Also, it was possible to observe that when K7M2:RAW 264.7 ratio was equal to 1:1, and the K7M2:RAW 264.7 ratio was equal to 1:2 the spheroids formation was more irregular and the average diameters were higher, indicating that starting with a higher proportion of K7M2 could benefit the spheroid formation. The average diameter obtained under each condition is shown in Table A5.

Table A5 – K7M2+RAW 264.7 spheroids average Feret's diameter for each cell ratio using 25% of NIH-3T3 after 3 and 6 days

Number of Seeded Cells (K7M2:RAW:NIH-3T3)	Days After Seeding	Feret's Diameter ( $\mu\text{m}$ )
132:68:50	3	312 $\pm$ 27
	6	555 $\pm$ 41
100:100:50	3	512 $\pm$ 81
	6	968 $\pm$ 139
68:132:50	3	577 $\pm$ 96
	6	1078 $\pm$ 185

Source: The Author (2023)

Figure A4 – K7M2+RAW 264.7+NIH-3T3 spheroids using 168:32:50 (A - B), 100:100:50 (C - D) and 32:168:50 (E - F) initial cells ratio; After 3 (A, C and E) and 6 days (B, D and F)



Source: The Author (2023)

After the result obtained from increasing the content of NIH-3T3 to 25%, it was evaluated how adding even more fibroblasts to the environment could impact the formation of spheroids. In this way, NIH-3T3 was increased to 33.3%, 60.6%, and 100% regarding the total amount of K7M2+RAW 264.7 in the ratios described in Table A6. However, to keep the growth condition closer to the ones used in the well succeeded K7M2+NIH-3T3 assay, 220 initial total cells were used, dividing each cell starting amount according to the desired percentage of NIH-3T3 and keeping the K7M2:RAW 264.7 ratio equal to 2:1. As can be seen in the Figure A5(A – F) after the increasing of the NIH-3T3 content no tight spheroids were formed in any of the ratios tested, being possible to identify individual cells in the edges of the structure after 6 days which indicates that the structures formed were loose.

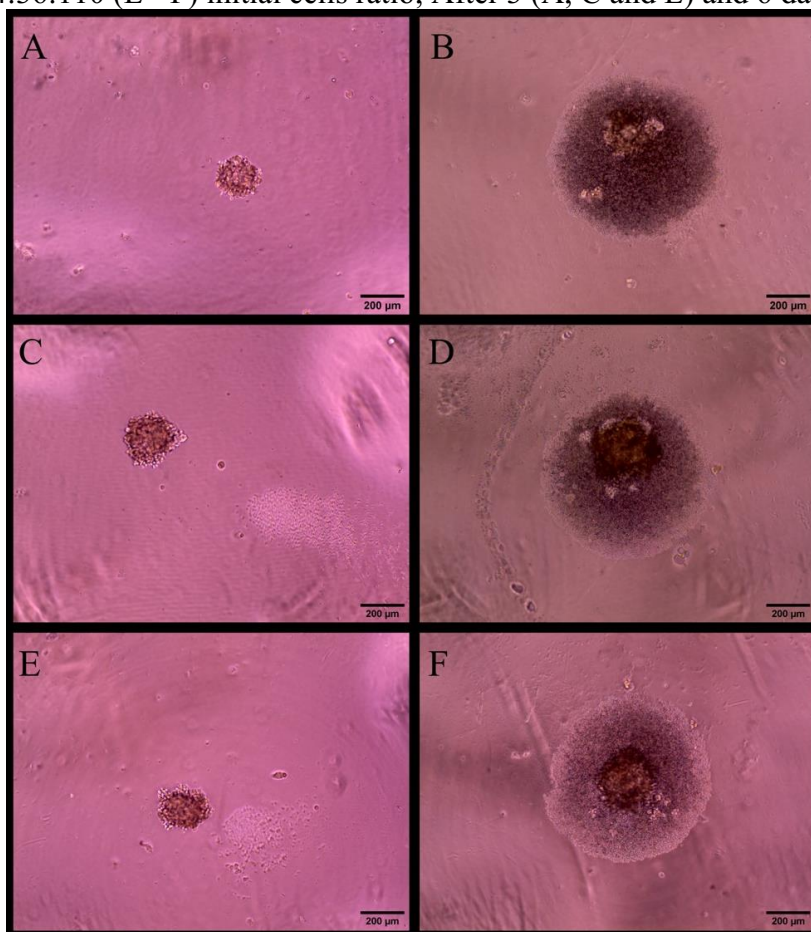
Table A6 – K7M2+RAW 264.7 spheroids average Feret's diameter using 2:1 cell ratio and 33.3%, 60.6% and 100% of NIH-3T3 after 3 and 6 days

Number of Seeded Cells (K7M2:RAW:NIH-3T3)	Days After Seeding	Feret's Diameter ( $\mu\text{m}$ )
110:55:55	3	224 $\pm$ 27
	6	724 $\pm$ 98
92:45:83	3	285 $\pm$ 9
	6	762 $\pm$ 119
74:36:110	3	292 $\pm$ 38
	6	623 $\pm$ 23

Source: The Author (2023)



Figure A5 – K7M2+RAW 264.7+NIH-3T3 spheroids using 110:55:55 (A - B), 92:45:83 (C - D) and 74:36:110 (E - F) initial cells ratio; After 3 (A, C and E) and 6 days (B, D and F)



Source: The Author (2023)

Again, cells grew irregularly in the early stages of the co-culture as can be observed by the pictures obtained from day 3, even though with the population reaching a bigger size compared to the spheroids made only by K7M2+NIH-3T3 this time after 6 days the structure formed had a spherical shape that is probably a result of the higher inclusion of fibroblasts to the co-culture (GOUDAR et al., 2021). However, the co-cultures still formed loose structures that were easily disrupted after being manipulated by pipetting, proving that the conditions to form singular and tight spheroids made of K7M2+ RAW 264.7+ NIH-3T3 were not reached yet.

The last assay that kept the ratio of 2:1 to K7M2: NIH-3T3 and increased the content of NIH-3T3 to three different levels showed an interesting pattern, of having a core spheroid in the inner of the structure formed after 6 days. Probably this core structure is a result of the initial spheroid growth observed in the images from day 3 and once K7M2 proved to be able to form spheroids in the absence of RAW 264.7, this early spheroid could be major composed by K7M2. It's important to highlight that after being manipulated by pipetting, the structures observed in Figure A5(B, D, and F)



were disrupted, however part of the inner core still was intact at the end of the procedure, indicating that the strategy of rising the initial percentage of NIH-3T3 had a positive impact over the formed structure and that a higher fibroblast content could be a key factor to achieve the successful formation of K7M2+ RAW 264.7+ NIH-3T3 spheroids.

Observing the images from day 6 it is possible to say that the enhancement in the initial fibroblast content supported the formation of more spherical structures, so the hypothesis is that to form spheroids from K7M2+ RAW 264.7+ NIH-3T3 co-culture the percentage of NIH-3T3 in the initial seeding must be higher than when using only K7M2+ NIH-3T3 co-culture. Also, based on the proliferation aspect of the structures obtained after 6 days using K7M2+ RAW 264.7+ NIH-3T3 reducing the amount of RAW 264.7 in the initial seeding could be beneficial to the spheroid formation and tightness due to the difference in the growth ratio of the cells, specially K7M2 and RAW 264.7.

## **Conclusion and Future Perspectives**

Osteosarcoma lung metastasis cells (K7M2) and fibroblasts (NIH-3T3) were successfully used to create 3D co-culture individual and tight spheroids. After 6 days the K7M2+NIH-3T3 spheroids reached a size around 500  $\mu\text{m}$  using 220 cells in the initial seeding stage with 10% of NIH-3T3. Attempting to create a more realistic *in vivo* model of the tumor microenvironment macrophage cells (RAW 264.7) were incorporated into the co-culture system. After the addition of macrophages to the co-culture no tight spheroids were formed after 6 days in any of the conditions tested. However, some essential aspects were identified for the further establishment of the K7M2 + RAW 264.7 + NIH-3T3 spheroids co-culture approach. When RAW 264.7 is present in the growing media, a higher number of NIH-3T3 cells in the initial seeding is necessary to lead to the formation of sphere structures and keep the organization and kinetics during the spheroid growth process. Also, the strategy of starting with a bigger amount of K7M2 regarding RAW 264.7 proved to be rational and effective, especially analyzing the data until half of the growing period (3 days). However, due to the faster doubling time of RAW 264.7, the hypothesis of starting the seeding stage with a proportion higher than 2:1 (K7M2:RAW 264.7) could be considered, because after three days apparently the growth rate RAW 264.7 negatively impacts the spheroid formation and tightness, being possible to observe individual cells growing in the edge of the spheroid structure after six days.

Relevant contributions were made for the establishment of a methodology for growing K7M2+ RAW 264.7+NIH-3T3 spheroids. Nevertheless, further studies need to be done to successfully reach the formation of single and tight spheroids from the co-culture of K7M2+ RAW 264.7+NIH-3T3. Thus, future attempts starting with a ratio higher than 2:1 (K7M2:RAW 264.7)

could have a positive impact on the spheroid formation and growth within six days, aiming to end up the culture period with a K7M2:RAW 264.7 ratio closer to 1:1, that could be verified by flow cytometry analysis to reach a percentage of macrophages close to 50% regarding the total amount of living cells. Also, after the positive results obtained with higher percentages of NIH-3T3 this high percentage of fibroblasts in the seeding step will be maintained, because apparently the presence of the fibroblasts is crucial for the formation of an early tight spheroid, which in turn will contribute to the even growth of the 3D spherical structure. Also, having a higher percentage of NIH-3T3 visibly had a positive impact in the spheroid formation after six days, but once that apparently there is no difference between the structures formed using 33% or 100% fibroblasts regarding the sum of K7M2+ RAW 264.7 the next tries will explore how 50% of NIH-3T3 can impact the co-culture and spheroid formation.

The aim of establishing a K7M2+RAW 264.7+NIH-3T3 co-culture was to be able to investigate the delivery, uptake, transfection, and endosomal scape of the LNPs in a more complex *in vitro* system. In this way, after having the 3D cell culture established the goal is to encapsulate enhanced green fluorescent protein (eGFP) encoding mRNA in the same formulations tested in the 2D *in vitro* model and investigate key aspects of the LNPs delivery such as how the co-existence of the three types of cells will impact the delivery of the LNPs, how the delivery will be distributed over the three types of cells, if the macrophages will have the higher bioluminescence expression level as they had in the 2D assays using the cells individually, and how will be the penetration of the LNPs in the 3D cellular matrix. These questions will be accessed using eGFP once that flowcytometry can quantify its presence in each type of cell and also sort the cells using antibodies for RAW 264.7 and fluorescent markers for K7M2 once The da Rocha and Sweet Labs has a modified K7M2 line that encodes the red fluorescent protein tdTomato. Also, one aspect that could be explored using the K7M2+ RAW 264.7+NIH-3T3 spheroids would be the use of confocal microscopy to visually identify where in the spheroids the mRNA is being delivered and translated. Again, this could be investigated using the eGFP encoding mRNA once that eGFP has a natural bioluminescence. Also, in the future both of preview's assays could be enhanced by adding a fluorescent dye to the LNPs matrix because this will allow the quantification of the nanoparticle location before and after being uptake by the cells. Using the dye to track the LNPs and eGFP to quantify the expressed protein, the transfection and translation efficiency of the formulation could be measured, which could significantly impact the design and composition of the LNPs formulation, considering the complexity of the 3D system regarding the 2D.

### ***Spheroids Dissociation and Cell Viability***

The capability of dissociating spheroids was investigated because to use the flowcytometry to identify and quantify in which cells the mRNA expression is occurring, the cells need to be individualized keeping the viability. The assay was performed on K7M2+ NIH-3T3 (200:20) spheroids after 6 days of incubation, and after disruption the cellular viability was 80%.

Initially, the tightness of the spheroids was checked by pipetting the whole volume of each well 10 times, using an EVOS™ XL Core Imaging System Olympus Microscope (Thermo-Fischer Scientific, Waltham, MA, USA) to observe how the shear promoted by the pipetting would interfere in the spheroid morphology. After, the whole volume of 10 wells, containing 1 spheroid per well was added to a 1.5 mL centrifugal tube, and centrifuged at 1200 rpm for 7 min to concentrate the spheroids. Following, the spheroids were redispersed in 100 µL of DMEM media and transferred to a single well of a 48-well plate to confirm the spheroids presence. Then, the 100 µL of DMEM media containing the spheroids were transferred to a centrifugal tube with 100 µL of 0.25% trypsin/EDTA, and the tube was placed in a 37 °C water bath for 2 min. Last, the 200 µL were transferred to a single well of a 48-well plate and gently pipetted 50 times. This cycle of water bath incubation and pipetting was repeated as many times as necessary to break all the spheroids. The disruption of the spheroids was visually checked using an optical microscope, and the viability was quantified using an automated cell counters (Thermo-Fischer Scientific, Waltham, MA, USA).